HIGH POWER DIODE LASER ASSISTED HARD TURNING OF AISI D2 TOOL STEEL

HIGH POWER DIODE LASER ASSISTED HARD TURNING OF AISI D2 TOOL STEEL

By

PETRE DUMITRESCU

A Thesis

Submitted to the Faculty of Graduate Studies

in Partial Fulfillment of the Requirements

for the Degree of

Master of Applied Science

McMaster University

Master of Applied Science   McMaster University

Mechanical Engineering   Hamilton, Ontario

TITLE:	High Power Diode Laser Assisted Hard Turning of AISI D2 Tool Steel
AUTHOR:	PETRE DUMITRESCU, B. ENG.
SUPERVISOR:	Dr. Philip Koshy
NUMBER OF PAGES:	xiv, 111

Abstract

Laser technology is being employed at an increasing rate in many industrial applications. The increasing demand for new engineered materials including ceramics, composites and hardened steel require manufacturing technologies alternative to traditional ones. The use of lasers in hot machining processes is one of them.

The current research presents a study on laser assisted turning of hardened AISI D2 tool steel ($\approx$ 60 HRC), widely utilized in the tool making industry, which poses problems with respect to the current state of machining technology due to hard chromium carbide particles present in its microstructure.

This research work relates to the application of an analytical model to predict the rate of heating and cooling of the surface of the workpiece material subject to laser heating. Experimental temperature measurements were performed using an infrared thermometer and a thermocouple in order to calibrate and validate the temperature model. The predicted temperature evolution was then used in designing the laser assisted turning process with respect to cutting parameters and kinematics.

Cutting tests were performed on a Nakamura Tome-450 CNC lathe on which a 2 kW diode laser (Laserline LDL 80-2000) was integrated. Two machining configurations: grooving and longitudinal turning were evaluated using carbide tooling with an emphasis on tool life, cutting forces, mechanism of chip formation, workpiece surface temperature, and surface integrity. Cutting tests performed on AISI D2 tool steel when using laser assist showed that an average temperature of about 300°C in the uncut chip thickness is sufficient for proper LAM.

The main mechanisms of tool wear identified during both conventional and laser assisted grooving were cutting edge chipping, flank face abrasion, and adhesion. Built

up edge (BUE) was invariantly present during LAM, which was very stable for low cutting speed (20 m/min) and became unstable with an increase in cutting speed to 30 m/min. The use of laser assist enabled the cutting up to a speed of 30 m/min in the grooving cutting tests with good tool performance which was not possible without the use of laser. LAM also significantly reduced chatter, which was consistently noticed during conventional machining. The use of laser assist in grooving changed the cutting to thrust force ratio F_c/F_p from ≈ 0.5 in conventional cutting to ≈ 1 during LAM, indicating material softening. Chip thickening was noticed when using LAM, which suggests a decrease of about $10°$ in the shear angle. No thermal damage was found in the generated subsurface for the grooving experiments.

Longitudinal turning tests were performed in two LAM configurations corresponding to two different laser beam orientations: spot slow axis parallel to the workpiece axis (LAM $\parallel$) and spot fast axis parallel to the workpiece axis (LAM $\perp$). Chipping and abrasion were identified as the main mechanisms of flank wear for both conventional and LAM tests. During both LAM tests (LAM $\parallel$ and LAM $\perp$) chipping was reduced and the tool life improved by about 100% compared with conventional turning. Chip analysis revealed that the segmented chips characterized both conventional and LAM $\parallel$, while for LAM $\perp$ chips transformed into continuous chips. This observation together with the measured surface temperature in front of the cutting edge ($\approx 400°$ C for LAM $\parallel$ and $\approx 600°$ C for LAM$\perp$) showed that LAM$\perp$ is the proper LAM configuration for longitudinal turning. No thermal damage was identified in the generated subsurface and surface roughness increased with the increase of temperature in the uncut chip thickness.

Acknowledgments

Contents

List of Tables

List of Figures

CHAPTER 1

Introduction

Machining is a method of fabrication that continues to evolve rapidly. Presently, developing novel machining processes capable of processing new engineering materials and enhancing machining productivity in order to reduce costs constitute important research directions.

Progress in the science and technology of materials has resulted in a number of new materials. Examples include titanium and nickel alloys for aerospace applications, ferrous alloys for die and mold industry, and engineering ceramics for seals and bearings. While the application domain of these new materials is expanding, their machinability remains poor due to their properties such as low thermal conductivity in case of titanium alloys, hard carbide particles in hardened ferrous alloys and brittleness of ceramics. It is interesting to note that the very properties that enhance the application potential of these materials are responsible for poor machinability. It is therefore imperative to develop appropriate machining technologies for commercially exploiting new materials.

The recent development of technology for cutting ferrous materials in the hardened state (50-62 HRC) represents a rapid advancement in terms of reducing processing time and cost. The traditional method of processing hard ferrous alloys consists of rough machining the parts to near net-shape with the material in soft state, followed by heat treating to the desired hardness, and then rough and final finish grinding to achieve the required geometrical tolerances and surface quality. This cycle is time consuming and resource intensive, with detrimental effects on productivity and cost.

In this context hard machining reduces processing time, while maintaining or even improving product quality, and in many instances replacing expensive post-treatment by grinding. Furthermore, hard machining is generally accomplished dry and is hence also environment-friendly.

This thesis details an enabling technology that uses a high power diode laser to assist turning of hardened steel with abrasive carbide constituents.

1.1   Hard Machining

Hard machining refers to machining ferrous alloys (high-speed steels, die steels, bearing steels, alloy steels, case-hardened steels, white cast iron, and alloy cast iron) in their hardened state (45-70 HRC). Hard machining enables bypassing of one or more processes (such as rough and finish grinding), or combining more processes in one setup (rough and finish machining).

With regard to higher cutting forces and increased chip-tool interface temperatures in hard machining as compared to conventional cutting, certain elements of the technology listed below are crucial for successful implementation [24]:

- Need for a very rigid spindle with adequate power, high-precision machine-tool and tool holders with high stiffness;

- Use of hard ($> \mathrm{HV}1800$) and tough ($\mathrm{K_{1C}} > 6\,\mathrm{MPa\,m}^{1/2}$) tool materials, such as cemented carbides, ceramics and poly-crystalline cubic boron nitrides (PCBN), see Table 1.1 for typical mechanical and thermal properties;

- Increased cutting edge strength (negative rake angles, high wedge angle, suitable insert shape and cutting edge preparation);

- Appropriate cutting conditions.

A few distinct characteristics of hard machining in relation to conventional cutting are [24, 1]:

- The ratio of cutting force to thrust force (F_c/F_p) is about 0.5, as opposed to about 2 in conventional (soft state) machining [24, 1]. This necessitates a higher system stiffness as well as a stronger cutting edge (negative rake geometry and large wedge angle $\geq 90°$).

- Different tool wear modes such as cutting edge chipping and/or severe abrasion on tool flank depending on the work material being martensitic transformation hardened or carbide precipitation hardened.

- Cutting tool materials require high hardness and fracture toughness to withstand high cutting forces, as well as good thermal properties (temperature stability, thermal conductivity and thermal expansion coefficient) to overcome the increased temperatures at the chip-tool interface, see Table 1.1.

- Mechanism of chip formation is characterized mainly by segmented or discontinuous chip, while flow-type chip is predominant in soft state machining (Figure 1.1).

- Surface finish achievable is similar to that in grinding, on the order of [0.1 - 0.2 μmR_a].

To facilitate the hard machining process, a possible avenue would be to locally reduce the shear strength of work material in the cutting zone, by heating it externally. This can address some of the issues described above such as high cutting forces, and change in the mechanism of chip formation from brittle to ductile which would obviate premature tool failure due to fatigue. This concept of improving material machinability by employing an external heat source is known as hot machining.

	Carbide K10	Ceramic	PCBN
Mechanical Properties			
Density [g/cm^3]	14.0-15.0	3.8-5.0	3.4-4.3
Hardness [HV30]	1500-1700	1800-2500	3000-4500
Youngs Modulus [GPa]	590-630	300-400	580-680
Fracture Toughness [MPa$\sqrt{m}$]	$\approx$10.8	2.0-3.0	3.7-6.3
Thermal Properties			
Temperature Stability [°C]	$\approx$800-1200	1300-1800	$\approx$1500
Thermal Conductivity [W/K·m]	$\approx$100	30-40	40-100

Table 1.1: Mechanical and thermal properties of different cutting tool materials for hard machining [1].
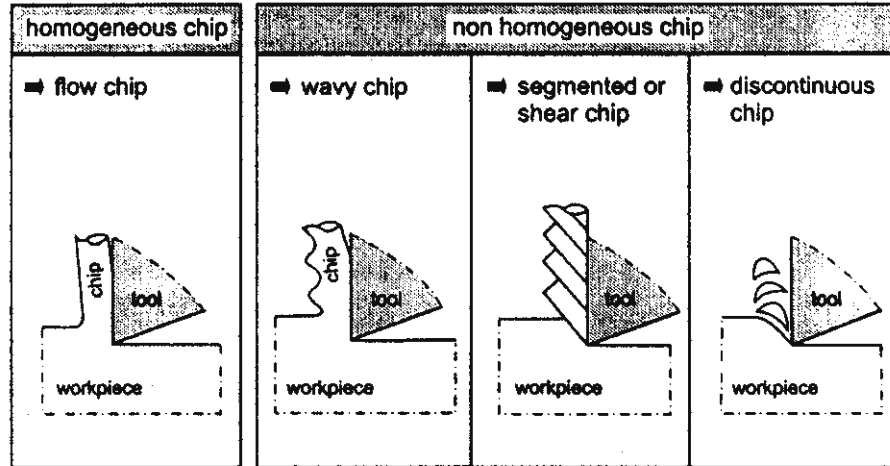
Figure 1.1: Classification of chip forms [1].

1.2   Hot Machining

Engineering materials undergo a reduction in strength at elevated temperatures (Figure 1.2) [4]. Considering that material removal in cutting processes take place by a shearing process, one possible avenue to enhancing the machinability of difficult to cut materials is to heat it locally in order to reduce its shear strength.

Hot machining is a chip forming metal cutting process involving a cutting tool with the difference that there is an external heat source to assist machining. Ideally the heating takes place just ahead of the cutting tool in the vicinity of the shear
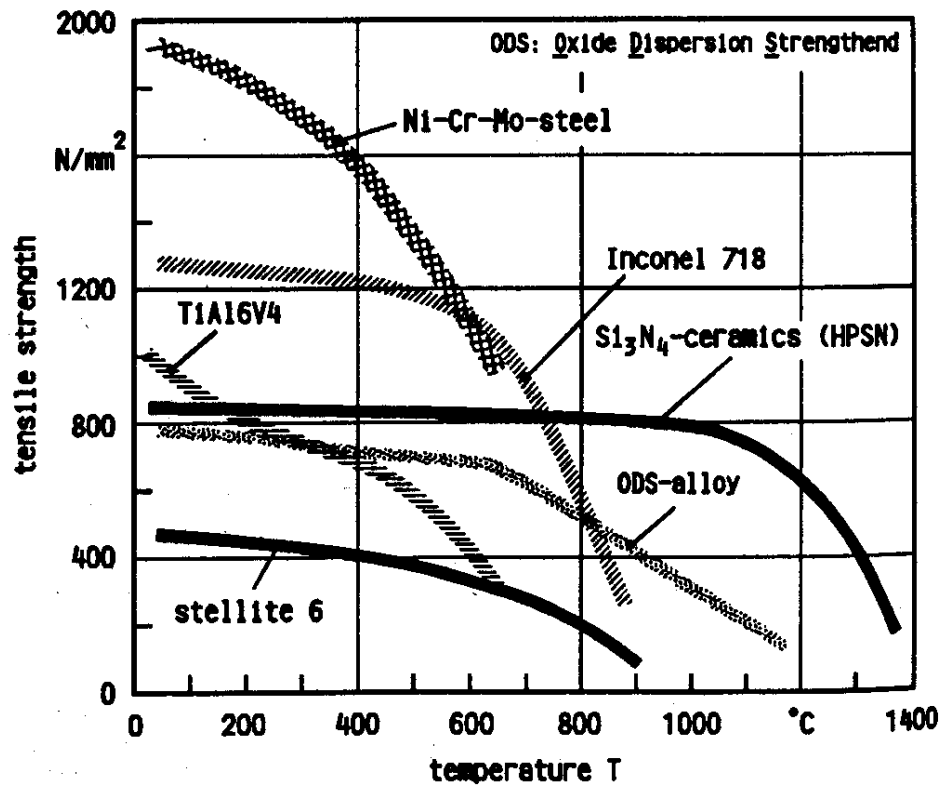
Figure 1.2: High-temperature strength of difficult to machine materials [4].

zone, softening the workpiece material to a depth comparable to the uncut chip thickness, leaving the generated surface and subsurface relatively undamaged. Figure 1.3 illustrates the concept involved.

Shearing of the material in the primary shear zone and chip-tool interface friction in cutting generates a large amount of heat which is considered detrimental to the cutting process. Inappropriate cutting parameters in conventional cutting could result in work material and cutting edge overheating, reducing surface quality and tool life. In hot machining, one could infer that additional heat supplied to the system could lead to such undesirable effects. It is deemed that in hot machining the reduction in the shear strength of the material entails lesser plastic deformation in cutting and thus the net temperature rise is in fact lower than that in a conventional cutting
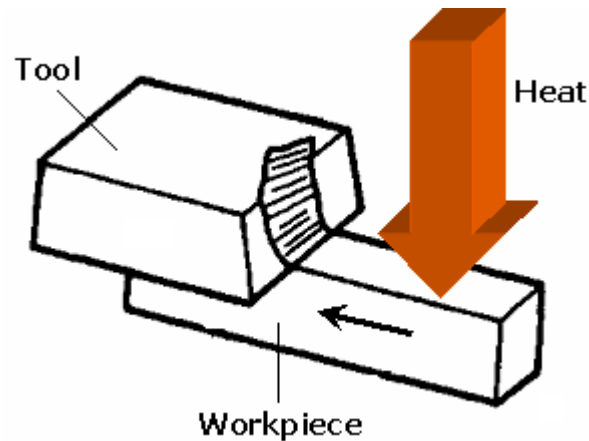
Figure 1.3: Hot Machining.

process. However, it is essential that the rate of heating need be commensurate with kinematic cutting parameters so as to restrain the heat to a thin layer below the work material surface such that most of the heat is carried away in the chip.

Typical advantages of Hot Machining include being able to cut rather than grind hard and brittle materials, decreased cutting forces and increased tool life. When machining heat resistant alloys such as Inconel or for turning chilled cast iron using plasma assisted machining [5], a significant decrease in cutting forces has been observed, Figure 1.4 a). Flame assisted machining of steel has been reported [5] to yield a substantial improvement in tool life, with the maximum tool life obtained at a workpiece temperature of about 650°C, Figure 1.4 (b).

Although the concept of Hot Machining has been around for a while, implementation of the technology has been limited by the availability of effective heat sources. The heat source for hot machining should provide localized and selective heating, have a high power density, be economical to install and operate, and be easily integrated into a machine tool. The heating should also be precise and not present any safety issues. Recent developments in new technologies capable of high specific heat input and the development of cutting tool materials that can handle high temperatures
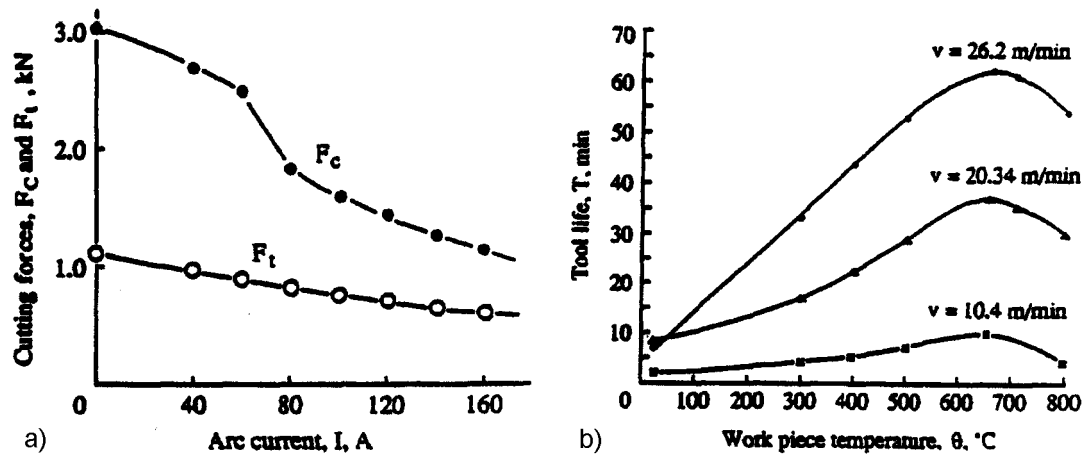
Figure 1.4: a) Cutting (F_C) and thrust forces (F_t) when turning cast iron with plasma assisted heating [5]; b) Tool life when hot machining an austenitic manganese steel utilizing flame heating [5].

have resulted in a renewed interest in hot machining.

Over the past years different heating sources have been tried in hot machining with varied success. Some of them are [5]:

- Furnace heating;

- Induction heating, (Figure 1.5 a);

- Flame torch heating (Figure 1.5 b);

- Tool-work electric heating, (Figure 1.5 c);

- Plasma-arc heating;

- Laser assisted heating.

Induction heating relies on eddy currents induced in the work material when placed in a high frequency magnetic field, which can develop high temperatures, but presents limitations in respect of materials with low permeability. The need
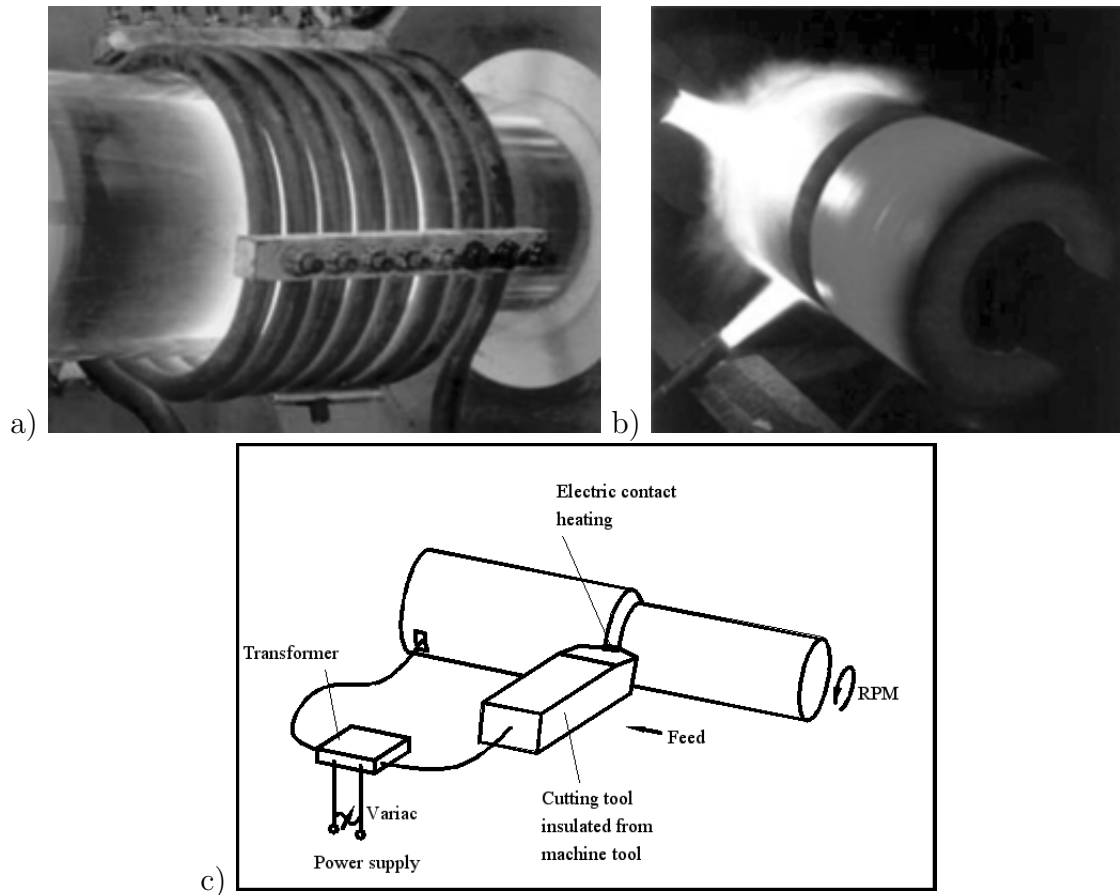
Figure 1.5: a) Induction heating [www.advancedenergy.org], b) Flame torch heating [www.linde-gas.com], c)Tool-work electric heating.

to accommodate the heating coil might also present problems in realizing processes kinematics. Flame heating is relatively safe to operate, but the power density is very low, resulting in a non-localized surface heating. Tool-work resistance heating involves the flow of a current through the cutting tool and the workpiece, is easy to implement, but when work or tool material is nonconductive this method is inapplicable. This precludes cutting non-conductive materials such as ceramics or the use of advanced ceramic cutting tools, well suitable for hot machining applications.

Among the heat sources listed above, plasma and laser heating seem to be the most effective with reference to high power density and ability to control the heating

process. However recent developments in the laser industry have resulted in safe, affordable, compact units with better output controls, which leave them the most desired heat source for hot machining, generally known as *Laser Assisted Machining* (LAM).

1.3   Laser Processing

Laser systems have started to be employed at an increasing rate in many industrial applications because of their multitude of advantages, such as high energy density, and the ability to heat a material selectively in a localized area. The increasing demand for processing difficult to machine materials including ceramics, glass, plastics and composites have promoted laser beam machining [25] to be a very promising alternative to traditional manufacturing.

In LM or *laser machining* material removal is realized by workpiece material absorbing part of the incident light energy that translates into high temperature in the vicinity of the point of incidence, resulting in material softening, local yielding, melting, burning or evaporation. For difficult to machine materials like ceramics, glass or composites this method represents an alternative to grinding or diamond cutting.

LAM or *laser assisted machining*, in contrast, makes use of laser energy just to assist a conventional cutting process, wherein material removal occurs by mechanical shearing using a wedge shaped cutting tool (see Figure 1.6).

Ideally, no evaporation of material occurs and minimal heat is conducted into the workpiece. The heat absorbed by the workpiece is utilized towards facilitating the shearing process by locally decreasing the material yield strength and counteracting the strain hardening phenomenon [26].
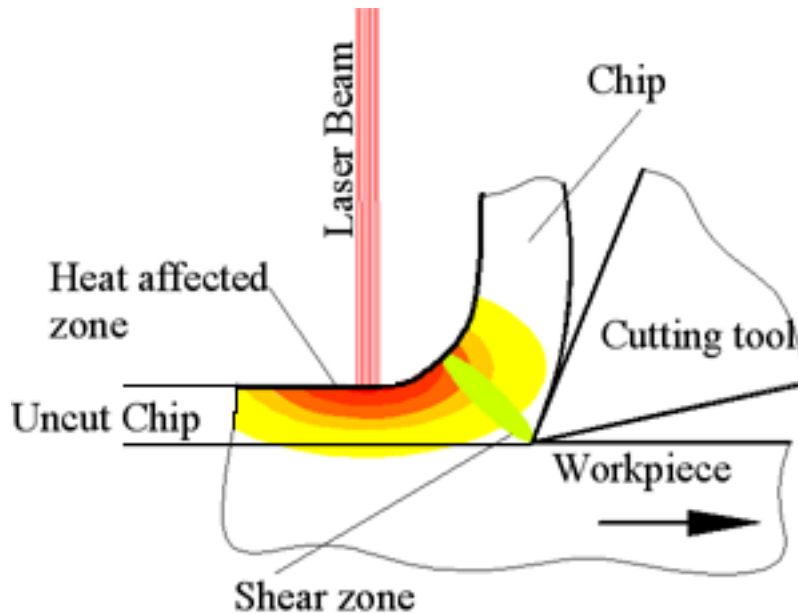
Figure 1.6: Laser assisted machining.

1.4   Scope and organization of present work

The present work deals with laser assisted hard turning of AISI D2 tool steel (1.4-1.6 %C, 11-13 %Cr) in its hardened state ($\approx$ 60 HRC). The motivation for this work was the poor machinability of this steel, which is widely used in stamping and other cold forming operations, as functional parts in dies and molds. A more detailed description of this material will be presented in Chapter 2.

Previous work published on hot machining is the focus of Chapter 2 with an emphasis on laser assisted machining of difficult to cut materials. Various aspects of this novel process such as laser-material interaction, tool life, cutting forces and mechanism of material removal are reviewed in light of conventional cutting.

The unique aspect of the research presented in this thesis is that LAM is accomplished using a high power diode laser (HPDL) as opposed to CO_2 and Nd:YAG lasers used elsewhere. HPDL are compact and more efficient in comparison with the CO_2 lasers. Moreover, the laser beam of HPDL can be conveyed using fiber optic,

which makes it easily integrable into a machine tool system and is hence more appropriate for LAM. Technical details and current industrial applications of HPDLs are discussed further in Chapter 2.

Chapter 3 gives a detailed description of experimental setup and equipment used. Experimental and analytical work aimed at characterizing laser absorption of D2 tool steel used as the workpiece in this research is presented in the first part of Chapter 4. Latter part of chapter 4 details experimental results in respect of various machinability aspects such as cutting forces, tool life and wear mechanisms/modes, mechanism of material removal and surface integrity. Conclusions derived from the present work as well as the scope for further work in this area constitute Chapter 5.

CHAPTER 2

Literature Review

2.1   Laser Assisted Machining

Laser Assisted Machining (LAM) is an enabling technology that has primarily been applied for the processing of difficult to machine materials such as engineering ceramics, nickel and titanium alloys, and hardened steel. LAM is showing great promise as a means of increasing productivity by exploiting the thermal softening characteristics of difficult to cut materials. In LAM, the material is heated selectively, prior to material removal, and subsequently the material is removed by shearing. Ideally no evaporation of the work material occurs as a result of laser heating, and the laser is employed only as a heating source for changing the material removal character from brittle fracture to plastic deformation. Material removal is performed, as it is in conventional machining by a cutting tool.

LAM process may produce higher material removal rates when compared with traditional cutting. It further offers increased productivity, improved tool life and surface quality, improved ability for geometry generation with significantly reduced cutting forces and the risk of chatter. Overall LAM is characterized by substantial cost savings and process improvements over conventional machining. Although in conventional machining a significant amount of experimental data is available for process parameters, and work material behavior, for LAM there are still unknowns and approximations in modelling of the process. For modelling LAM, the following additional process variables have to be considered:

- Laser-material interaction (dictates the temperature distribution in the material

subsurface) characterized by:

- Laser type (beam wavelength);

- Laser power density (laser power, laser spot size and shape);

- Workpiece material type, surface finish (roughness, color, presence of an oxide layer);

- Laser beam incidence angle on the workpiece surface.

• Thermo-mechanical material behavior: stress/strain relationship at elevated temperatures;

• Process geometry and kinematic setup:

- Laser beam - work surface relative velocity (scanning speed);

- Orientation of the spot for noncircular spot shape;

- Laser beam - tool lead distance (the distance between the laser spot on the work surface and the cutting edge).

Initial temperatures in conventional machining refers to ambient conditions, with heat generated by plastic deformation of the work material. Thus room temperature stress strain curves that characterizes the work material can be used in process modelling as a first approximation. Comparatively, during LAM, workpiece material used is already preheated to 500 - 1300°C at the start of the cutting process, therefore the models will have to be altered appropriately. A complete analysis of a machining process is difficult to perform, but many researches have focused on studying different aspects that could give an insight into the interaction between laser-tool-chip-workpiece such as:

- Influence of laser parameters on cutting forces and/or cutting power;

- Influence of the cutting parameters (cutting speed, feed and depth of cut) on cutting forces with and without laser assistance;

- Tool wear monitoring and tool life optimization;

- Mechanisms of chip formation (brittle fracture to ductile flow transformation) at elevated temperatures;

- Surface integrity and roughness measurements.

The focus of the present chapter is to review some of these aspects presented in the literature, especially in studies related to laser assisted hot machining. The reviewed applications of LAM are in research stage, with no large scale industrial implementations reported. Research referred to in this work are listed in Table 2.1, indicating the workmaterial and process employed.

MATERIAL	LAM Process	Reference No.
XC42 - steel	turning	[10, 9, 27]
35NCD16 - steel	milling	[11, 8]
Inconel 718	turning	[11, 27]
TA6V - Ti alloy	milling	[11, 8]
Cold-hard cast iron	turning	[13]
Si_3N_4 ceramics	turning	[11, 28, 29, 15, 30, 6, 14, 31]
Al_2O_3 particle/Al matrix composite	turning	[7]
Sintered mullite ceramics	turning	[12, 32]
Zirconia	turning	[33]
AISI D2 tool steel	turning	[34]

Table 2.1: **Applications of LAM.**

2.1.1 Mechanism of Chip Formation in LAM

Limited work has been published in terms of chip morphology. A few groups of researchers have developed investigation techniques and experimental models to study chip formation for materials, such as: titanium alloys, Inconel, hardened steel, and ceramics. As can be seen, all these materials are part of the group of difficult to machine materials, characterized by brittle fracture as the main mechanism of chip formation in conventional machining. The aim of using LAM with regard to these materials is to change the mechanism of chip formation from brittle fracture to plastic deformation, which would have a benefic effect on surface integrity and tool life.

Lei et al. [6, 14] have reported on the mechanism of material removal during LAM of silicon nitride ceramics. They have indicated two different mechanisms of chip formation, namely, plastic deformation in the shear zone enabled by viscous flow of the glassy grain boundary phase material, and initiation and propagation of intergranular micro-cracks Figure 2.1. Even at temperatures as great as $> 1000°C$ they observed that brittle fracture of $\beta - \mathrm{Si_3N_4}$ grains was not totally eliminated. Since the viscosity of the glassy phase decreases with an increase in temperature, the $\mathrm{Si_3N_4}$ grains initially slide and rotate into the liquid-like bond. Cracks were fount to initiate, coalesce and propagate at the grain boundaries, due to the absence of liquid-like glassy phase material, resulting in chip separation. LAM improved chip formation by inducing plastic deformation due to the temperature controlled viscosity of the glassy phase. They also developed a constitutive equation to describe the deformation behavior of $\mathrm{Si_3N_4}$ over a range of cutting conditions pertaining to LAM.

In a related work, Rozzi et al. [31] classified the chips produced during the LAM of silicon nitride ceramics, into three different categories as a function of the shear zone temperature: fragmented chips (T < 1151°C), semi-continuous chips (1151°C < T < 1305°C), and continuous chip (T > 1329°C). Cutting forces and surface tem-
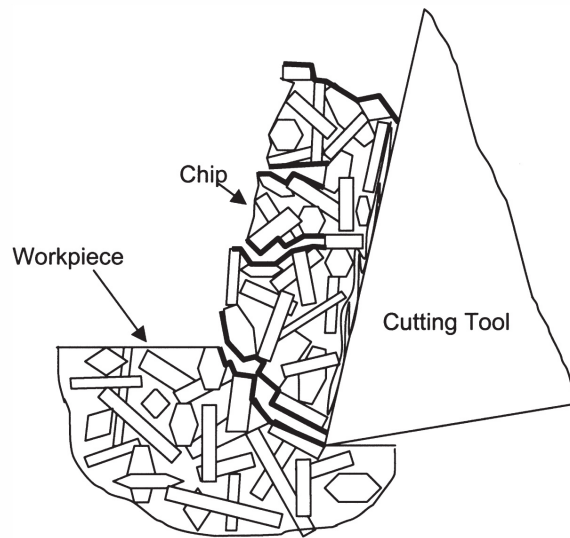
Figure 2.1: Chip formation in LAM of silicon nitride [6].

perature data associated with LAM indicated that the lower bound temperature for precluding fracture of the cutting tool or the workpiece corresponded to the glass transition temperature of $920° - 970°$C. They presented relevant images of surfaces generated during LAM showing parallel tool marks, a clear evidence of ductile mode of chip formation. At nominal LAM operating conditions a surface roughness of about 0.39 μmRa with no detectable sub-surface cracking or significant changes in microstructure. In relation to grinding that is widely used to machine ceramic materials, the advantage of LAM is the ability to achieve higher material removal rates and machining of complex shapes.

A similar mechanism of chip formation was observed by Rebro et al. [12] during LAM of mullite ceramic (sintered ceramic consisting of Al_2O_3 grains in a SiO_2 bond). At low laser power (temperatures $< 800°$C) the mechanism of chip formation was brittle fracture due to accumulation of strain energy within the workpiece, leading to crack initiation and propagation through the work material in the proximity of the cutting tool. With the increase of laser power, if the temperature of the workpiece at

the cutting location exceeds a critical value ($1000°C < T < 1300°C$), the glassy phase begins to flow, producing semi-continuous chips; further increase in laser power (for temperatures $> 1300°C$), as a result of continuous softening and resolidification of material near the cutting zone, continuous chips were formed.

Wang et al. [7] applied LAM for cutting Al_2O_3 particle reinforced aluminium matrix composite. During conventional machining of this material it was observed that the hard Al_2O_3 particulates were embedded into the softer aluminium matrix by the cutting tool. This phenomenon was observed to be more prominent during cutting of this material using laser assist. The white layer beneath the generated surface (Figure 2.2 b) was considered by the authors to represent an increased density of hard alumina particles enhancing the wear resistance of the surface. This was a direct consequence of the softening of the Al-matrix, which permits the pushing of more alumina particles into the subsurface by the tool, and the squeezing out of the metallic Al matrix (Figure 2.2 c).
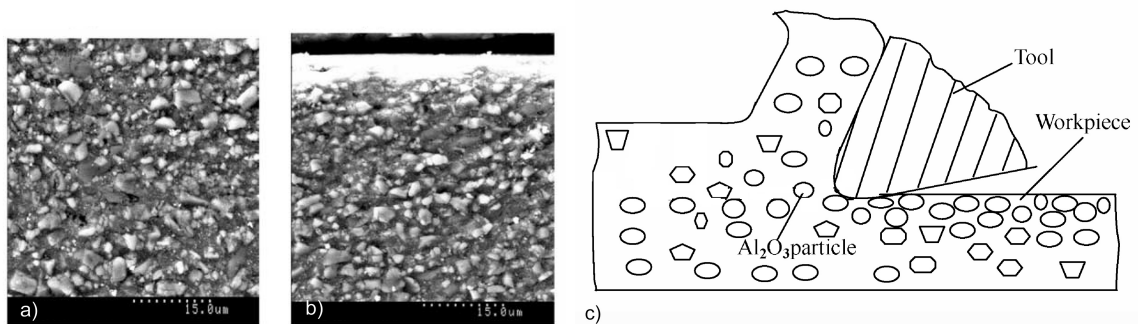
Figure 2.2: a) Unmodified material microstructure; b) White layer after LAM; c)Schematic diagram of cutting Al_2O_3 particle reinforced aluminium matrix composite [7].

Lesourd et al. [8] observed a dramatic change in the mechanism of material removal of a titanium alloy TA6V on applying laser assist which yielded continuous chips as opposed to segmental chips obtained in conventional cutting due to catas-

trophic shear localization. In their work, chip segmentation was quantified in terms of the thickness of the shear band which decreased systematically, on the application of laser heating. On reaching a critical level of heating the shear bands were not visible anymore, at which point the chip could be considered continuous, see Figure 2.3. This was explained as due to inhibition of the catastrophic shear instability during material removal on account of the laser induced preheating of the material.
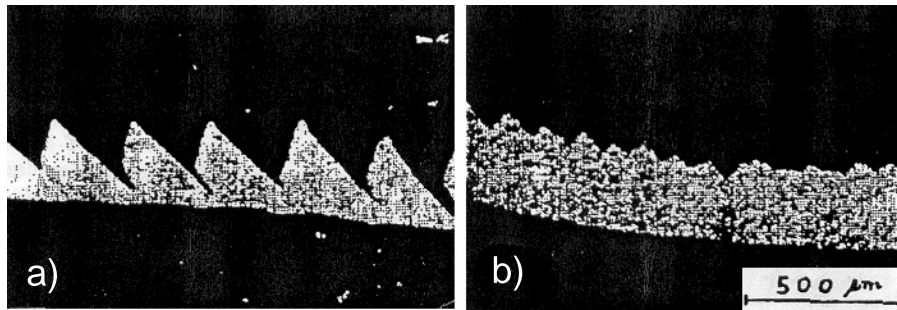
Figure 2.3: Chip formation in titanium alloy TA6V : a) Conventional cutting, b) Laser assisted cutting [8].

The studies reviewed above indicate that elevated temperatures in the proximity of the material removal zone has a beneficial effect on the chip formation process.

2.1.2 Cutting Forces

One of the important factors in evaluating machining performance is the cutting force which has a direct influence on machining accuracy and stresses imposed on the tool. It serves as a parameter to characterize the effectiveness of LAM with reference to conventional cutting. Different researchers have reported reduced cutting forces during LAM, a review of which can be found below.

Salem et al. [9] used a CO_2 laser with 10.6 μm wavelength and a maximum output power of 3.5 kW to study the influence of induced heat on cutting forces in turning of hardened XC42 steel (equivalent to AISI 1042 steel). The graphs showed in Figure 2.4 reflect the reduction in cutting forces in comparison with conventional
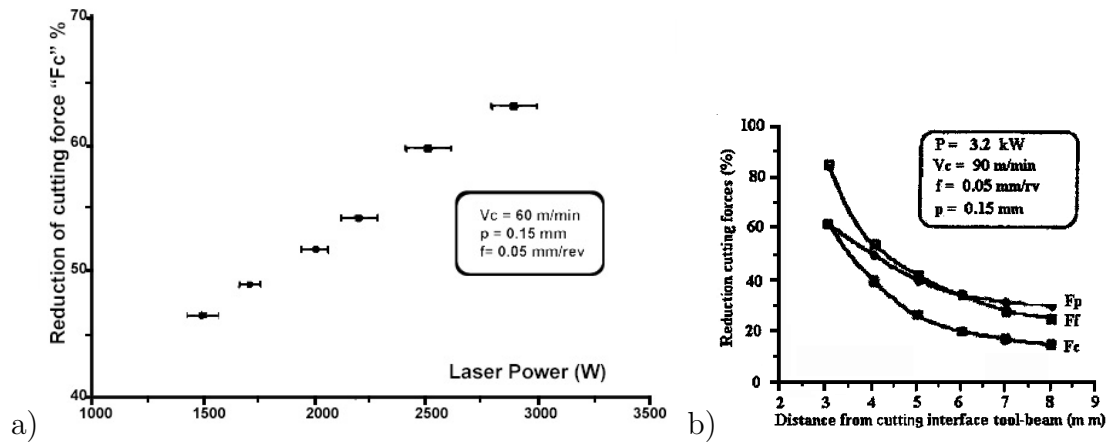
Figure 2.4: a) Reduction in cutting forces with an increase in laser power when machining XC42 steel; b)Reduction in cutting forces with the increase of tool-beam distance [9].

machining as a function of laser power, and the distance between the point of incidence of the laser and the cutting edge [9]. It can be seen that the reduction in cutting forces increases linearly with laser power whereas it reduces with an increase in laser-tool lead distance.

Similar results (for the same XC42 steel) were reported by Gratias et al. [10] in respect of laser power and laser beam-tool lead distance (Figure 2.5). These parameters have a substantial influence on the shear zone temperature and the level of work material softening thereby reducing cutting forces by values as high as 80%. Both
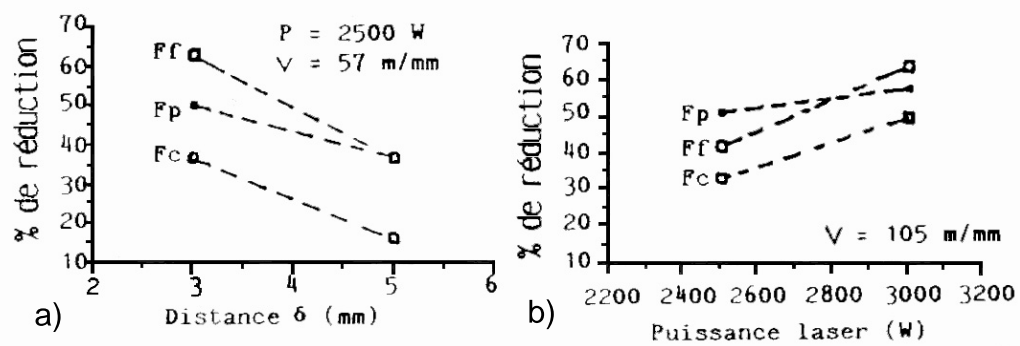
Figure 2.5:   Reduction in cutting forces as a function of: a)Laser-tool lead distance (δ); b) Laser power [10].

these parameters proved to have high impact over the temperature in the shear zone, and thus over the softening level of the work material during cutting.

Lesourd et al. [11] experimented with LAM on several difficult to machine materials : *TA6V* (a titanium alloy with 5.5-6.75 % Al, 3.5-4.5 % V, less then 0.4 % Fe, 0.015 % H, 0.1 % C, and 0.05 % N), known for its low machinability, 35NCD6 temperature resistant steel (similar to 36 NiCrMo16 - DIN Standard, with 0.36 % C, 0.2 % Si, 0.45 % Mn, 1.8 % Cr, 0.35 % Mo and 3.85 % Ni), Inconel 718, a hardenable nickel-chromium alloy, suitable for high temperature applications, and also Si_3N_4 ceramics. For all these materials they reported machinability improvements when using laser assistance. The reduction in cutting forces was 30-50% and 50% for TA6V and 35NCD6 steel, respectively. It was observed that laser assistance enabled cutting of 35NCD6 steel at speeds on the order of 200 m/min. Heating of the Si_3N_4 workpiece above 1100°C permitted material removal by cutting of the material at a cutting speed of 65 m/min, a feed of 4 mm/min, and a depth of cut of 1 mm (Figure 2.6). The most remarkable results were obtained for machining Inconel 718. The laser assistance expanded the range of machinability from the usual 20 m/min cutting speed in conventional machining to incredible values of 350-400 m/min (Figure 2.7).

Ma Li-xin et al. [13] describe LAM experiments conducted on cast iron (3.5% C, 0.6% Si, 0.3% P, 0.12% S, with a surface hardness 52 HRC), using a YAG solid continuous beam laser, with a maximum output power of 200W, and report that cutting force decrease by 23.2% on average. At constant laser power, they observed that the effectiveness of the laser in terms of a reduction in cutting forces decreased with an increase in both cutting speed and depth of cut, due to insufficient work material softening. Although the low power employed in this work limited the range of cutting parameter values over which the tests were performed, LAM was noted to be beneficial even at low laser powers.
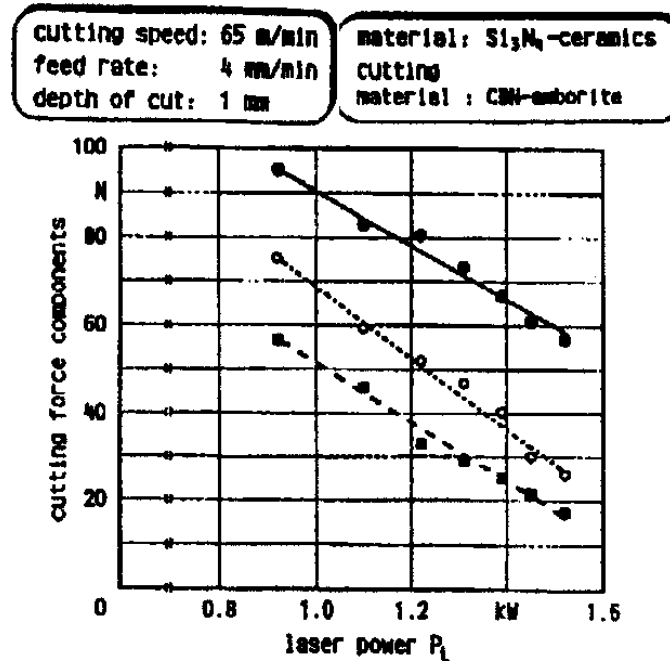
Figure 2.6: Cutting forces in LAM of Si_3N_4 **ceramics [11].**

Wang et al. [7] studied cutting forces, tool wear and residual stress in LAM of aluminum matrix composites (Al_2O_3p/Al). They concluded that LAM is a very effective method for machining Al_2O_3p/Al composite, in that the cutting forces and tool wear are significantly reduced in comparison to conventional machining, and that LAM can increase the compressive residual stress in the machined surface, giving the machined surface an improved fatigue strength and surface quality. The hard Al_2O_3 particles, initially even distributed in the metallic aluminum matrix are pushed into the workpiece surface by the cutting tool nose. This leads to relatively high cutting forces in the case of conventional machining. During LAM the induced heat softens the aluminum matrix facilitating the sinking of Al_2O_3 particles into the subsurface. As can be seen in Figure 2.8, the thrust force F_y and the axial force F_x are reduced by approximately 50%, while the cutting force F_z is reduced just by 10%.

Lei et al. [6] developed a constitutive equation for predicting the shear zone
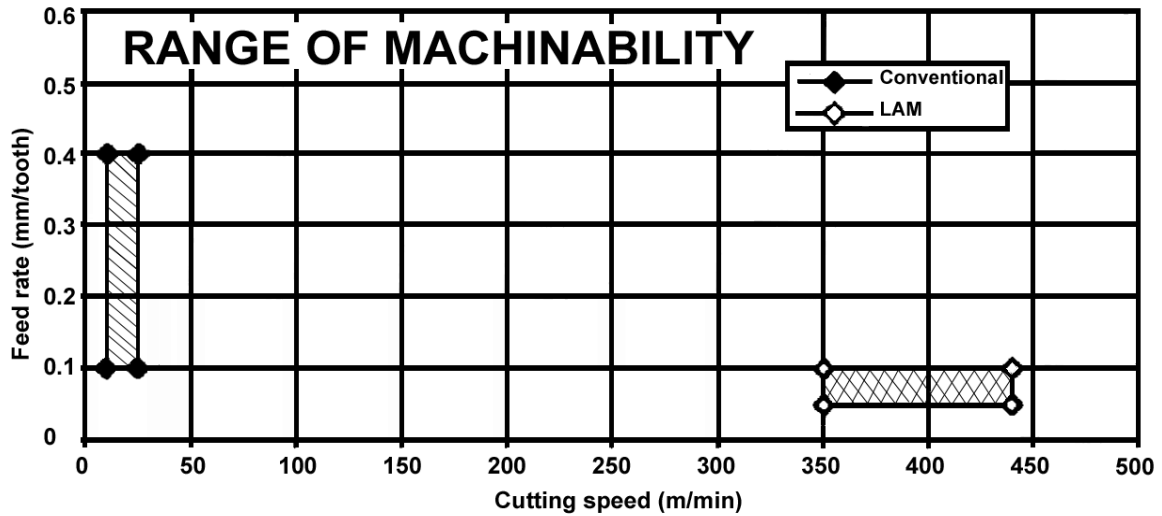
Figure 2.7: Machining range for Inconel 718 [11].
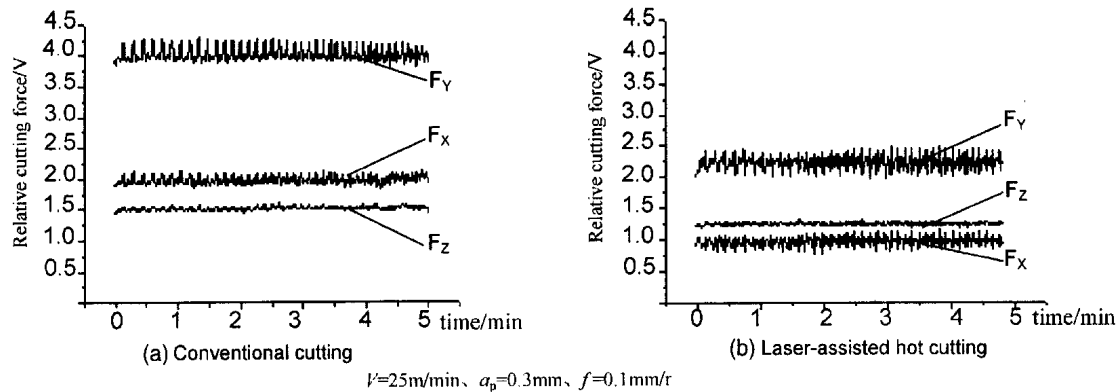
Figure 2.8: Cutting forces when machining Al_2O_3 particle reinforced aluminum matrix composite [7].

stress as a function of workpiece temperature, when LAM of silicon nitride ceramics. They compared the values for the shear stress predicted with data obtained from experiments and found good agreement between them (Figure 2.9). From the computational and experimental results they concluded that the shear stress decreased with increasing temperature due to a reduction in material strength, in fact the viscosity of glassy phase decreased, facilitating the flow of the material over the cutting tool face. They found that for the range of speeds employed (0.4-1 m/s) the shear stress
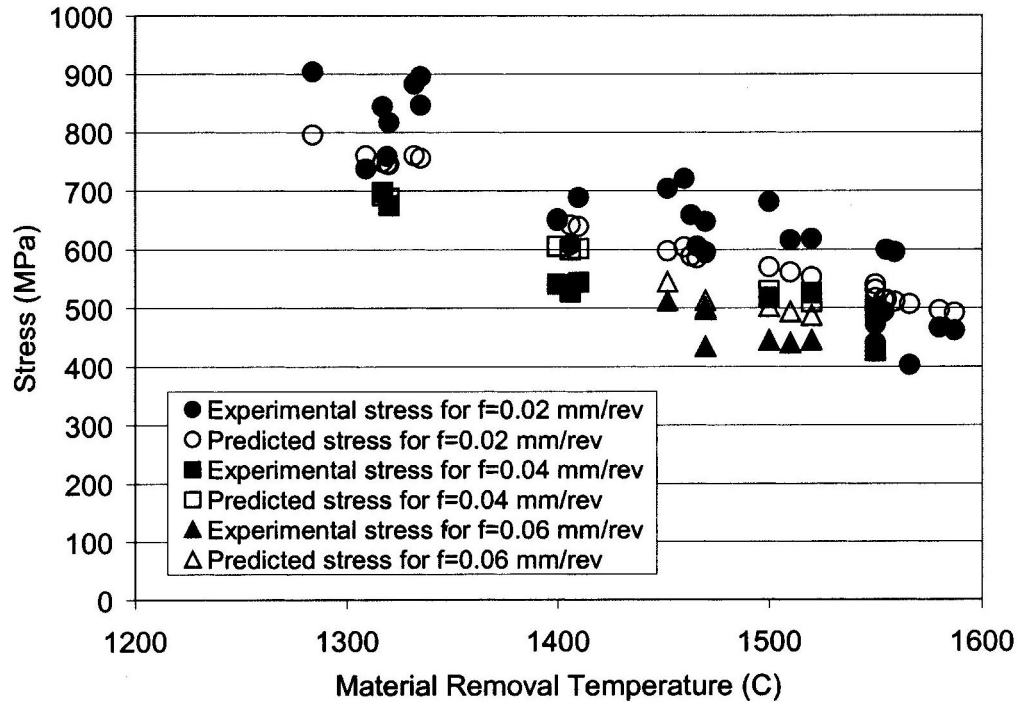
Figure 2.9: **Comparison of shear stress predicted by model and experimental results in LAM of silicon nitride [6].**

variation was insignificant.

For LAM of mullite ceramics (Al_2O_3 grains in a SiO_2 bond, sintered ceramic) Rebro et al. [12] found that a low maximum power of 210 W was sufficient for heating the workpiece. A higher laser power was found to generate thermally induced tensile stresses, resulting in thermal cracks ultimately leading to thermal fracture. The authors studied the ratio between the feed force and the cutting force F_f/F_c in a laser assisted (at laser powers up to 210W) turning operation. The comparison presented in Figure 2.10 provides additional evidence on the benefits of LAM in terms of inducing material softening in the vicinity of the cutting zone.

Khan [34] conducted experimental investigations on LAM of hardened AISI D2 tool steel and reported reduction in cutting forces for cutting speeds in the range of 200-300 m/min.
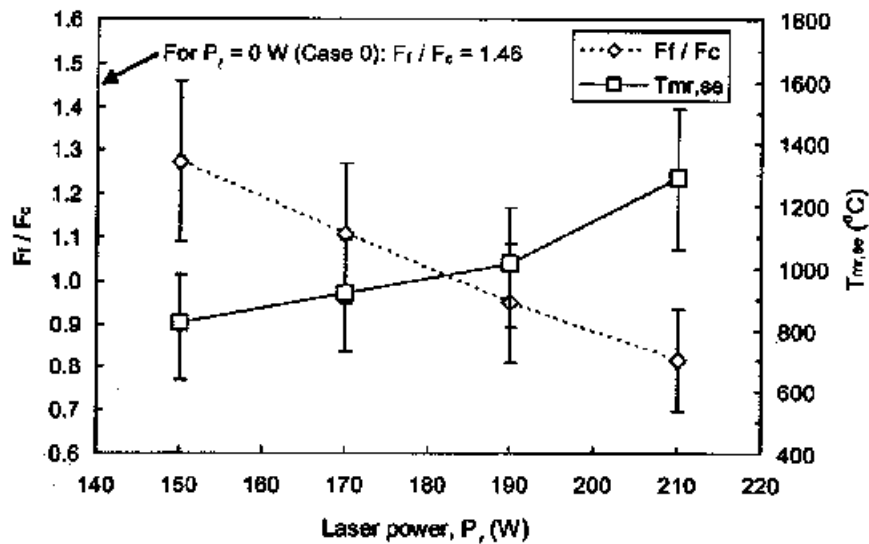
Figure 2.10: **Material removal temperature and feed/cutting force ratio vs. laser power in LAM of mullite ceramics [12].**

2.1.3   Tool Wear and Tool Life

Tool wear in cutting operations is generally attributed to abrasion, adhesion, and diffusion mechanisms on account of the mechanical and thermal influences on the tool. The application of LAM can be expected to improve tool life when machining difficult to cut materials due to the fact that the material is thermally softened in the shear zone, provided that this does not impose an additional load on the cutting tool. In general in LAM can be expected to bring about significant reduction of wear due to abrasion.

Ma Li-xin et al. [13] reported a 50% reduction of in tool wear for LAM of cast iron, in comparison with the conventional machining Figure 2.11.

Tool wear was monitored by Wang et al. [7] for LAM of Al_2O_3 particles reinforced aluminum matrix composite, by measuring the variation in workpiece diameter over the life of the tool, which was assumed to be the direct result of the flank wear. The absolute value for flank wear was not measured, but the dimensional variation of
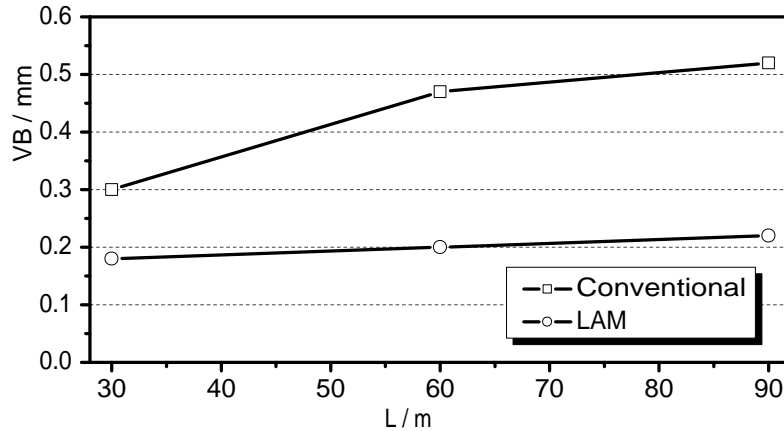
Figure 2.11: Comparison of flank wear when machining cast iron using conventional and LAM as a function of length cut [13].

the workpiece during conventional cutting when compared with LAM (Figure 2.12) reflects the beneficial effect of LAM in reducing tool wear. Tool wear when conventionally machining this material is primarily due to alumina particles giving rise to abrasive wear. LAM improves tool life by softening the Al matrix which renders the hard and abrasive alumina particles ineffective in terms of inducing abrasive wear.

Tool wear and failure modes in LAM of Si_3N_4 ceramics were identified by Lei et al. [14] as being highly dependent on the temperature induced in the uncut chip thickness, Figure 2.13. In general it was found that flank wear decreases with an increase in temperature. However, above a certain temperature ($> 1500°C$) they indicated a 25% probability for catastrophic failure to occur due to high temperature induced into the tool material, which suggests that there is a limiting temperature for realizing successful LAM. At lower temperatures ($< 1400°C$), the cutting forces were higher and the mechanism of tool wear observed was abrasion, with limited adhesion. With the increase of temperature a thin layer of shiny material was noticed on the wear land, which was believed to be molten glassy grain boundary material, adhering
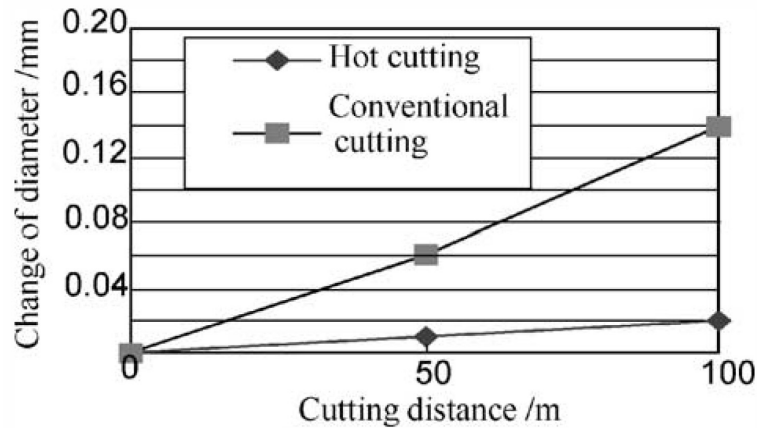
Figure 2.12: **Comparison of change in workpiece diameter as an indication of flank wear between conventional and LAM of** Al_2O_3 **particles reinforced Al matrix composite [7].**

to the tool surface.
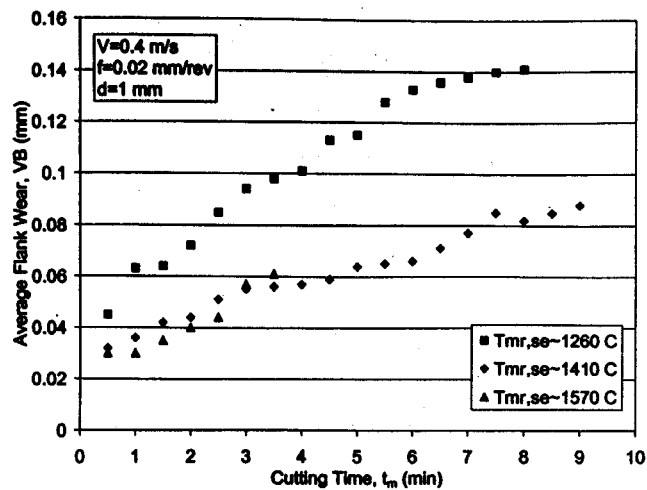
Figure 2.13: Flank wear when LAM of silicon nitride [14].

Rebro et al. [12] also concluded that the temperature developed in the material removal zone which is a function of the laser power had a substantial influence on flank wear during LAM of mullite ceramics. As shown in Figure 2.14, for the K313 uncoated carbide inserts employed in their experiments, they found an optimum temperature (T = 1043°C) for which tool life was maximum. Below this temperature the flank

wear was higher due to insufficient reduction in workpiece material strength, while above this value the tool strength was compromised due to excessive heat diffusing into the tool.
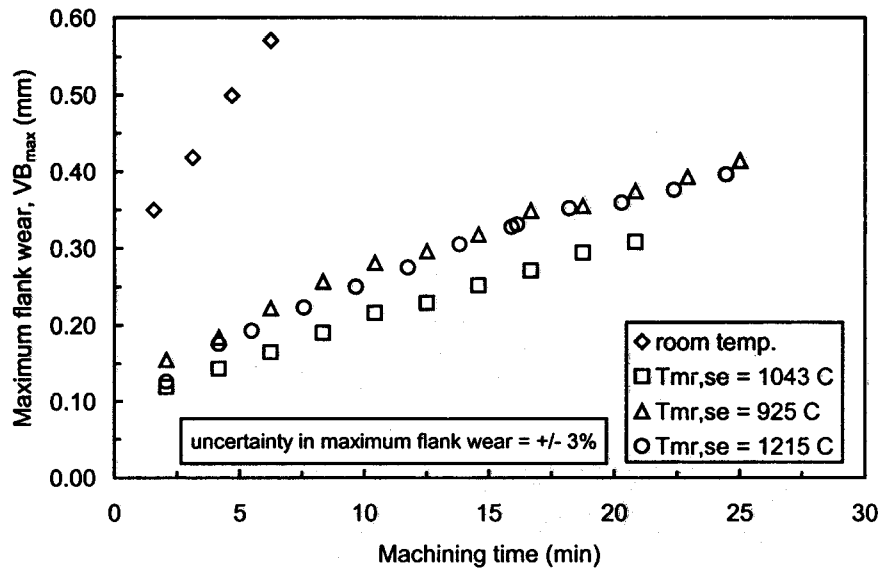
Figure 2.14: Flank wear for LAM of mullite [12].

Based on the foregoing it can be concluded that the important factors that determine tool wear during LAM are the material machined, tool material, and the laser power used. The general trend for all the applications reviewed here is a significant improvement in tool life in LAM in comparison to conventional machining.

2.1.4   Laser-material Interaction - Analytical Modelling

During LAM, part of the laser beam energy is absorbed by the workpiece surface, generating local heating and resulting in a steep temperature gradient that depends on the the work material, the spot size, energy distribution of the beam and the scanning velocity (the relative motion between the beam and the workpiece). Since finding optimal cutting conditions for LAM is both time consuming and difficult when adopting a trial and error experimental technique, analytical and numerical

modelling could give a better understanding of the process and thus facilitate the selection of parameters.

Experimental results show that the thermo-physical process of laser-material interaction consists of two phases:

- The *heating phase* which occurs when the laser beam irradiates the workpiece surface. The surface temperature increases rapidly, generating a temperature gradient in the thickness of the workpiece, and softening the workpiece material up to a certain depth. Being able to predict the temperature field in the workpiece material thickness would provide important information for identifying appropriate process kinematic parameters and the laser power for LAM .

- The *cooling phase*, starts immediately after the laser beam passes by. During this phase the surface temperature decreases rapidly. This phase is of particular interest with regard to designing the machining set up, especially for positioning the laser spot in front of the cutting tool. If the laser spot is positioned too far from tool tip the benefits of heating the workpiece are lost, whereas if the spot is too close to the tool tip, this would have an unfavorable influence on tool wear.

The rapid succession of the two phases has an important influence in LAM, because the scanning velocity should be chosen as a function of heating/cooling cycle. This parameter characterizes the relative motion between the laser beam and the material surface, and influences the laser irradiation time, and thus the amount of thermal energy delivered to the workpiece.

The maximum uncut chip thickness should be determined with reference to the temperature distribution into the depth of workpiece material in order to realize an effective LAM process. If the workpiece material is not sufficiently heated, catas-

trophic failure of the tool could occur, and for brittle materials, the surface integrity could be affected due to appearance of cracks. If the workpiece material is overheated, microstructural transformations or thermal residual stresses could be induced into the workpiece subsurface.

The interaction between a laser and the work material is complex and depends on many factors related to both the laser beam (wavelength, beam intensity and distribution, spot size, incidence angle), and the work material (thermal properties and surface optical properties). The efficiency of the heating process by a laser beam scanning the surface of a particular material is determined by the amount of energy absorbed into the volume of material and converted into thermal energy and the proportion reflected back.

As can be seen in Figure 2.15, the reflectivity is not only dependent on the work material surface, but also the laser wavelength. With decreasing wavelength, the reflectivity decreases (i.e. absorptivity increases) and therefore the laser-material interaction efficiency is higher.

Reflectivity/absorptivity is also a function of temperature for a particular laser-material combination. As the temperature increases, the electrons are more likely to interact with the structure rather than oscillate and radiate, leading to a decrease in reflectivity and increase in absorptivity.

In respect of the mechanism above, Yilbas [35] developed a mathematical model involving heat conduction, phase change, convection processes and mass removal mechanisms to study the temperature distribution and material evaporation speed inside the workpiece material, during laser irradiation. He measured the surface temperature of the workpiece using an optical method, which was in good agreement with values predicted by the theoretical model. His model also pointed to the interesting fact that the maximum temperature was below the free surface of the material for
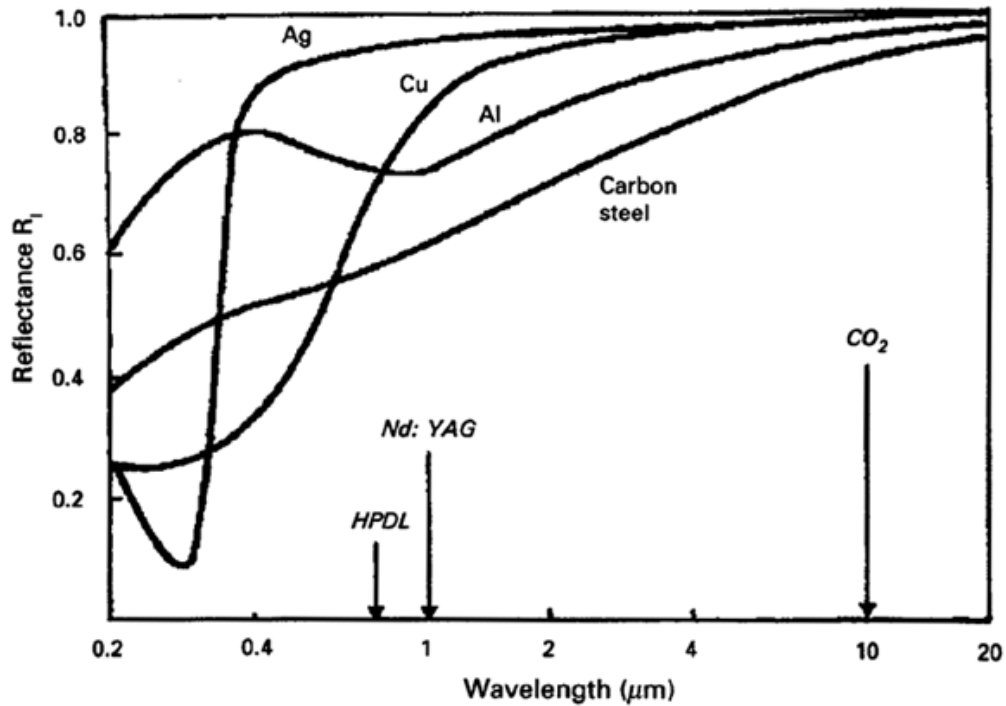
Figure 2.15: Reflectivity spectrum of various polished metal surfaces [2].

high laser intensities, which suggests that material removal mechanism is initiated from inside the material by a burst of liquid, or explosion of vapor bubble through the free surface. His experiments also revealed that high temperatures were reached within a radius 1/e of the laser beam intensity distribution, whereas beyond this radius a very rapid decay of temperature was observed, which suggested that the energy gained by the material through absorption is considerably higher than the losses due to the radial effect of heat conduction.

Rozzi et al. [36, 15] developed an analytical three dimensional heat transfer model for LAM which predicts the thermal response of a rotating silicon nitride workpiece undergoing a LAM process. The analytical model accounts for the workpiece material physical properties, the kinematics and the workpiece geometrical changes associated with the turning process. They also used an infrared pyrometer to measure

the workpiece surface temperature subject to laser heating and found good agreement with the theoretical results. A schematic of the experimental setup can be seen in Figure 2.16, with the mention that the pyrometer measuring locations were stationary (N1, N2, N3), whereas Figure 2.17 shows the numerical and experimental temperature histories for the three different pyrometer locations.
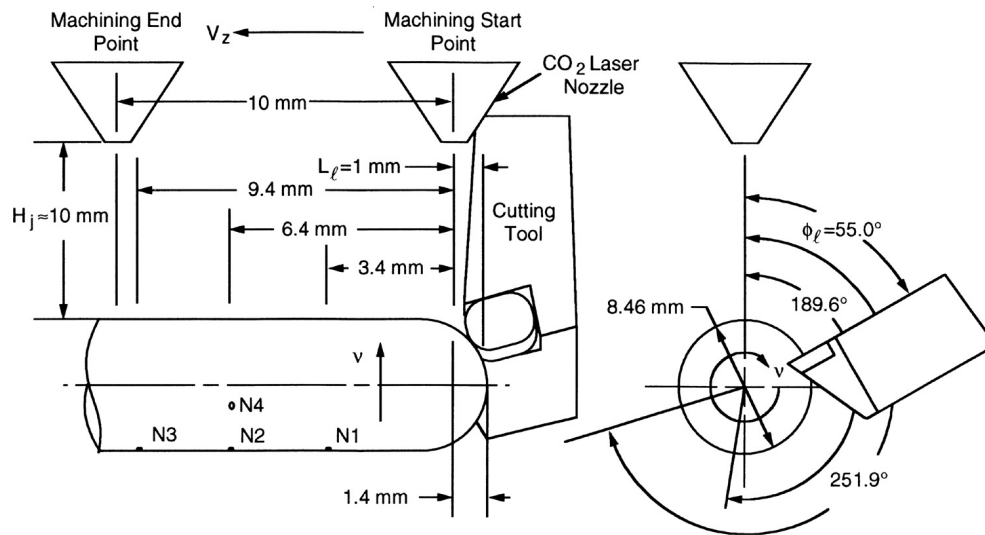
Figure 2.16: Surface temperature measurement locations during LAM of silicon nitride [15].

The same analytical model [36] is used by Rebro et al. [32], and Pfefferkorn et al. [33] to assess the LAM process for other ceramic materials: mullite $(2Al_2O_3 - 2SiO_2)$ and magnezia partially stabilized zirconia. They also found good agreement between predicted and measured temperatures.

Rozzi et al. [14] conducted a study to evaluate the laser assisted turning of a silicon nitride workpiece and identified temperatures for its successful implementation. Due to workpiece rotation and poor accessibility to the small machining zone, the temperature measurement was done in a different location on the workpiece surface and employed a semi-empirical method to evaluate the temperature at the material
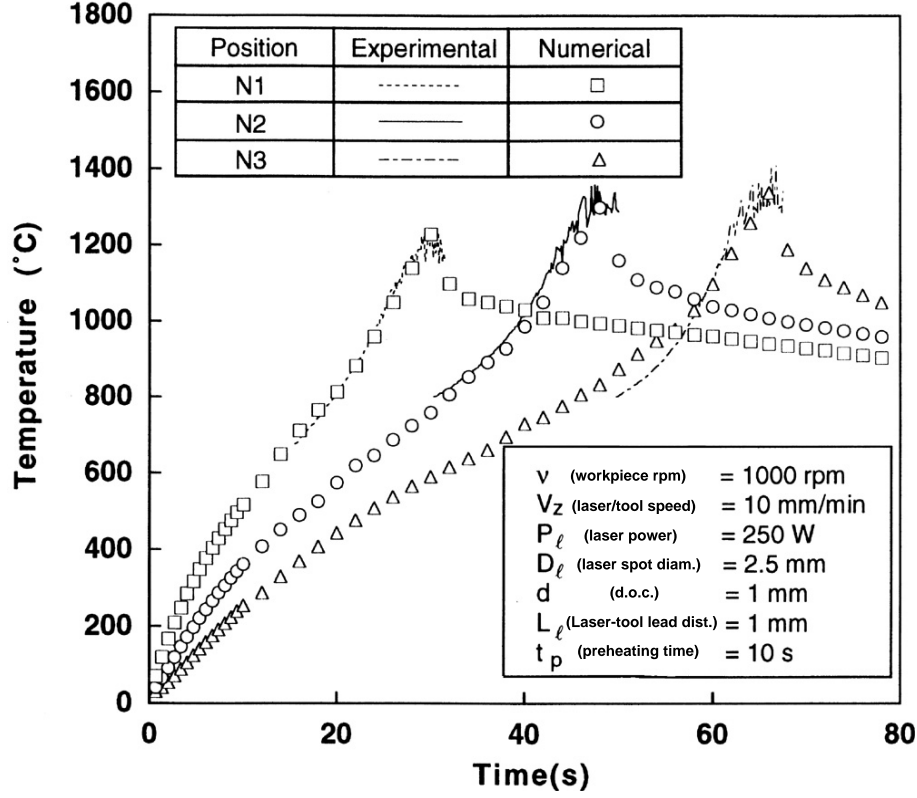
Figure 2.17: Experimental and numerical surface temperature histories at N1, N2, respectively N3 locations [15].

removal location. They obtained the temperature field around the material removal location (T_{mr}), respectively at the pyrometer measuring location (T_{py}), based on a transient three dimensional thermal model developed based on [15, 30]. The difference between these two predicted temperatures $\Delta T = T_{mr} - T_{py}$ was considered as a correction factor for the experimental measured temperature in order to obtain the temperature in the material removal zone: $T_{mr,se} = T_{meas} + \Delta T$. The maximum surface temperature T_{max} (Figure 2.18) was also obtained from the numerical modelling of the workpiece temperature corresponding to the center of the laser spot.

Gratias et al. [10] observed that by irradiating a XC42 steel workpiece using a laser, the material develops a heat affected zone beneath the surface. The XC42 structure consists of ferrite and pearlite while the layer that can be seen in Figure 2.19
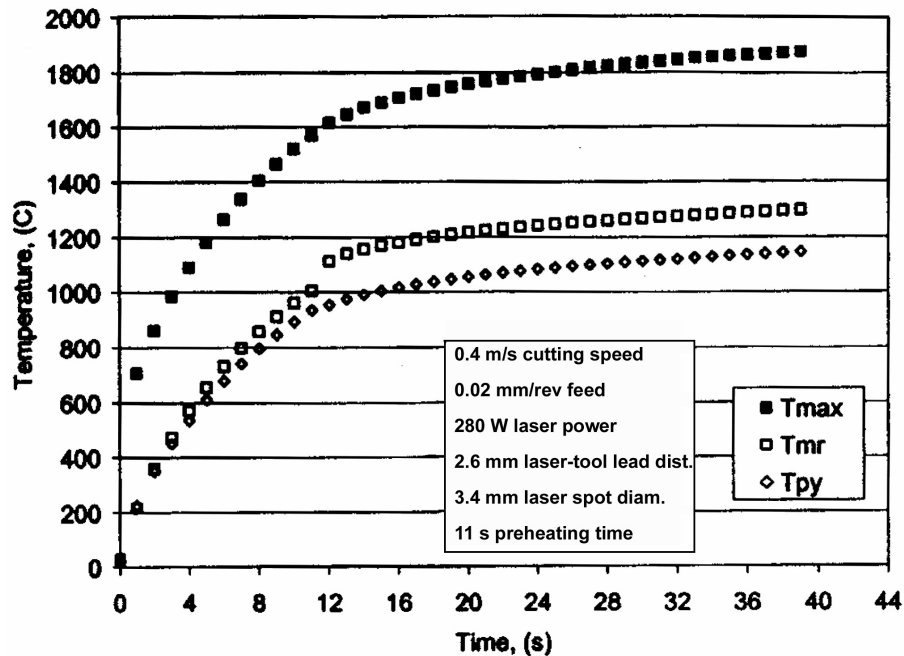
Figure 2.18: Predicted temperatures at the center of the laser spot, in the material removal plane, and at the measurement location [14].

is martensite which forms as a result of heating above the austenizing temperature (780°C), and rapid cooling, thus offering a very good method for visualizing the heat affected zone during LAM. They also proposed an empirical relation to determine the depth of the heat affected zone (e), see Figure 2.19:

$$e = \frac{A \cdot P}{\sqrt{v}} + B$$

where P is the laser power, v is the speed of laser beam travelling along the workpiece surface, A and B are experimental constants. This method could be applied when using the laser for surface heat treatment, but could also be useful to determine the maximum uncut chip thickness during LAM. Figure 2.19 reveals the depth of heat penetration into the workpiece when the laser beam is scanning the surface. The martensitic transformation takes place in zone E. Due to its hardness, martensite is

unfavorable for the cutting process. Knowing the heat penetration depth and the length of zone E could aid in selecting the cutting parameters for LAM in order to avoid martensite formation in front of the cutting tool.
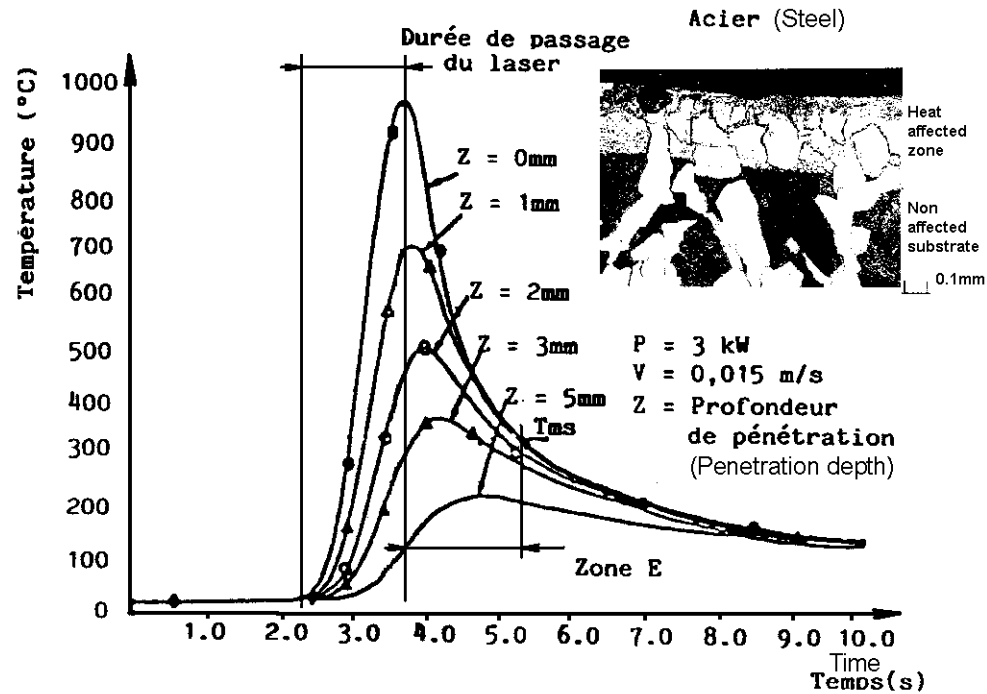
Figure 2.19: Temperature distribution for a steel sample and micrograph of a heat affected zone [10].

Ashby et al. [16] utilized an approximate solution of the equations of the heat flow, combined with kinematic models to predict the near surface temperature gradient of plain carbon steels after laser irradiation. Their model is associated with laser case hardening of steels, and focuses on the structural changes and the depth at which these occur in the microstructure of carbon steels due to laser heating. Although experimental validation was not performed, the model could be considered valuable due to its simplicity and ease of numerical implementation. The depth of the hardened layer as it was obtained from model computation can be observed in Figure 2.20 as a function of laser power and beam spot dimension and scanning velocity. A more detailed description of their approach is to be given in the next chapter of this work.
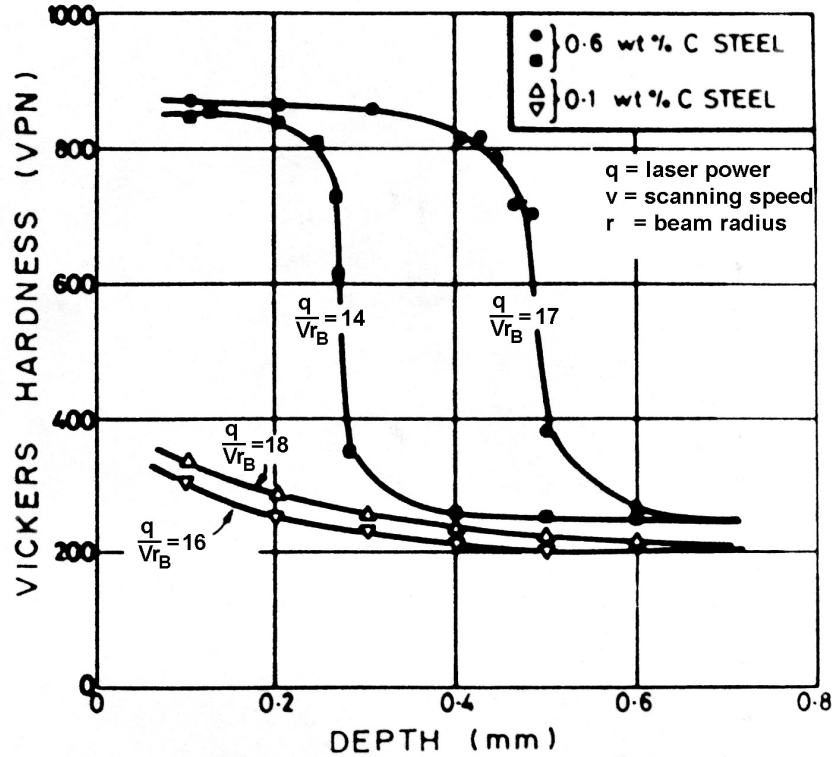
Figure 2.20: **The hardness profile in two different steels and two sets of parameters [16].**

Metal cutting is a process that implies very high strain rates during chip formation (on the order of $10^5\,\mathrm{s}^{-1}$), and that generates a large amount of heat as a result of material shearing. Material behavior data (strain, strain rates, flow stress) at elevated temperature is difficult to measure during cutting tests, therefore these values have to be approximated by other means. Using tests results from tensile tests for the flow stress is not appropriate, because of the corresponding low strain rates ($10^3\,\mathrm{s}^{-1}$). A good approximation to cutting conditions are impact tests, which can reach strain rates up to $2 \times 10^4\,\mathrm{s}^{-1}$, similar to those obtained in metal cutting. These tests can be also carried out at elevated initial temperatures, simulating hot machining conditions.

Jaspers et al. [17] performed impact tests using the Split Hopkinson Pressure

Bar (SHPB) method at elevated temperatures. Their results (Figure 2.21) show the effect of thermal softening at high strain rates. A high dependency of the flow stress on strain rates and temperature can be observed, and also the fact that strain hardening is apparently independent of temperature.
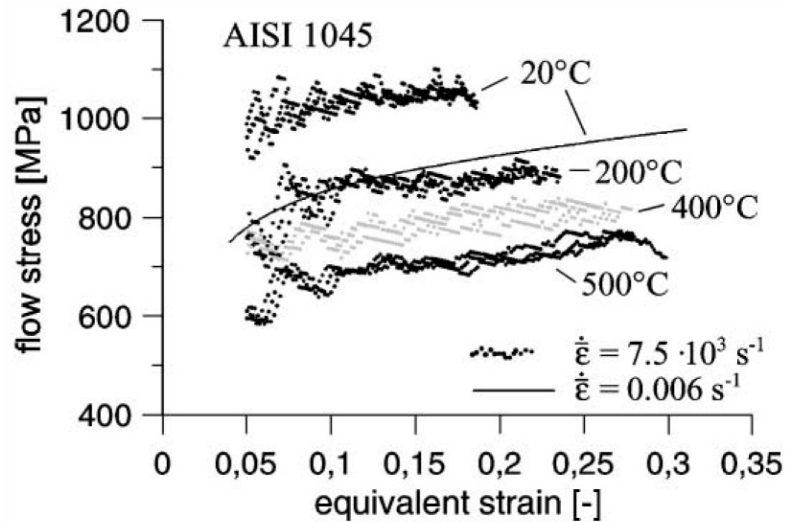
Figure 2.21:   Flow stress of ANSI 1045 steel in low (continuous line) and high strain rate (markers) at various temperatures [17].

A knowledge of flow stress at the high strain rates and elevated temperatures combined with the ability to measure or predict the temperature during LAM could ease and shorten the process of optimizing the machining parameters for successful implementation of LAM. This would also enable the use of numerical techniques to replace expensive and time consuming experiments that involve a trial and error approach.

2.1.5   LAM - Perspectives

As a manufacturing process LAM has not yet reached the stages of industrial application. However the advent of new and difficult to cut materials, is expected to accelerate the development of LAM, and its subsequent industrial implementation.

The improvements in laser technology, especially in the optical manipulation of the laser beam could lead to the implementation of laser based technologies in the machine tool systems. The introduction of laser incorporated machine tools would represent the next step in manufacturing technology in order to satisfy the continuous demand for flexibility, accuracy, quality and cost reduction.

Experimental studies carried out until now prove that LAM possesses significant advantages over conventional machining applications, especially for difficult to machine materials in terms of reducing cutting forces, improving surface finish and surface integrity, and significantly enhancing tool life. LAM also provides the opportunity to cut materials that otherwise need be ground, thus substantially increasing process productivity.

In order to determine LAM applicability range and limitations, more systematic studies and experiments for various machining conditions and a range of materials have to be carried out. Several physical phenomena occur simultaneously or successively during LAM in a very short time interval (heating, cooling, primary and secondary zone shearing, friction, etc.). Modelling of these phenomena gives the possibility of better understanding the processes involved, and enables the optimization of cutting parameters, considering that conventional machining parameters cannot be applied as such to LAM.

A better understanding of laser-material interaction will definitely lead to an improvement in laser assistance of machining operations. Future research in this field will provide valuable information for proper implementation and use of this method for improving the machinability of materials.

LAM is not meant to complectly replace finishing operations like grinding and diamond cutting, techniques that are able to generate better surface finish and less subsurface damage than LAM. Due to its flexibility in generation complex geometries,

and higher material removal rates, it is believed that it could replace the above mentioned techniques in shaping and roughing operations, especially for very difficult to cut materials, resulting in a substantial increase of cutting efficiency.

2.2 Laser Technology

2.2.1 Types of Lasers

The design and application of industrial lasers have advanced considerably since their introduction in the 1960's. During this time, lasers have evolved from being a laboratory curiosity to a real and powerful industrial tool, rapidly finding their way into many fields of manufacturing.

In 1964, Patel at Bell Laboratories developed the first CO_2 laser, capable of generating power in the range of 1 mW with an efficiency of 0.0001%. The first commercially available laser was built by Coherent in 1966 with an output power of 100W, and two years later upgraded it to 250W. In 1970's Avco Everett research laboratory developed the first high power CO_2 laser with an output power of 15 kW. The CO_2 lasers had a gas mixture of $CO_2/N_2/He : 0.8/1/7$ and are capable of generating power densities in the range of $10^9 - 10^{15} W/cm^2$ [25]. A Nd-YAG laser was also developed by Bell Laboratories in 1964, but was not used until Quanta-Ray introduced the first reliable high performance YAG laser in 1976. These lasers used neodymium (Nd) as the lasant material doped in a YAG (yttrium aluminum garnet) crystal.

In 1974 Ewing and Brau developed the first excimer laser at Avco Everett research laboratory [37], based on noble gas halides (krypton fluoride and xenon chloride), capable of generating high power densities, in the range of $10\,MW/cm^2$ to $200\,TW/cm^2$.

Diode lasers are based on semiconductors such as AlGaAs, AlGaInP or InGaAs. The first diode laser application was reported in the early 1990's for soldering and used a 15W laser. Since then, continuous development of semiconductor technology aided the development of high powers diode lasers, comparable with CO_2 and Nd-YAG lasers. Presently, 6kW diode lasers are available commercially. Diode lasers with output powers in excess of 0.5 W are considered to be in the range of high power and are referred to be **H**igh **P**ower **D**iode **L**asers (HPDLs) [2]. Since a HPDL is used in this work, typical characteristics and industrial applications of this laser are detailed in the following. Table 2.2 provides a comparison of certain technical characteristics of HPDL with YAG and CO_2 lasers.

	Diode Laser	YAG Laser	CO_2 Laser
Laser Power (kW)	< 6	< 4	< 40
Power Intensity (W/cm^2)	up to 10^6	up to 10^9	up to 10^8
Wavelength (nm)	$790 - 980$	1640	10600
Metal Absorption	$25 - 40\%$	$25 - 35\%$	$5 - 10\%$
Efficiency	$25 - 40\%$	$3 - 5\%$	$10 - 15\%$
Size of laser head (cm^3/W)	1	10	1000
Beam handling	Lens/Fiber	Fiber	Mirrors
Running Cost	Low	High	Middle
Investment cost (CAD/W)	$60 - 180$	$145 - 220$	$60 - 145$

Table 2.2: **Comparison of different type of lasers [Laserline GmbH].**

2.2.2   Diode Lasers: Characteristics and Industrial Applications

2.2.2.1   Characteristics of HPDL

The materials used for the manufacture of diode lasers are based on semiconductors of group III-IV compounds. Comparing HPDLs with other types of high power lasers available, it can be emphasized that HPDLs are different, from the point of view of its optical properties, including a wide spectrum band (2-20nm), large beam divergence, non-symmetrical beam distribution (2.5-6 times difference in beam

divergence in the two orthogonal axis) and astigmatism.

Unlike the other lasers listed in Table 2.2, for which the laser active medium generates a single high power beam, the HPDL system combines multiple beam clusters from small semiconductor diodes into a single bundled beam. Each of these multiple beams are collimated by cylindrical micro-lenses to obtain parallel light, the beam bundle is then double collimated, first by a cylindrical lens in order to parallelize the beam in both directions, and then by a spherical lens for final focusing of the spot (Figure 2.22). For this reason it could be assumed that there are no physical limitation for the future development of HPDLs regarding the maximum power, and that the multiple integration of diode stacks enables HPDLs to deliver beams with more time stable intensities than other high power lasers.
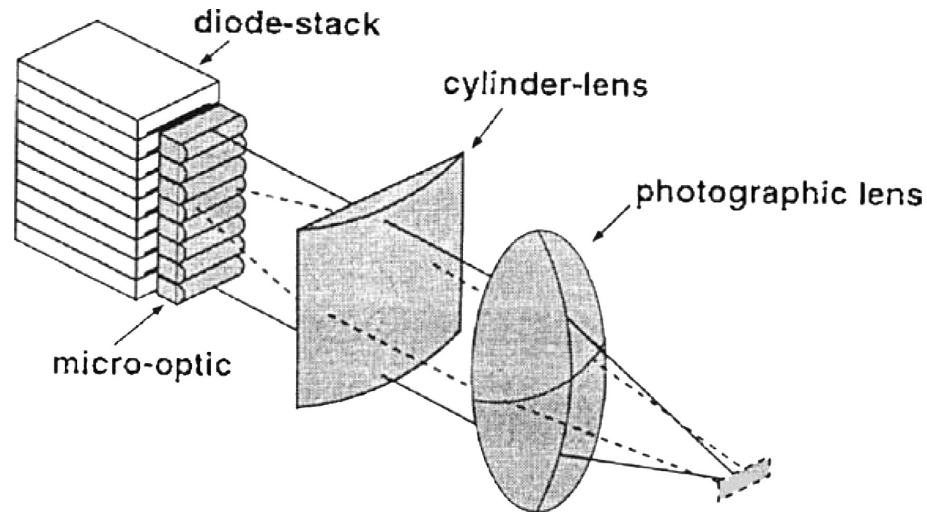
Figure 2.22: Visualisation of focusing of light from a diode laser stack [18].

The wavelengths of the diode lasers are in the IR spectrum range, and vary depending on semiconductor material, temperature of the stack and current drawn. Table 2.3 lists the wavelengths of a selected range of HPDLs according to reference [2].

In practice, HPDLs have broader wavelength bands than CO_2 and Nd:YAG

Materials	AlGaAs	InGaAs	AlGaInP
Wavelengths (nm)	720 - 880	940 - 990	630 - 690

Table 2.3: Wavelengths of selected range of diode laser materials [2].

lasers. Currently the maximum power of commercially available diode lasers is 5W to 6kW continuous wave, and 2.5kW if the beam is fibre-delivered. The lasers at or below 120W are air cooled while the ones above 120W are water cooled. At this time the only limitation imposed on the laser stack assembly is the compactness of the cooling system which is designed to ensure overall dimensions of the laser head. The typical electrical to optical conversion efficiency for HPDL is 20-30%, with a maximum of 50%, which is significantly higher than the values for CO_2 lasers (10-15%), or Nd-YAG (1-5%) [2].

Due to the non-circular cross-section of the active region and the construction of the diode laser head, the output radiation is differently divergent on the two orthogonal axes, leading to a beam asymmetry, which can be corrected with appropriate optics. This divergence also leads to difficulties in obtaining a precise focused spot, resulting in short working distance for diode lasers, and larger spot area leading to low power densities ($\approx 2.6 \times 10^5 \, \text{W/cm}^2$) [2]. Accordingly, most current applications of HPDLs in material processing are limited to surface treatments, conduction limited welding, soldering, scribing and marking (Figure 2.23).

Overall the main advantages of HPDLs in comparison to conventional lasers are:

- Compact size, which facilitates easy incorporation into machine tools;

- High efficiency, well above conventional lasers;

- Easy maintenance;
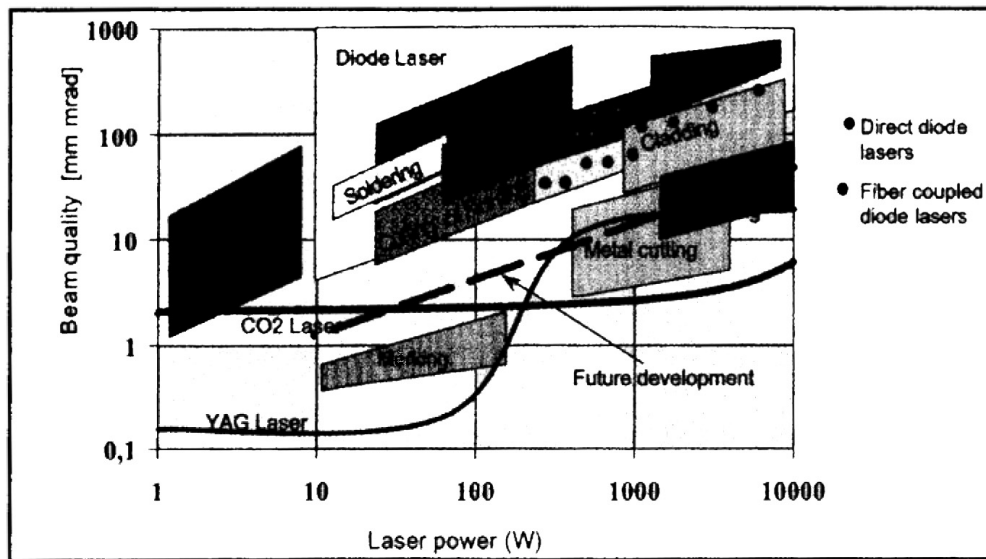
Figure 2.23: **Laser power, beam quality and typical application domains [Laser Line GmbH].**

- The possibility of beam guidance by optical fibers;

- Higher absorption on metallic surfaces (compared with CO_2 and Nd-YAG lasers)

2.2.2.2   Industrial Applications of HPDLs in Materials Processing

Typical industrial applications of HPDLs [38] include:

○ Esthetic welds in kitchen sink manufacturing, replacing TIG welding and allowing for a considerable reduction in afterwork.

○ Brazing of Zn-coated steel sheets (0.9mm) with CuSi hard solder using a 2.5kW laser, resulting in very smooth seams.

○ Hardening of car door torsion springs using a two laser head setup.

○ Cladding of stellite powder on a steel substrate using a laser with power density of $2 \times 10^4 \, \text{W/cm}^2$.

○ Soldering of small components sensible to mechanical contact or electrostatic discharges. HPDL provides a good accessibility in this case with no need of mechanical contact.

○ Polymer welding resulting in reliable joints.

Zaboklicki et al. [39] also reported hardening and welding by thermal conduction of metals using HPDLs:

○ Laser hardening of 42CrMo4 steel using a 650W continuous wave laser, with feed rates of 300-7000 mm/min.

○ Welding of X5CrNi18 9 steel using the same laser power as above, with feed rates in the range of 200 to 1800 mm/min. The study compared the welding of samples with no edge preparation and samples with ground edges, and achieves a complete penetration weld on a 1mm thick sheet metal at 450 mm/min. In all cases the quality of the welded track was better than that achieved by conventional methods.

Rudlaff and Haag [40] also reported on a transformation hardening of a steel component, and welding of stainless steel sheet of 0.8 mm thickness, using HPDL. A specific application of a pulsed diode laser described in this paper is the welding of very thin titanium foils (0.08 mm) with helium protective gas, with 55W laser power at a 1 m/min feed rate. The superior beam stability of the diode laser over other types of lasers permits a good control over process parameters and yields a clean weld. Other applications such as laser cutting of steel plates up to 10 mm thickness, or 6mm thickness stainless steel welding using HPDLs are mentioned in reference [41].

Although currently the use of HPDLs is limited by its low power density, progress is being made in developing more powerful diode lasers and new applica-

tions are arising, such as cutting and drilling. The suitability of fiber optic delivery systems in HPDLs systems also can increase the power density delivered to the work surface and the flexibility of positioning the laser spot. These characteristics give HPDLs an added advantage over other lasers for further development and industrial implementation that currently are dominated by CO_2 and YAG lasers. To the best of the author's knowledge the work presented in this thesis is a first attempt at investigating the application of diode lasers in assisting a cutting process.

2.3 AISI D2 Tool Steel

High carbon high chromium tool steels (Group D) were first commercially developed as a substitute for high-speed steel. However, they could not be used for this purpose because of their high brittleness. However, it was found later that the high wear resistance of this tool steel, due to extremely hard chromium carbide particles, combined with remarkable non-deforming post-quenching qualities make these steels useful in the manufacture of cold work dies and moulds.

2.3.1 Material Properties and Applications

AISI D2 is an air-quenching steel, alloyed with molybdenum and vanadium. It is characterized by high wear resistance, high compressive strength, good through-hardening and good resistance to softening due to tempering.

A typical chemical composition of D2 tool steel is given Table 2.4.

%C	%Si	%Mn	%Cr	%Mo	%V
1.55	0.3	0.4	11.8	0.8	0.8

Table 2.4: Chemical composition of AISI D2 cold work tool steel [3].

Physical properties of AISI D2 steel as a function of temperature is given in Table 2.5.

Physical Data (Hardened and tempered to 62 HRC)			
Temperature	20°C	200°C	400°C
Density kg/m^3	7700	7650	7600
Coef. of thermal expansion			
ˍ low temperature tempering (/°C from 20°C)	-	$12.3 \cdot 10^{-6}$	-
ˍ high temperature tempering (/°C from 20°C)	-	$11.2 \cdot 10^{-6}$	$12 \cdot 10^{-6}$
Thermal conductivity W/m°C	20.0	21.0	23.0
Modulus of elasticity GPa	210	200	180
Specific heat J/kg°C	460	-	-

Table 2.5: Physical properties of AISI D2 tool steel at room and elevated temperatures [3].

The recommended heat treatment industrial practice for D2 consists of [42]:

○ Hardening: preheat at 815°C and austenitize at $980 - 1025$°C, hold at temperature for 15 - 45 min. depending on part size, quench in air and cool as evenly as possible on all sides.

○ Tempering: at $205 - 540$°C, or double tempering, allowing tool to cool to room temperature after first temper.

○ Stabilizing (optional) - stress relieve tempering at $150 - 160$°C for a short period before refrigerating at -85°C.

The domain of application of AISI D2 generally refers to components that require high wear resistance combined with moderate toughness (shock-resistance). Typical applications include:

○ Cutting: tools for blanking, fine-blanking, punching, cropping, shearing, trimming, clipping, short cold shears, shredding knives, granulator knives, circular shears, wood milling cutters, reamers and broaches.

○ Forming: tools for bending, deep-drawing, rim-rolling, spinning and flow-forming, coining dies, cold extrusion dies, punches, tube and section forming rolls, plain rolls, dies for molding of ceramics, bricks, tiles, grinding wheels, and abrasive plastics, thread-rolling dies, and crushing hammers.

The steel is also used in the manufacture of precision tools such as gauges, measuring tools, guide rails, bushes, sleeves, knurling tools, sandblast nozzles.

The wear resistance of AISI D2 in its hardened state (58-62 HRC), is due to the M_7C_3 chromium carbides formed in the hardening process due to high percentage of chromium and carbon, bring this steel in the class of difficult to cut materials.

2.3.2 Hard Machining of AISI D2

Traditionally, D2, like other steels, is processed in the following succession of operations:

- Rough machining;

- Stress relieve (optional);

- Finish machining;

- Heat treatment (quenching and temper/double temper);

- Grinding to final size.

Grinding operations are time consuming and limited in the range of geometries that can be produced. Therefore improved technologies such as hard machining are emerging as a substitute for the final grinding operation. Due to wide area of application of D2 in the tool making industry, where complex workpiece geometry is required, AISI D2 tool steel is a very well justified candidate for hard machining.

Due to the relatively recent development of advanced cutting tool materials, such as cubic boron nitride (CBN), the interest in cutting hardened steel has increased substantially. Although the use of AISI D2 in the die and mould industry is widespread, the machinability of this material has not received sufficient attention. Research on hard machining and high speed machining of D2 reported in the literature is reviewed below.

Hodgson et al. [43] investigated machinability aspects when turning hardened (59-62 HRC) AISI M2, D2, and D6 tool steels, using CBN cutting tools at cutting speeds in the range of 80-120 m/min. Analyzing the difference in tool life values they assumed that the high hardness, similar for the three materials, was not the only factor that influences tool performance. Cutting tool edge preparations (sharp vs chamfered) were compared with regard to tool life and it was concluded that chamfering of the cutting edge of CBN tooling was detrimental for cutting tool performance.

Kishawy [44] studied the influence of cutting parameters on the cutting edge temperature during high speed hard turning of D2 using PCBN tooling employing a tool embedded thermocouple technique. Increasing cutting speed and feed rate proved to increase the cutting edge temperature from about 500°C at a cutting speed of 150 m/min to about 1000°C at a cutting speed of 500 m/min, while an increase in the cutting tool nose radius reduced the cutting edge temperature due to the increase of contact area between tool and workpiece which facilitates heat transfer. The effect of the rake angle was also studied in this research and a critical rake angle of $-20°$ was found for which the cutting edge temperature reaches a minimum.

Poulachon et al. [45, 19] studied the influence of work material microstructure on the wear behavior of PCBN tooling. Four different hardened steels, AISI D2 being one of them, were employed in this study. Tool wear rate was the maximum for D2 steel with the flank wear morphology comprising deep grooves (Figure 2.24 a).

They reported that the main factor responsible for the rapid tool wear was the high concentration of hard carbide particles in the steel microstructure (Figure 2.24 b).
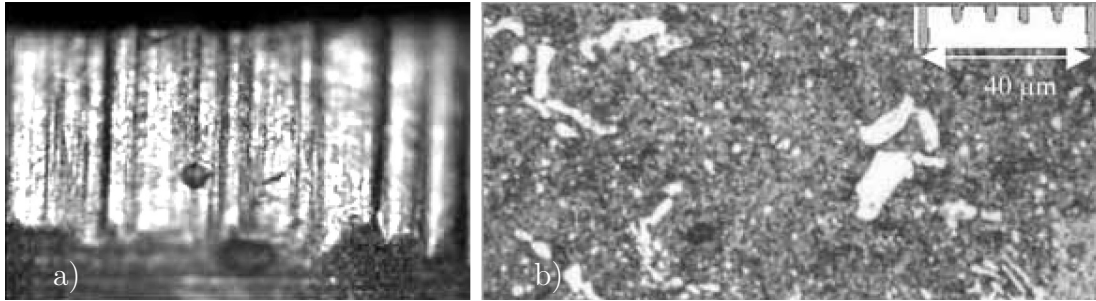
Figure 2.24: a) Flank wear in turning D2 steel, CBN tool, 180m/min cutting speed, 0.08mm/rev feed rate, b) Carbide particles in D2 microstructure [19].

Koshy et al. [46] reported a comparison between end milling of AISI H13 and D2 tool steels using carbide and PCBN tooling. Tool life values obtained from machining tests on D2 (58 HRC) were an order of magnitude lower than those with H13 material (52 HRC). Chipping, adhesion and attrition were identified as the mechanisms responsible for tool wear, and PCBN tools were observed to fail by catastrophic fracture.

El-Wardany et al [20, 47] studied the effects of cutting conditions on chip morphology and surface integrity during high speed turnning of AISI D2 using PCBN tools. They identified a critical pressure exerted in the direction of cutting speed of approximately 4000 MPa, only above which segmented chips form. Plastic deformation of carbide particles due to very high temperature generated during high speed machining, as well as a limitation to 10-15 μm thickness of the layer with deformed grains was observed (Figure 2.25).

Becze et al. [48] performed mechanical testing on fully hardened AISI D2 tool steel at strain rates comparable to that of machining processes ($5 \times 10^4 \text{s}^{-1}$) utilizing the Compressive Split Hopkinson Bar technique for various initial temperatures (296-873 K). Studying the microstructure of the sheared specimens they identified
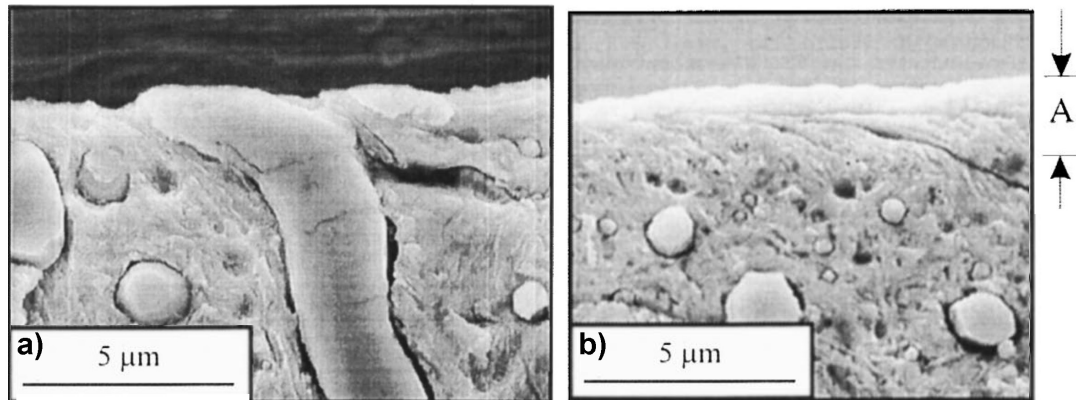
Figure 2.25:   a) Carbide particle deformation due to high temperature b) Deformed layer beneath machined surface for 350 m/min, 0.1 mm/rev and 0.2 mm d.o.c [20].

two different shear localization mechanisms. At temperatures below A3 ($< 720°$C), deformation shear bands (corresponding to segmented chip formation in cutting), was the dominant failure mode, whereas above A3 temperature, transformation shear bands (corresponding to continuous chip formation in cutting) were observed. This observation suggests that AISI D2 tool steel is a good candidate for LAM.

CHAPTER 3

Experimental Details

3.1 Laser Assisted Machining System

Machining tests were performed on a Nakamura Tome SC450 turning center (Figure 3.1) with a FANUC-21TB CNC controller, 30 kW spindle output, and a maximum spindle speed of 2500 rpm . The laser system consists of laser head, laser power supply, cooling system, and laser controller.

Figure 3.1: LAM system: Laser power supply and turning center

A schematic of the laser assisted machining system indicating the machine tool and various components of the laser equipment are shown in Figure 3.2. A data acquisition system was used for acquiring temperature and cutting force signals during

cutting tests.
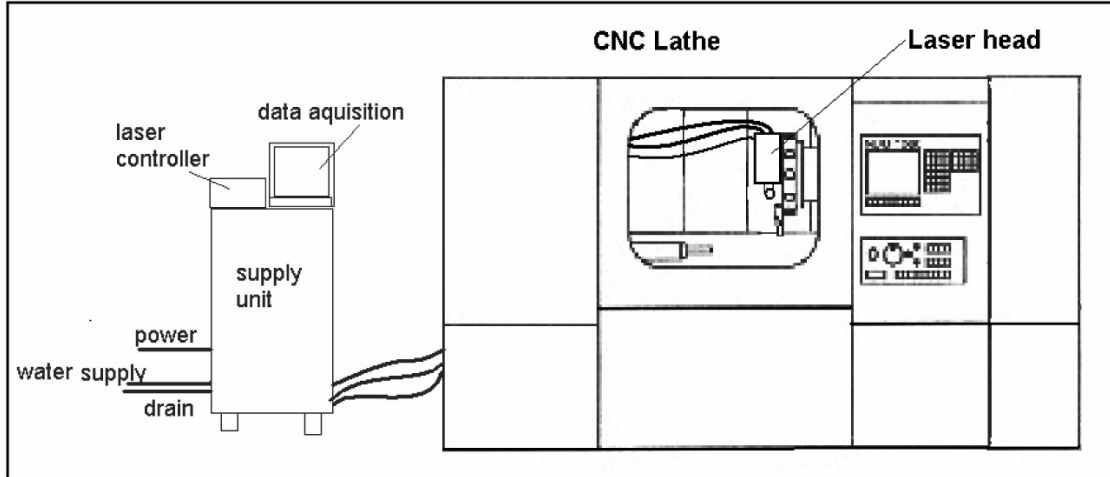
Figure 3.2: Laser integration into the CNC-lathe.

The laser employed in this work is a Laserline GmbH 2kW Diode Laser LDL80-2000 the technical specifications of which are listed in Figure 3.3.

Laser technical specifications	
Maximum Laser Power	2000 W
Spot size	4 mm x 0.9 mm
Wavelength	808 nm - 940 nm
Beam focusing distance	85 mm - 90 mm
Divergence angle	20 degree
Laser head dimensions	410 x 150 x 130 mm

Figure 3.3: LDL 80-2000 diode laser head.

For laser integration, several modifications and adaptations were made to ensure safe operation of the machine tool:

- The sliding door of lathe is equipped with an interlock which automatically shuts the laser down in case of accidental opening of the door.

- The process observation window of the machine tool is covered with a laser

absorbent glass with an optical density of 6.5, in order to stop any direct or reflected laser beam;

- The chip conveyor is disabled during laser operation;

- Cooling water supply/return hoses and power/electical control line are brought into the machine tool through three dark colored plastic elbows to avoid any diffusion of reflected beam;

- An air blower tube using compressed air at a pressure of 2 bar is used during laser operation to protect the laser optics from any debris or fumes resulting laser heating or the cutting process.

- The laser head was mounted on the machine tool turret using a holding and positioning fixture, designed to allow high flexibility and stiffness in positioning the laser spot in relation to the workpiece surface.

- Although manufacturer's specifications of the laser classify it as a Class 4 laser, the safety audit performed on the laser assisted machining system by Photonics Research of Ontario in compliance with American National Standard for Safe Use of Lasers ANSI Z136.1 (2000) establishes it is a Class 1 laser, due to the laser being enclosed within the machine tool system.

3.2   Fixture for Laser Head and Thermometer

In order to rigidly hold the laser head inside the machine tool and to precisely position the laser spot on the workpiece surface, the fixture illustrated in Figure 3.4 was designed and built.

The fixture has six degrees of freedom and provides translation and rotation about the X,Y,Z axes. This allows precise positioning of the laser spot with respect
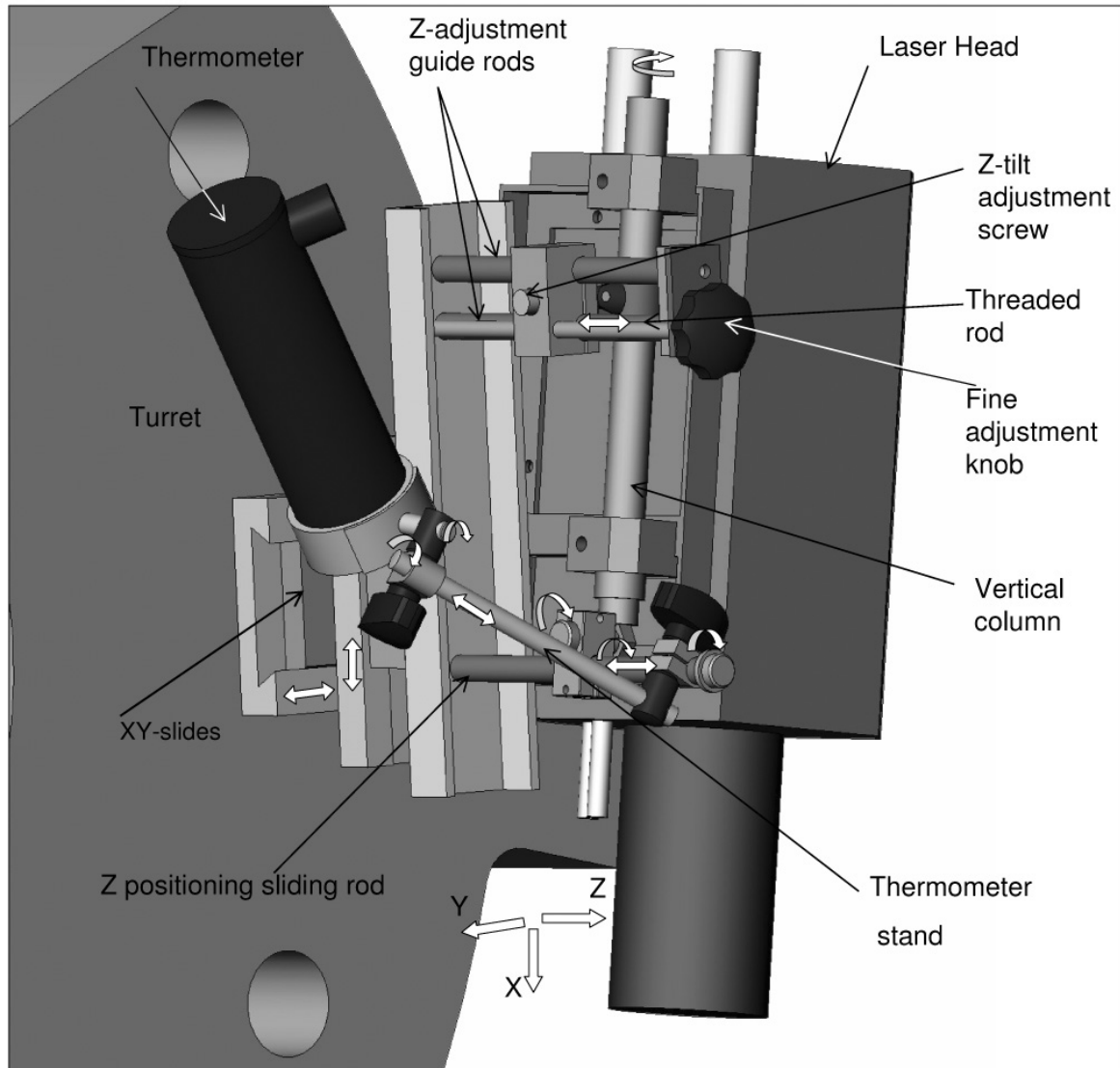
Figure 3.4: Laser head and thermometer positioning fixture

to the workpiece, and facilitates easy focussing of the laser spot independent of the position of the cutting tool. The thermometer was held in an articulating stand (Figure 3.4) which allows for a very flexible and precise positioning of the thermometer sighting direction.

The laser spot was positioned in relation to the workpiece with the laser in the pilot mode (4 mW at 800 nm wavelength) using an infrared visualization card,

while the thermometer direction was set using the built-in laser pointer. Once the position/orientation of the laser head and the location of the thermometer are set, the fixture provides means for rigidly locking the system in place.

3.3   Temperature Measurement Sample and Equipment

In order to calibrate and validate the model used for numerical temperature predictions, described later in Chapter 4, the temperature during laser heating was measured on the work material free surface and at a depth of 1mm, at a fixed location on the specimen, with the laser traversing past. To simulate a flat work surface and linear traverse of the laser spot on the surface, the setup shown in Figure 3.5 was used.
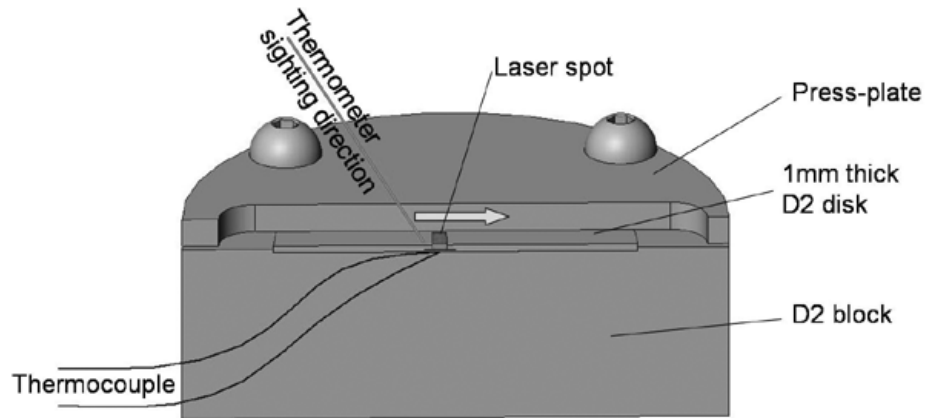
Figure 3.5: Sectional view of temperature measurement setup.

The D2 steel block was meant to simulate the volume of the workpiece. The thermocouple was cemented between the D2 steel block and the 1mm thick D2 disk. The press-plate holds the disk and the thermocouple in place and prevents any deformation of the disk that might occur during the heating process. The slot machined in the press-plate permits the translation of the laser beam across the measurement spot.

The temperature calibration experiments were performed on the laser assisted

machining system described above. During temperature measurement tests, the spindle was kept locked from rotating. The temperature measurement sample was accommodated in a specially designed vise held in the machine chuck. The linear travel of the laser beam across the sample surface was realized with the feed motion of the lathe turret along the Z axis.

The temperature on the free surface of the sample was measured using an infrared thermometer, Raytek MA2SC (Figure 3.6). For temperature calibration experiments the thermometer was held stationary by attaching it to the machine tool base in order to measure the evolution of temperature on a particular spot on the sample free surface, exactly above the position of the thermocouple (refer to Figure 3.5). Temperature data was acquired on a PC using the Marathon Graphic Setup and Display software at a sampling interval of 20 ms.

MA2SC Thermometer Specifications	
Temperature Range	$300° - 1400°C$
Nominal Spectral Response	$1\mu m/1.6\mu m$
Accuracy	$\pm(0.30\%\mathrm{T_{meas}} + 1°C)$
Repeatability	$\pm(0.10\%\mathrm{T_{meas}} + 1°C)$
Temperature Resolution	$1°C$
Response Time	1ms or 10ms
Emissivity Adjustment	0.10 to 1.0 in 0.01 increments
Focus Distance	300 to 500 mm
Spot Size at Min Focus Dist	1.0 mm dia.

Figure 3.6: Raytek MA2SC infrared thermometer [www.rayteknorthamerica.com].

The temperature at 1mm depth was measured using a type CO2-K thermocouple, mounted in between the 1mm thick disk and the D2 block. Its specifications are given in Figure 3.7. Temperature data was acquired on a PC using National Instruments data acquisition system (SCC-TC02) and Labview Software, with a sampling rate of 10 ms.

CO2-K Thermocouple Specifications	
Thermocouple Type	K CHROMEL-ALUMEL
Length	150mm
Maximum Temperature	540°C
Response Time	2 to 5 ms

Figure 3.7: Specifications of Omega CO2-K thermocouple [www.omega.com].

3.4 Cutting Tools

In this work, the efficacy of using a diode laser for LAM was studied in both grooving and longitudinal turning operations. The cutting tools employed in these cutting tests were:

- Sandvik parting blade using a TiN coated Sandvik GC1015 (K15) flat face carbide insert with a 0° rake angle and 7° relief angle, for grooving operations (Figure 3.8), and
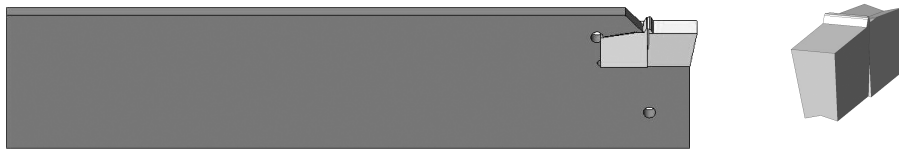
Figure 3.8: Cut-off blade and insert used in the grooving experiment.

- Kennametal CSSNR-164 tool holder with -5° rake angle and 45° side cutting edge angle, using a TiAlN coated Sandvik H13A (K15) flat face carbide insert with a 0° rake angle and 11° relief angle for longitudinal turning operations (Figure 3.9).
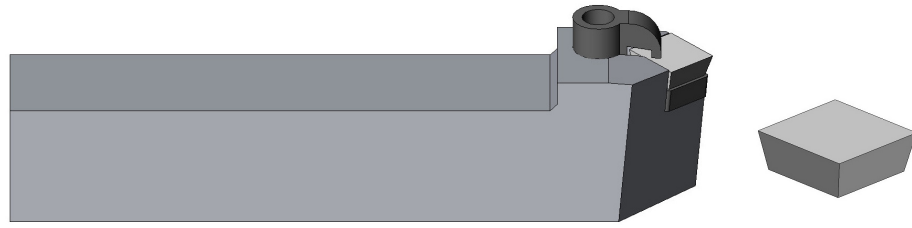
Figure 3.9: Tool holder and insert used for longitudinal turning.

3.5   Workpiece and Workpiece Fixturing

Preliminary LAM grooving tests performed on bar workpiece pointed to the fact that the thermal history of the workpiece could influence the material subsurface. To minimize this effect, and to ensure through hardening of the workpiece, experiments were conducted on a disk shaped workpiece of diameter 100 mm. The thickness of the disk was 3.5 mm (Figure 3.10 a) which is less than the width of the grooving insert (4 mm). The same setup was used for also longitudinal turning experiments, with the length cut per pass corresponding to the width of the disk. The workpiece was assembled on a mandrel, held between the machine chuck and the tail stock. The washer nut system at the end of the mandrel allowed for rapid workpiece removal for cooling inbetween successive cuts to prevent tempering of the workmaterial (Figure 3.10 b). Radial run-out on the workpiece measured during cutting tests was less than 0.01mm.

3.6   Cutting Configurations

Cutting tests were performed in two basic configurations:

- ***Grooving / Part-Off***. Cutting configuration and parameters can be seen in Figure 3.11. This setup represents a simplified version of a more general groov-ing configuration (see Figure 4.10). Due to the cutting edge being perpendicular
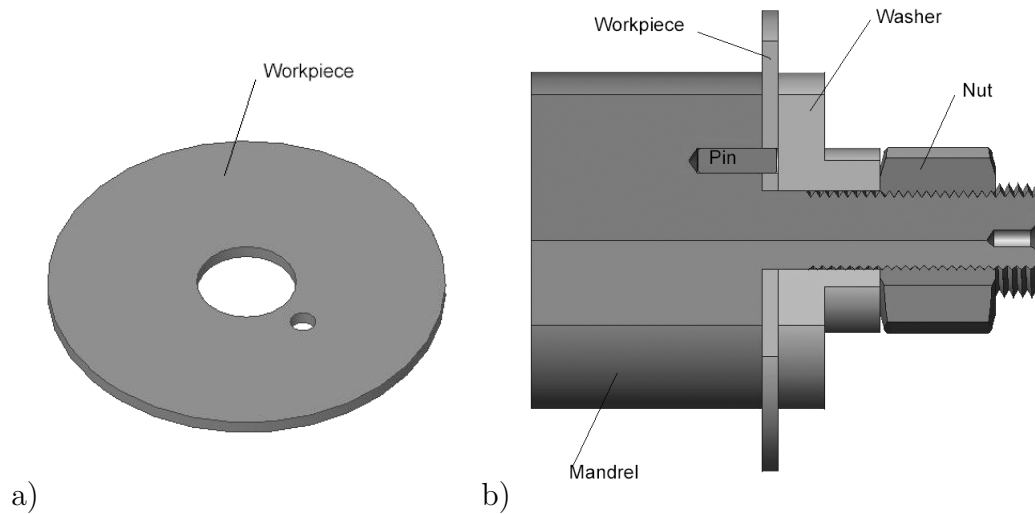
Figure 3.10: a) Disk shaped workpiece b) workpiece mandrel assembly.

to the cutting velocity and width of the tool being greater than the workpiece thickness, there is no force in the axial direction and the configuration refers to orthogonal cutting.
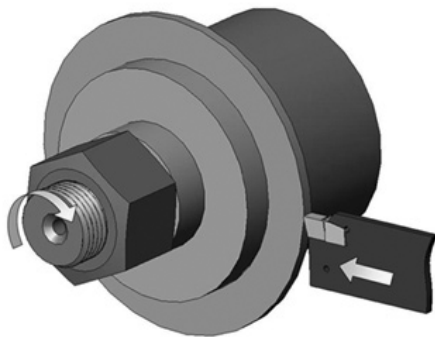
Laser power	0 & 2000 W
Cutting speed	20 and 30 m/min
Feed rate	0.05 mm/rev
Cut width	3.5 mm
Spot orientation	longitudinal axis (slow axis) parallel to workpiece axis

Figure 3.11: Grooving / part-off configuration and parameters employed.

- **_Longitudinal Turning_** For this turning operation, the length cut for each pass is limited to 3.5mm, which facilitates a better control over the amount of heat induced into the workpiece during LAM. In order to avoid workpiece subsurface overheating the workpiece was removed for cooling after each pass.

Laser power	0 & 2000 W
Cutting speed	100 m/min
Feed rate	0.05 mm/rev
Depth of cut	0.2 mm
Length cut/pass	3.5 mm
Spot orientation	longitudinal axis (slow axis) parallel & perpendicular to feed direction
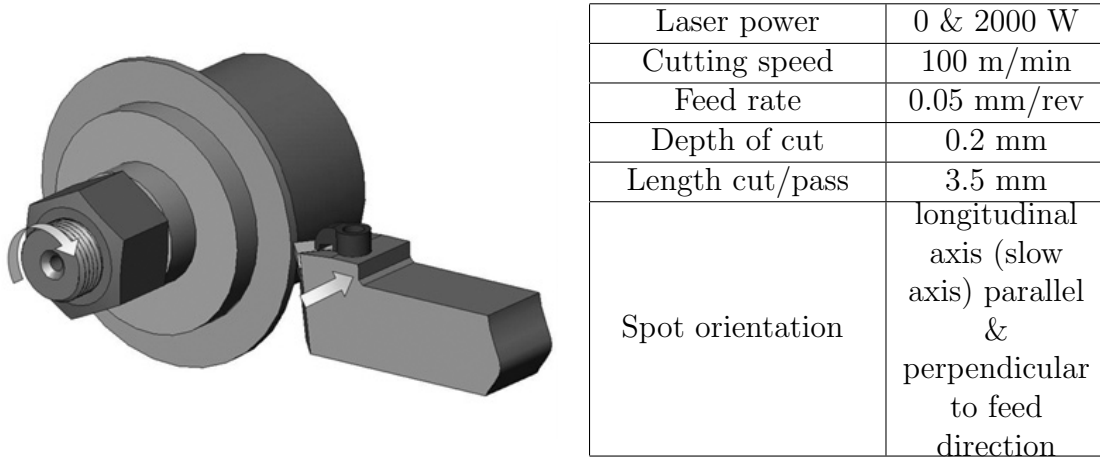
Figure 3.12: Longitudinal turning configuration and cutting parameters.

Cutting parameters and geometry are given in Figure 3.12.

3.7   Experimental Setup

Figure 3.13 illustrates the cutting test set-up, which shows the laser head held in the fixture attached to the turret, and the dynamometer with a tool mounted. The mandrel on which the workpiece is mounted is held between the lathe chuck and the tailstock. The figure also shows the air blower that was specially designed to protect the laser optics against fumes and particles that could result from laser heating. All the parts and equipment as shown in Figure 3.13 refer to longitudinal turning operation. The inclination of the laser head with respect to the turret face was realized to prevent back reflection of the beam into the laser head.

Although the laser head holding and positioning fixture allows positioning of the laser spot in the immediate vicinity of the cutting zone some limitations for decreasing the laser-tool lead distance were identified during the initial setup and cutting trials:

• Chip flow interfering with the laser beam resulting unwanted beam reflection;

• Beam reflections from the workpiece onto the tool that can lead to tool damage;
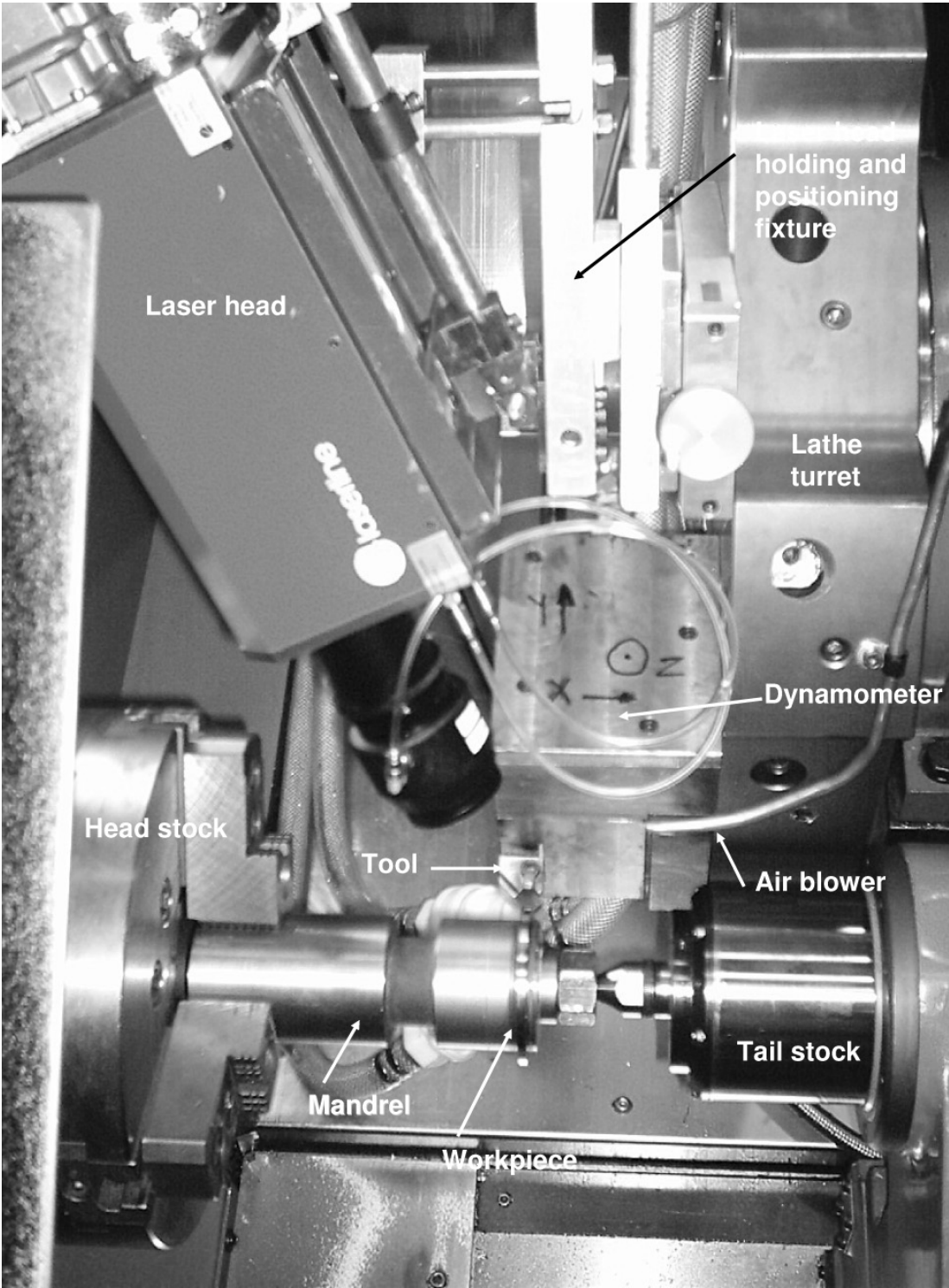
Figure 3.13: Experimental setup.

- Physical interference between laser head optics and the dynamometer body.

Considering the above the laser spot tool lead distance was set at 25 mm for a workpiece of 100 mm diameter.

3.8　Experimental Procedure and Limitations

Preliminary conventional cutting trials, details of which are discussed later, were performed at various cutting speeds for both grooving an longitudinal turning configurations, to determine the mechanical limitations of the chosen tooling. Based on these trials, grooving experiments were conducted at a cutting speed of 20 and 30 m/min for grooving, and longitudinal turning esperiments refer to a cutting speed of 100m/min.

The temperature predictions indicated that a laser power of 2000 W was required for effective softening of the work material. Therefore all experiments that employed laser assist were conducted using this power level and the influence of laser power on process performance was not studied.

Dynamometer dimensions combined with the small focal distance of the laser head (90mm) limited the minimum laser spot-cutting tool lead distance to be 25mm for a 100mm diameter workpiece.

Cutting forces, surface temperature, and tool wear were monitored during cutting tests for the two configurations described above, with and without laser assist, for comparison and quantification of the effect of laser in terms of improving the cutting process.

Flank wear was monitored using a tool-makers microscope. A maximum flank wear land of 300 μm was adopted as the tool failure criteria. Cutting forces and surface temperature were measured, recorded and analyzed.

Chips were collected from all cutting tests, mounted in an epoxy base, polished, etched with Nital 2% solution, analyzed under microscope, and photographed. The workpiece was sectioned and parts containing the generated surface were also embedded in resin, polished, etched, analyzed under a microscope, photographed. The micro-hardness measurements were performed on the workpiece subsurface using a LECO micro-hardness tester (model M-400-H2), with a load of 1kg.

CHAPTER 4

Experimental Results and Discussion

The material presented in this chapter consists of:

- Analytical modelling and numerical computations carried out to predict temperatures in the workpiece due to laser heating, with a view to enabling selection of appropriate cutting parameters for successful implementation of the process. Experimental temperature measurements are also presented for model validation.

- Results of cutting tests that were conducted to characterize the performance of high power diode laser in assisting hard turning of AISI D2 tool steel in grooving and longitudinal turning configurations. Cutting forces, temperature, tool life, chip formation mechanisms, subsurface hardness and surface roughness are studied and discussed.

4.1 Analytic Modelling and Experimental Calibration

LAM is a hybrid process, combining a cutting process with laser heating. The approach used in this work to predict the workpiece temperature is described below.

4.1.1 Laser Heating of Solids

In addition to the parameters specific to any machining operation (process kinematics, cutting parameters, tool geometry and workpiece material characteristics), in a LAM process the laser-material interaction introduces more variables. These can

be divided into laser parameters that are independent and dependent on cutting parameters.

- LAM parameters independent of conventional machining:

  ○ Laser power;

  ○ Laser spot size that determines the power density and area of the workpiece that is heated;

  ○ Laser wavelength that determines the amount of energy absorbed into work material during irradiation.

- LAM parameters dependent on cutting parameters and kinematics:

  ○ Scanning speed is the relative motion between the laser spot and the workpiece material which influences the amount of heat absorbed into the workpiece material and therefore controls the temperature gradient. This relative motion is dependent upon the cutting process, for instance, in case of turning and milling operations, the scanning velocity relates to the cutting speed and feed rate respectively. This parameter determines the depth of heat penetration, a parameter that is critical in LAM since ideally the uncut chip thickness should relate to the depth to which material softening has occurred;

  ○ Laser-tool lead distance, (see Figure 4.1), determines the temperature reached in the superficial layer of the workpiece at the moment immediately preceding the cutting process, and the amount of heat absorbed into the body of the workpiece. Since heating is due to conduction, the rise in temperature at a particular depth is not instantaneous. Under ideal

conditions, the laser-tool lead distance should be such that the work material domain that corresponds to the uncut chip thickness is softened by the time the material reaches the shear plane.
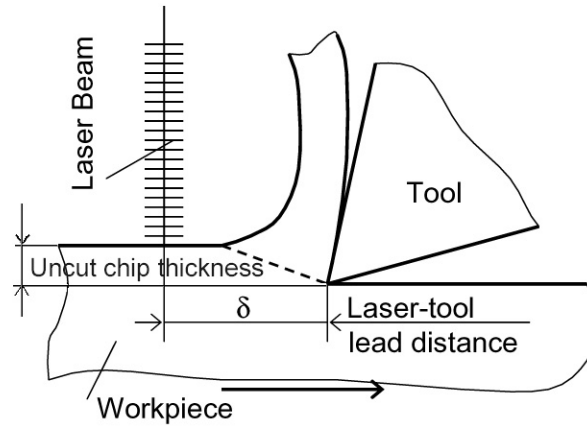
Figure 4.1: **Laser-Tool Lead Distance.**

In respect of laser heating, LAM shows several similarities with another laser assisted process: case hardening of steels. Temperatures achieved in laser case hardening of steels are $700 - 800$°C, the range in which the austenitic transformation takes place. The case depth has been found to be ([16], [49], [21]) highly dependent not only on the laser power and laser power density (derived from the size and shape of the laser spot), but also on the scanning speed (velocity of the beam travelling along the work surface). In light of the similarities between LAM and laser case hardening with regard to temperature distribution in the work material due to laser heating, research already done in the laser case hardening of steels is taken into consideration in the present work.

4.1.2   Case Hardening Temperature Field & Penetration Depth

Ashby and Easterling [16] derived an equation by combining the approximate solutions to the equation of heat flow with a kinetic model to predict the near surface

temperature field. The temperature $T(z,t)$ in a particular point along the beam track, at a depth z beneath the free surface and at a particular moment in time t is given by equation 4.1. The parameters involved as well as the methodology used are briefly described below:

For a laser beam of power q and spot size of radius r_B that is displaced along a flat surface at a constant scanning speed v (Figure 4.2), the temperature field is given by equation 4.1:
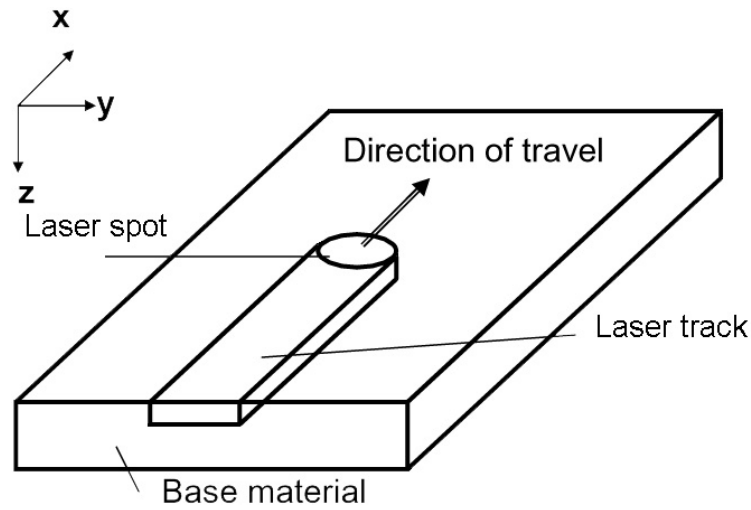
Figure 4.2: Linear heating [21].

$$T = T_0 + \frac{Aq/v}{2\pi\lambda[t(t+t_0)]^{1/2}} \exp[-\frac{(z+z_0)^2}{4\alpha t}] \tag{4.1}$$

where

- α is the material thermal diffusivity, given by:

$$\alpha = \frac{\lambda}{c\rho} \tag{4.2}$$

where:

- c is the material specific heat capacity, $(Jkg^{-1}K^{-1})$

- λ is the material thermal conductivity, $(\mathrm{Js}^{-1}\mathrm{m}^{-1}\mathrm{K}^{-1})$

- ρ is the material density, (kgm^{-3})

  and:

- T_0 is material initial temperature (K);

- A is the material surface absorptivity (1-emissivity) (%);

- r_B is the beam radius for a circular spot shape Figure 4.3, at which the beam intensity decreases to $1/e$ times the maximum beam intensity.
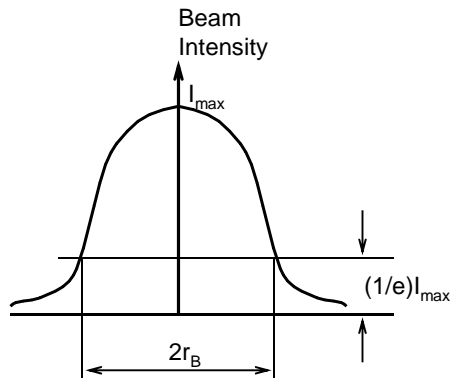
Figure 4.3: Definition of r_B for a beam with a gaussian energy distribution.

In the same equation 4.1:

- t_0, is the characteristic heat transfer time that refers to the heat diffusion time over a distance equal to the beam radius

$$t_0 = r_B^2/4\alpha$$

and:

- z_0 is the characteristic length that represents the distance over which the heat can diffuse during the beam interaction time, r_B/v being chosen in such a way that it gives the correct surface temperature for all q, v and r_B. z_0 has the function of limiting the surface temperature to a finite value due to the finite heat injection time.

z_0 is evaluated considering two limits, $t >> t_0$, and $t << t_0$.

For $t << t_0$:

$$z_{01}^2 = \frac{\pi}{2e} \frac{\alpha r_B}{v}$$ (4.3)

For $t >> t_0$:

$$z_{02}^2 = \frac{\pi^{1/2} r_B}{e} \left(\frac{\alpha r_B}{v}\right)^{1/2}$$ (4.4)

Using this approach and equations 4.1, 4.2, 4.3, 4.4, a Matlab code was used for numerical evaluation of the temperature field in the superficial layer beneath the free surface of the material, as well as the heating and cooling rates with the mention that the material physical properties were considered constant.

In order to accommodate the rectangular spot shape, which is characteristic of the diode laser beam, an equivalent radius r was derived using the spot area equivalence:

$$r = \sqrt{\frac{ab}{\pi}}$$ (4.5)

where a and b are the length and width of the diode laser spot. and

$$r_B = \kappa r$$ (4.6)

where the κ is the beam radius coefficient.

Although the diode laser considered for verification of the Ashby and Easterling

[16] model does not have a strict Gaussian power distribution on the long axis, the top hat distribution has been considered to have sufficient similarities to validate the model's applicability to the situation presented in this work.

The plots in Figure 4.4 generated in MatLAb for AISI D2 (physical properties listed in Table 2.5) give an indication of the maximum temperature reached at a particular depth z from the free surface, as well as the rates of heating and cooling for different values of absorptivity and beam radius.
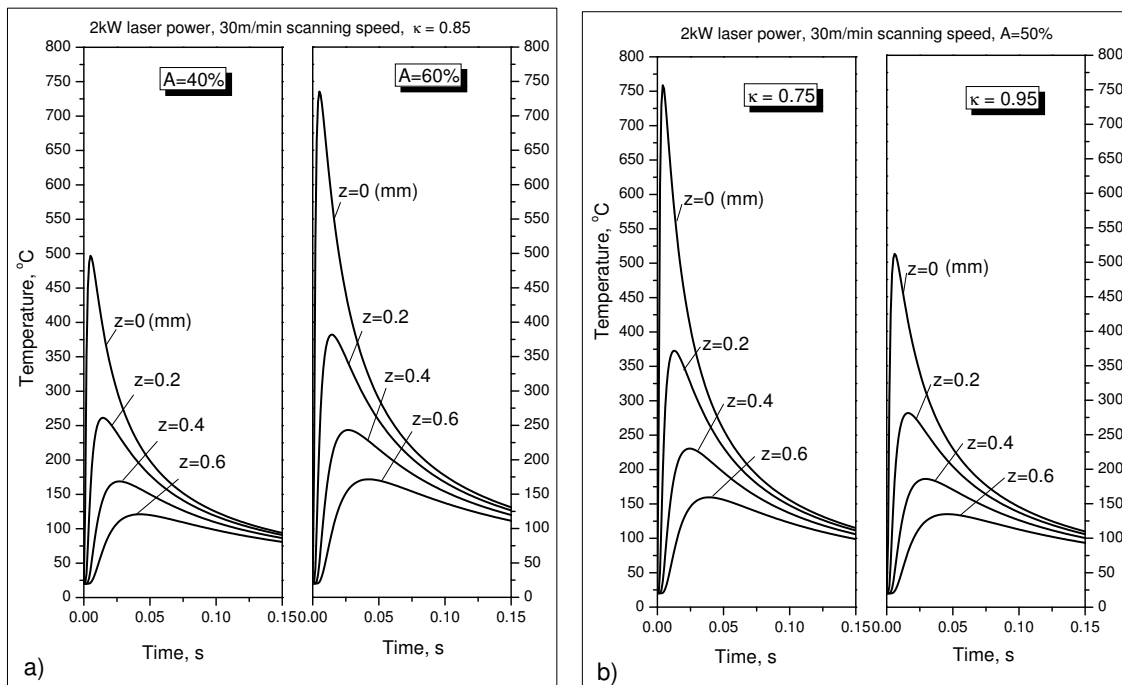
Figure 4.4: The effect of: (a) absorptivity, and (b) beam radius on the transient temperature distribution.

For this numerical approach, input data consist of physical properties of the workmaterial such as thermal conductivity λ, specific heat capacity c, and density ρ (parameters considered constant in this work with respect to temperature), the laser power q and the scanning speed v, and also the two parameters that have to be calibrated experimentally:

- A is the material surface absorptivity (emissivity, %), specific for each work material - laser type combination, and also influenced by the state of the work material surface (the level of oxidization, surface roughness, etc.);

- r_B, the beam radius, which for a gaussian distribution of the laser beam intensity (Figure 4.3) is the distance from the center of the beam to the position at which the intensity falls bellow $1/e$ from the peak value. This value is determined by the real laser beam distribution and can be measured experimentally.

These parameters have a high influence on the peak temperature, as can be seen in Figure 4.4. A set of experimental tests were designed and performed to calibrate the A and r_B parameters.

Information presented in Figure 4.4 can be used for predicting the temperature distribution in the workpiece during LAM, for machining methods where the laser spot has a linear trajectory on the workpiece surface, not for processes where the laser scanning occurs on a more complex path. However the model presents first approximations for laser power levels required for implementing LAM for a given set of process kinematic parameters.

4.1.3   Calibration - Results and Discussion

The data in Figure 4.5 (a) were generated with a MatLab code and represent the predictions for temperature on the work surface and at a depth of 1mm, for a laser power of 1000W and a scanning velocity of 3m/min. The data in Figure 4.5 (b) are the corresponding temperatures measured using the infrared thermometer and the thermocouple on the experimental setup described earlier (Figure 3.5).

The values for A (absorbtivity), and κ (beam radius percentage of 1/e beam maximum intensity) were set by comparing the measured temperature at the depth
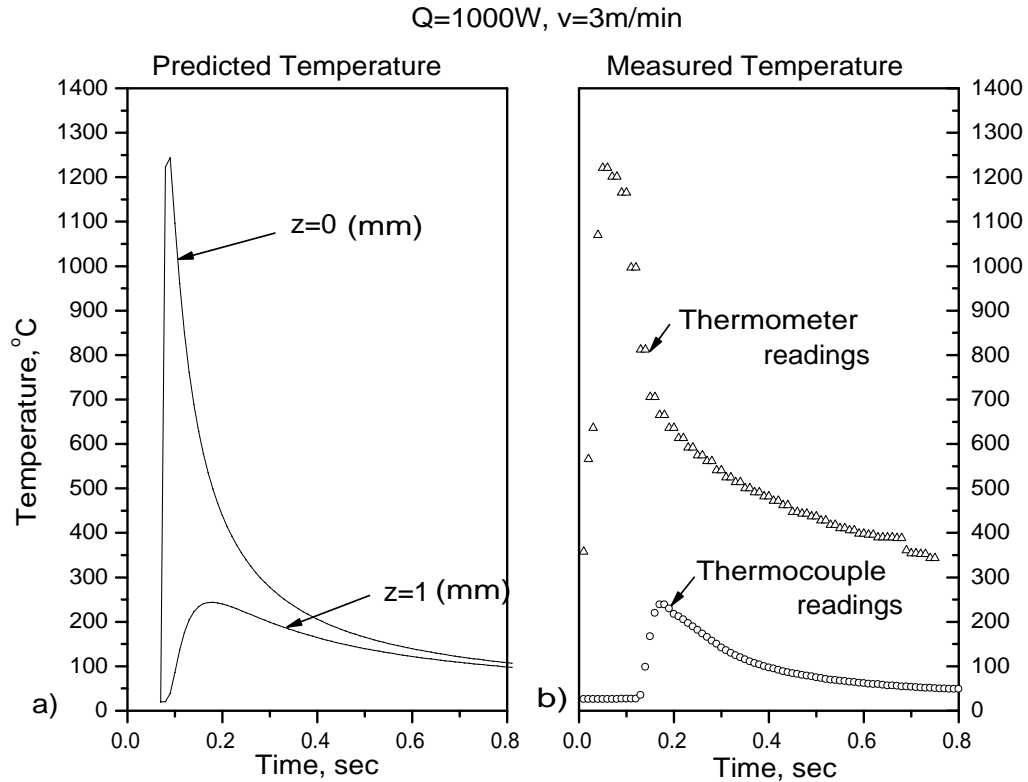
Figure 4.5: Transient temperature due to laser heating: a) predicted, b) measured

of 1 mm with model predictions for the same depth z=1 mm. The maximum temperature achieved matched for the values of $A = 45\%$, and $\kappa = 0.85$. Using this values, the surface temperature was predicted and the infrared thermometer emissivity was adjusted such that the measured temperature matched the predicted one. The value found for the thermometer emissivity was 0.75 which is in the range of 0.4-0.8 recommended by the thermometer user manual for steel as the workmaterial.

Multiple iterations performed revealed that the two factors with the higher influence on the work material temperature are laser power and laser scanning speed. The influence of laser power for various scanning speeds on the predicted surface

temperature of a D2 workpiece is shown in Figure 4.6.
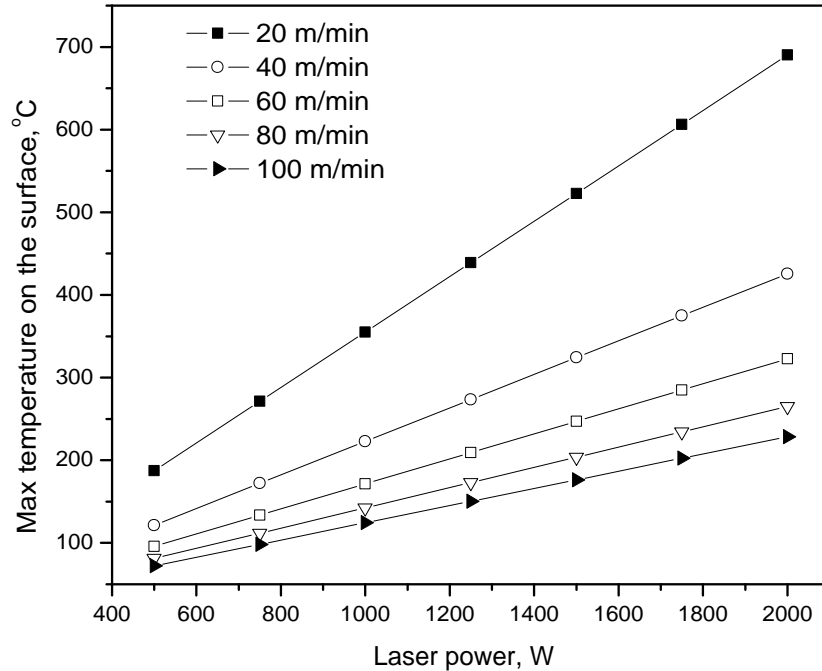
Figure 4.6: Influence of laser power for different scanning speeds on workpiece surface maximum temperature.

Hot hardness data for AISI D2 tool steel given in (Figure 4.7) reference [22] shows that at about $300 - 400°C$ the material hardness decreases from the initial 60HRC at room temperature to about 52-55HRC. It can be assumed that starting with this temperature in the uncut chip thickness, and with additional rise in temperature at the shear zone the D2 steel softens adequately for enabling the cutting process.

Using the analytical model for predicting the temperature in the uncut chip thickness as a function of cutting speed for a tool lead distance of 25 mm and the maximum laser power of 2 kW, the variation of temperature is shown in Figure 4.8 as a function of cutting speed. The shaded area indicated in Figure refers to the tem-
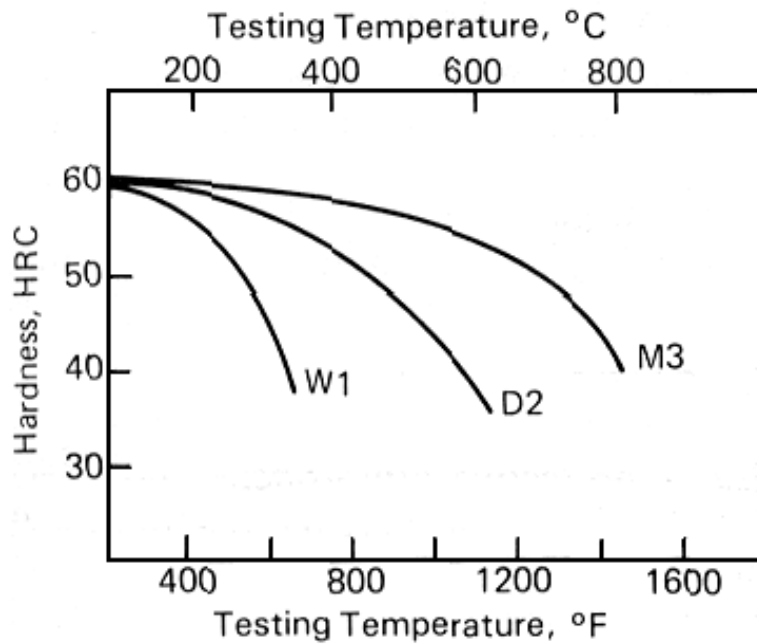
Figure 4.7: Tool steel hardness at elevated temperatures [22].

perature range of about $300 - 400°C$ mentioned previously as being the appropriate temperature in the uncut chip thickness for successful LAM. It can be seen that, for an uncut chip thickness of 0.05 mm, the cutting speed cannot exceed 25-30 m/min. This hypothesis suggests that for a successful LAM the cutting speed corresponding to the uncut chip thickness of 0.05 mm should be chosen at around 20-30 m/min value.

4.1.4 Cycling Heating in Laser Assisted Turning

In the case of longitudinal turning the laser does not follow a linear path on the work surface. Similar to the cutting tool tip, the trajectory of the laser spot is a helix with the diameter equal to the workpiece diameter and the pitch equal to the feed per revolution. If the laser spot dimension along the workpiece axis is larger than the feed per revolution only a fraction of the induced heat is removed by the chip and the
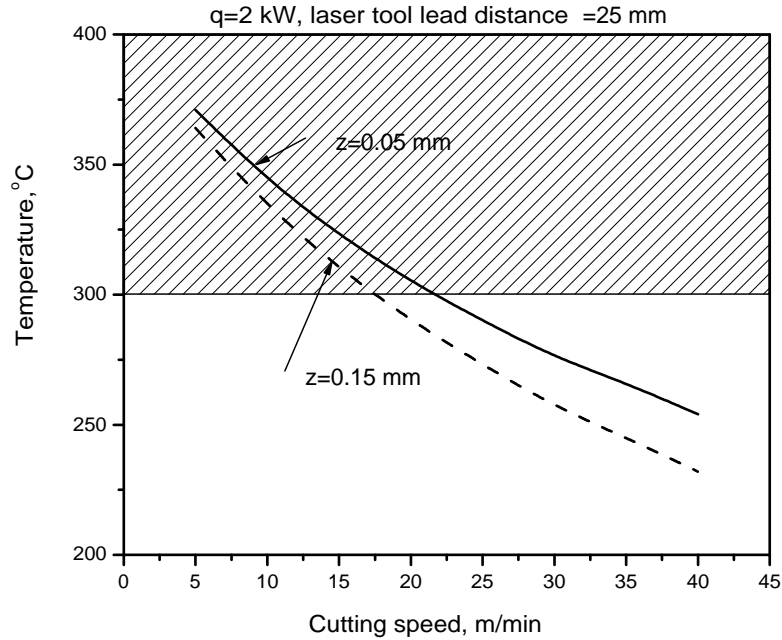
Figure 4.8: Temperature in the uncut chip thickness due to laser heating

rest is absorbed by the workmaterial. This implies that a location on the workpiece will be heated repeatedly before material removal takes place. For the setup shown in Figure 4.9, the number of cycles is given by $[n_c]$:

$n_c = a/f$

where f is the feed in mm/rev, and a is the width of the focused laser spot. Since the diode laser has a rectangular laser spot the width a can assume various values depending on the orientation of the laser about its own axis.

Therefore, the model previously described cannot be used for workpiece temperature predictions in this case. A new model, that will take into consideration the heating cycles and the accumulated heat into the workpiece with each revolution, will have to be developed, but this does not constitute the scope of the present work.

However, temperature predictions accomplished using the Ashby and Easterling
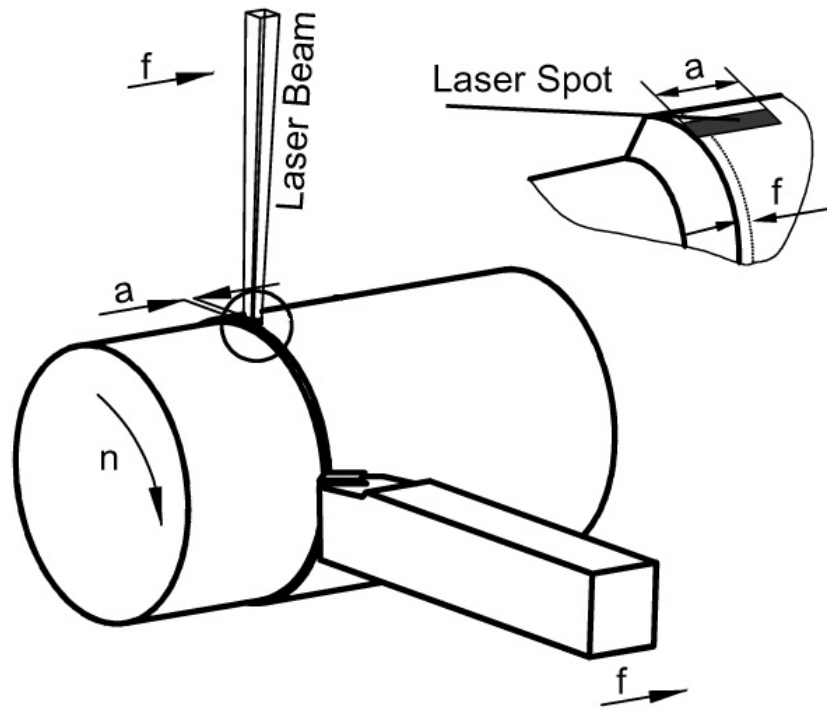
Figure 4.9: Longitudinal laser assisted turning

model is applicable to a grooving/parting off operation which is a particularly difficult operation to realize when conventionally machining hardened tool steels. This was realized by using a parting tool with a width w equal to the width of the spot a (see Figure 4.10). There will still be some residual heat transferred into the workpiece subsurface due to previous passes of the laser over the surface, but most of it can be assumed to be transported through the chip. In this configuration cyclic heating effects are minimal and hence the Ashby and Easterling model can be used for process design and for comprehending process performance.
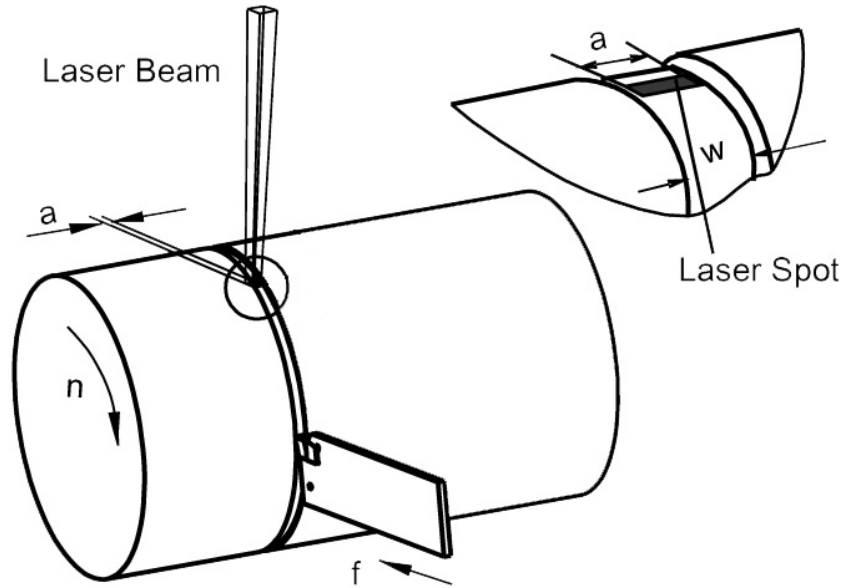
Figure 4.10: Laser assisted grooving/parting off

4.2 Grooving Tests

4.2.1 Tool Life and Tool Wear Mechanism

Conventional grooving experiments were performed at cutting speeds of 20, 30, 40 and 50 m/min in order to determine the capability of the coated carbide cutting tool when machining hardened D2 tool steel. The feed was kept constant at 0.05 mm/rev for all the experiments. At 20 m/min the tool performance was acceptable, while at 30 m/min and above, the tools failed catastrophically in the first pass. With the application of laser assist, for acceptable tool life the cutting speed could be increased roughly by a factor of 2 up to a speed of 40 m/min. Speeds higher than 50 m/min could not be implemented with respect to acceptable tool life even with laser assist on account of the limitations of maximum laser power of 2 kW.

During conventional machining at 20m/min the tool wear was progressive and uniform along the cutting edge. No chipping of the cutting edge was observed. The wear pattern on the flank face of the tool can be seen in Figure 4.11 (a). During
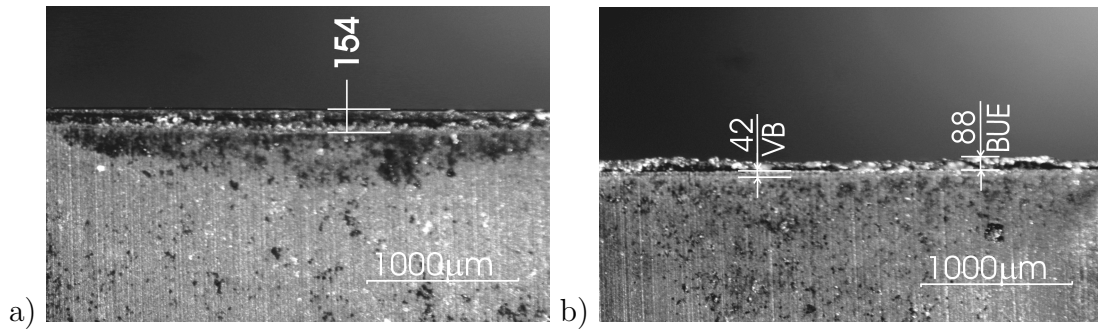
Figure 4.11: **Flank wear of the grooving tool at 20 m/min: a) Conventional cutting, b) Laser assisted (2 kW) cutting.**

LAM built-up edge formation on the cutting edge was noticed, Figure 4.11 (b). It appears that due to laser induced material softening prior to cutting and additional heat generation due to mechanical shearing, the temperature pertaining at the cutting edge was conducive to the formation of built-up edge (BUE). During the experiments, it was observed that the built-up edge formation was stable which tends to shield the cutting edge from wear.
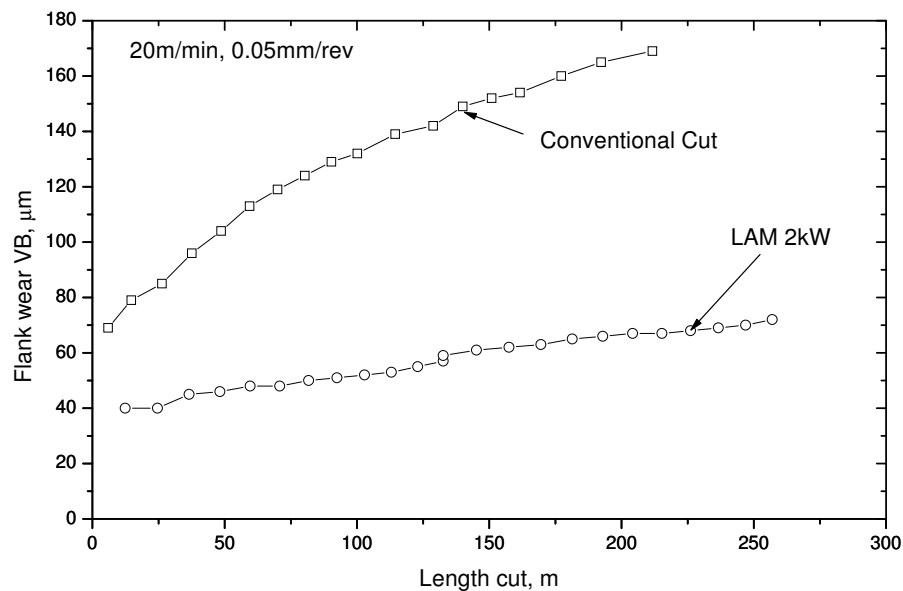
Figure 4.12: **Flank wear: conventional vs. laser assist cutting at 20m/min.**

The plots in Figure 4.12 show a substantial decrease in tool wear when machining is assisted by the laser. Experiments were halted at a maximum flank wear of about 160μm (as opposed to generally adopted tool wear criterion of 300μm) due to the slow progress of wear. Depending on the length cut, the flank wear associated with LAM is about 100-150 % lower in comparison with conventional cutting.

Conventional grooving experiments carried out at a cutting speed of 30 m/min resulted in tool failure in the very first pass (length cut $\approx$ 6 m). To ensure that this was not an isolated incident this cutting test was repeated several times and the results were observed to be consistent, indicating that a cutting speed of about 20 m/min represented the limit for this tool.

Observation of the flank wear morphology indicated that the tool failure was either due to severe abrasive wear (Figure 4.13 a) that could be attributed to the hard and abrasive chromium carbide particles in D2 tool steel, or large scale chipping of the cutting edge which leads to substantial friction between the tool flank and the workpiece that ultimately results in thermal damage of the cutting tool (Figure 4.13 (b).

a)   b)
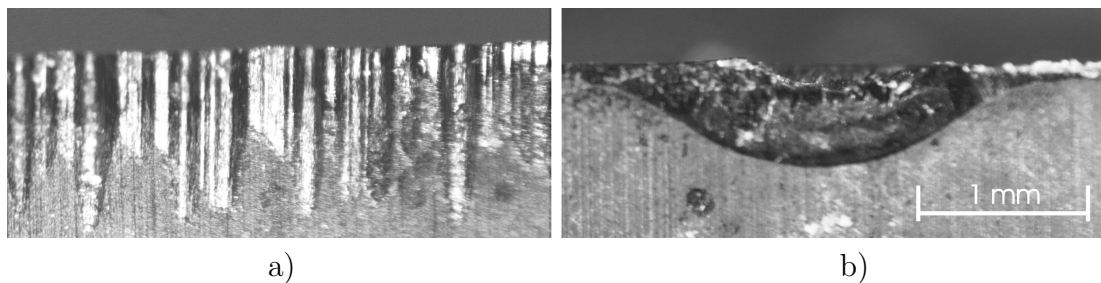
Figure 4.13: **Flank wear for conventional cutting after length cut of $\approx$ 6 m, for 30m/min: a) abrasive wear, b) thermal damage brought about by edge chipping.**

When machining with laser assist at a cutting speed of 30 m/min, BUE formation was observed on both the rake and flank faces (Figure 4.14 a) at the cutting edge

similar to that at a cutting speed of 20 m/min. However the scale of BUE formation at 30 m/min cutting speed was lower and the BUE was unstable. There were also indications of abrasive wear although it was very mild in comparison to conventional cutting, but less severe than at 20 m/min. The BUE was repeatedly removed during machining revealing flank wear. Traces of abrasive wear were also present, (see Figure 4.14 b). The flank wear after LAM was not distributed uniformly along the cutting edge. When cutting with laser assist it was observed that wear rate was observed to be constant up to a length 140 m (or a flank wear of about 160 μm), after which the flank wear was localized half way through the width of the cutting tool leading to rapid wear. This particular experiment was repeated three times and the evolution of flank wear was remarkably consistent (Figure 4.15). This indicates that at a cutting speed of 30 m/min laser assist brings about a manifold improvement in tool performance in comparison with conventional cutting. Furthermore laser assist also renders consistent tool performance.
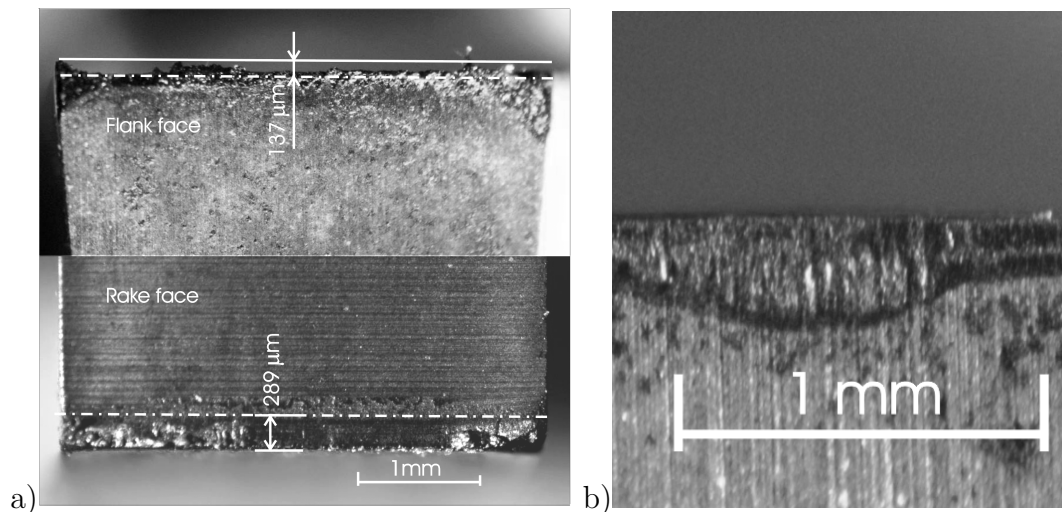
Figure 4.14:   a)Built-up edge when cutting with laser assist at 30m/min b) Traces of abrasive wear on the flank face of the tool for LAM at 30 m/min.

Comparing the results for 20 and 30 m/min it can be said that tool life decreases
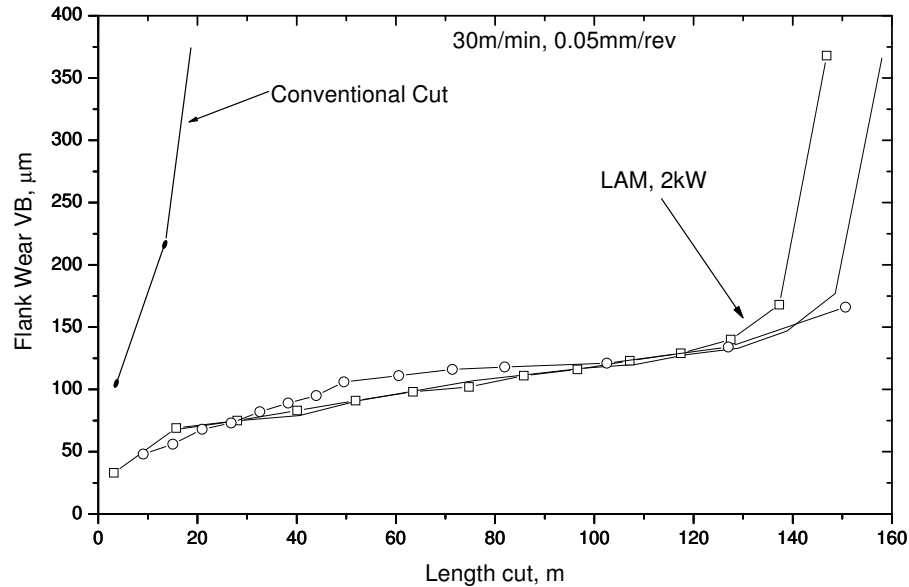
Figure 4.15: Flank wear - conventional vs. laser assist for 30m/min cutting speed

with an increase in cutting speed. It is not just the higher cutting speed that is responsible for this but also the lowered laser influence due to increased scanning velocity.

4.2.2 Cutting Forces vs. Temperature

Cutting forces and workpiece temperature were measured in order to compare conventional cutting with LAM and quantify the influence of laser heating on the cutting process.

Figure 4.16 provides a comparison between cutting forces in conventional and laser assisted grooving for a cutting speed of 20 m/min. The significant variation in all three components of the cutting forces recorded during conventional cutting (Figure 4.16 a) is an indication of the difficulty in machining hardened D2 steel. Although the machining configuration was two dimensional, it can be seen that there

were cutting forces in the axial direction presumably due lateral displacement of the tool owing to high thrust forces. The cutting process was also extremely loud. The advantages of using laser assist in this process in terms of the cutting force is very conspicuous (Figure 4.16 b) indicating a relatively smooth cutting operation. Overall it can be noted that laser heating had a higher influence on the thrust force than over cutting force. Thrust force was reduced by 50% on an average, while cutting force was reduced just by 20% in comparison with conventional cutting. A cutting force to the thrust force ratio F_c/F_p of about 1 was obtained in LAM as opposed to 0.7 in conventional cutting indicating the role of heating induced material softening in LAM.

The surface temperature measured using the infrared thermometer is also shown in Figure 4.16 b which indicates that LAM is characterized by repetitive heating due to grooving kinematics. Each workpiece revolution induces a new temperature gradient into workpiece and the workpiece experiences a continuous increase in temperature. Consequently the thrust force in laser assisted machining reduced from $\approx$ 750 N to $\approx$ 600 N and the cutting force from 600 N to 500 N. Such accumulation of heat into the workpiece would be detrimental in terms of subsurface material softening, however this phenomenon might not be of concern in certain applications like parting off.

Forces measured at a cutting speed of 30 m/min Figure 4.17 a indicate reduced chatter in comparison to cutting at 20 m/min. However the three fold increase in the thrust force during the duration of the cut implies rapid wearing of the tool which is in concurrence with tool wear data shown in Figure 4.14. Furthermore the sudden fluctuation observed in thrust and cutting force data relate to chipping of the cutting edge that probably led to suggest chipping of the cutting edge see Figure 4.13.

Application of laser heating can be seen to not only substantially reduce the cutting and thrust forces but also eliminate chatter and render the forces stationary
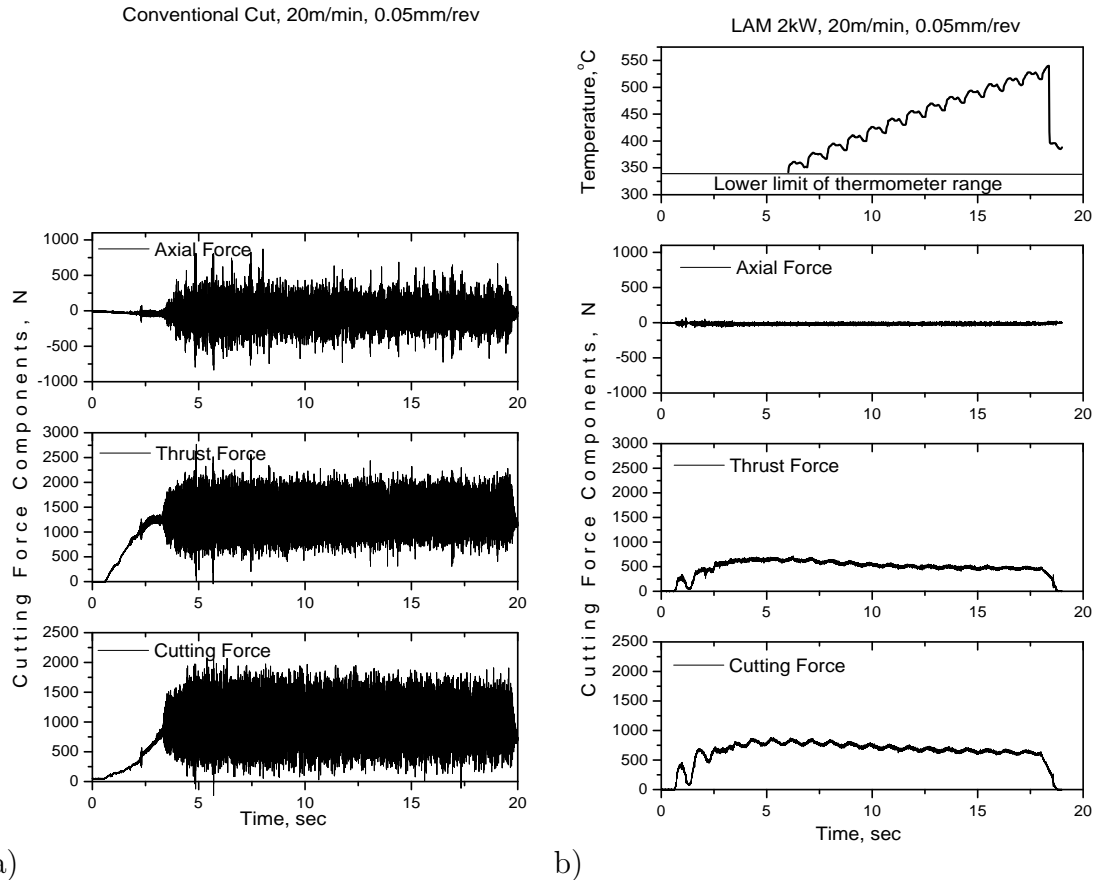
Figure 4.16:   a) Cutting forces in conventional cutting at 20 m/min cutting speed: b) Cutting forces in LAM and associated temperatures.

due to reduction in tool wear (see Figure 4.15). The correlation of the force data with the temperature data (Figure 4.17 b) seems to indicate the process becomes stable when the surface temperature reaches values higher than about 300° C. The fact that the cutting force ratio F_c/F_p is ≈ 1 in LAM is indicative of thermal softening of the workmaterial.

4.2.3   Mechanism of Chip Formation

Figure 4.18 presents typical chips obtained during conventional grooving/cut-off tests at a cutting speed of 20 m/min, and during LAM at 20 and 30 m/min. As
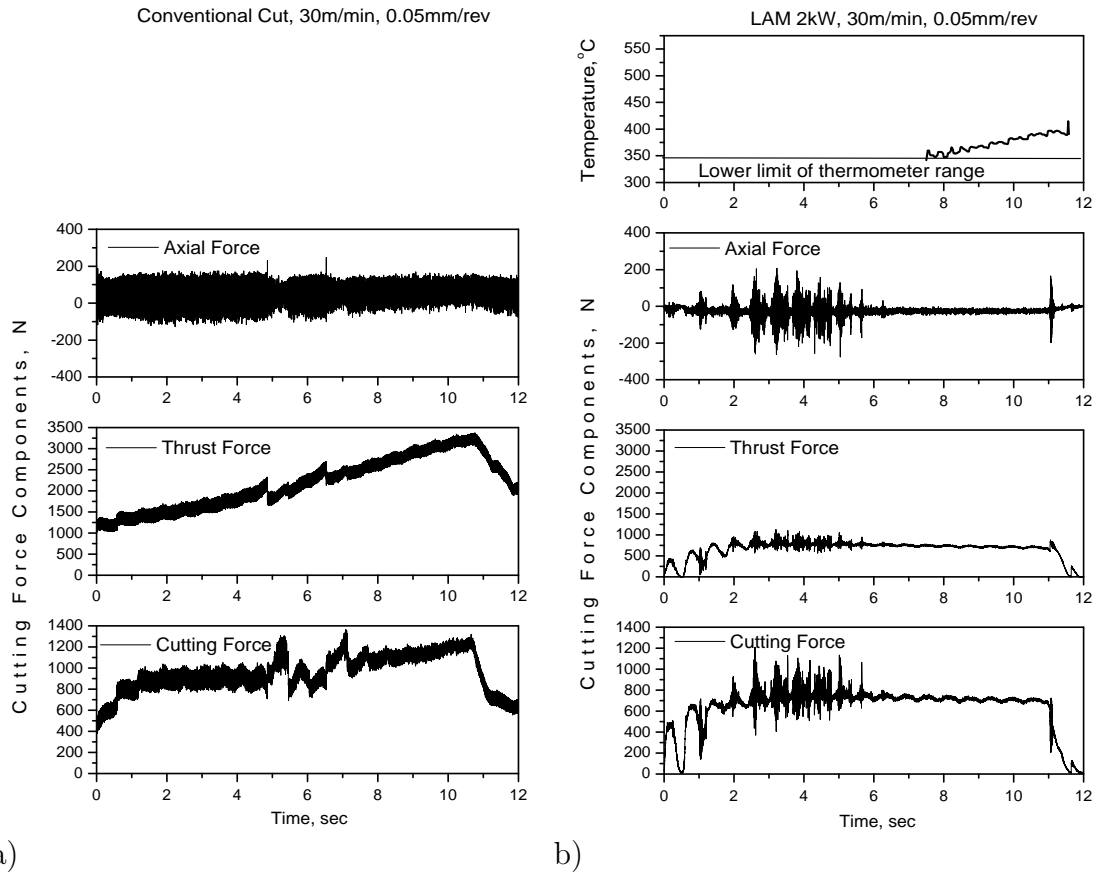
Figure 4.17: **a) Cutting forces in conventional cutting at 30 m/min cutting speed: b) Cutting forces in LAM and associated temperatures.**

expected, during conventional machining at 20m/min, the chips formed were segmental, referred to in the literature as saw-tooth chips. The mechanism of saw-tooth chip formation has been analyzed in detail by Vyas and Shaw [50] who identified two types of cracks:

○ gross cracks, which extend across the chip width, and

○ microcracks, which are discontinuous and distributed across the chip.

Vyas and Shaw proposed that the material in the bands between the gross cracks undergoes adiabatic shear, sliding over the surface formed by the next crack.

Although a relatively steady cycle of shear band formation for which the frequency can be calculated has been reported in [45, 50, 51], Davis et al. [52] have observed the phenomenon of uneven segment spacing at low cutting speeds. They also report that on increasing the cutting speed, the shear band pitch becomes more stable but they do not provide an explanation for this behavior. In the present work, the uneven segmentation observed at the low cutting speed of 20 m/min could be due to chatter at this speed.
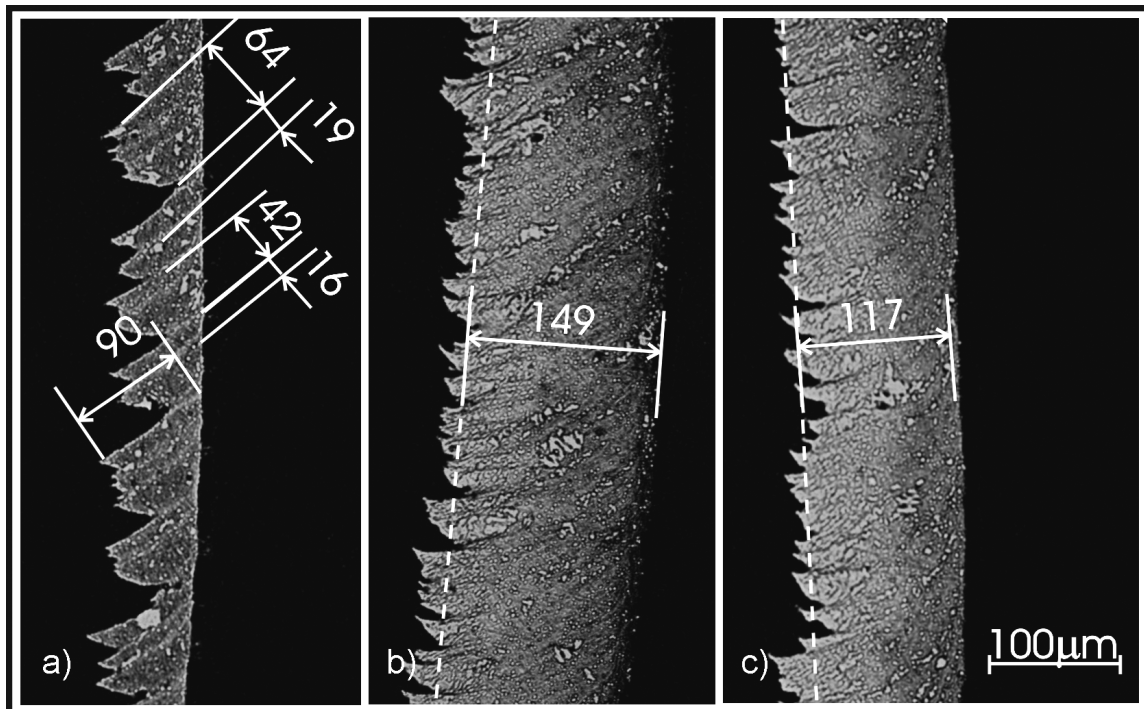
Figure 4.18: Chip obtained in: a) Mechanical cutting, b) LAM 20 m/min, c) LAM 30 m/min.

The chips shown in Figure 4.18 (b) and (c), correspond to machining with laser assistance at the maximum power (2 kW), at cutting speeds of 20m/min and 30m/min respectively. The chip morphology in this cases is entirely different in reference to chips obtained in conventional machining in that while the micro-cracks are still present, gross cracking has been eliminated complectly. Chip segmentation does not

occur anymore and the chip can be considered continuous. Shearing appears to occur on a curved path which is well pronounced in the vicinity of the tool edge visible but the gross cracks disappeared completely.

Reference [8] explains that in the case of conventional machining the shear strength of the workmaterial can be considered, and the value of F_s is minimum for the shortest path between tool edge and the free surface. In laser assisted machining this situation changes. Due to laser power entering the workpiece an important thermal gradient develops in the superficial layer, the temperature varies from about 400°C at the tip tool to about 600°C on the free surface, leading to a non linear mechanical resistance field curving from the tool edge through the highest temperature gradient Figure 4.19.
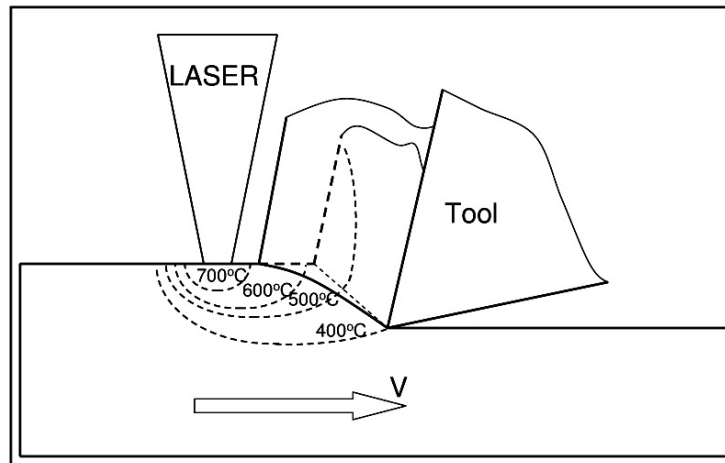
Figure 4.19: Chip formation in LAM [8].

Examination of the cutting edge when machining with laser assist indicated built-up edge formation at both 20 an 30 m/min. In this regard it seems that chip formation in these cases was associated with the BUE. This could have been a factor in reducing tool wear when machining with laser assist at least at a cutting speed of 20 m/min for which BUE formation was stable.

An important difference that is evident when comparing the chips obtained at 20 m/min, without and with laser assist (Figure 4.18 a, b) is that the chip thickness has increased substantially, from about 60-70 μm in conventional cut to 150 μm in laser assisted cut.
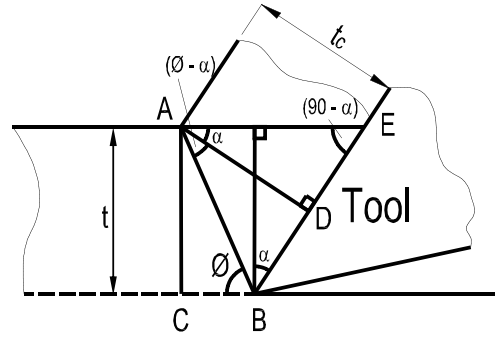
Figure 4.20: Geometrical relation between uncut chip thickness, chip thickness, and shear and rake angles.

Refering to Figure 4.20 uncut chip thickness and chip thickness can be related by:

$$\frac{t}{t_c} = \frac{sin\phi}{cos(\phi - \alpha)} \tag{4.7}$$

And for the present case where the rake angle $\alpha = 0$, Equation 4.7 reduces to:

$$\phi = tan^{-1}\frac{t}{t_c} \tag{4.8}$$

For the uncut chip thickness of 0.05 mm, considering an average chip thickness, Equation 4.8 gives a shear angle of about 40° for conventional cutting which changes to ≈ 19° for laser assist cutting at 20 m/min. On increasing the cutting speed to 30 m/min when using laser assist the shear angle increases to ≈ 23°. Such a reduction of shear angle on application of laser assist has been reported in reference [8] as well. The fact that the reduction in cutting forces in LAM has materialized despite the increase in shear plane angle is an indication of heating induced workmaterial softening. The

increase in the shear angle from 19 to $\approx 23°$ corresponding to the increase in cutting speed from 20 to 30 m/min is again indicative of the reduction in laser heating at the higher speed due to lower laser exposure time.

4.2.4 Surface Quality

The functional characteristics of a machined part depends of workpiece geometry and surface integrity. In order to determine the influence of LAM on surface integrity, metallographic samples from machined surfaces were prepared to characterize the subsurface hardness profile. The geometrical accuracy of the machined part was not the focus of this work.

During hard machining, surface integrity can be affected due to a combination of extremely high temperatures and mechanical loads in the tool workpiece contact zone. Tönshoff et al., [1] explains that during hard machining of steel, temperature of the workpiece material rises to above austenizing temperature in contact times of approximately 0.1 ms, and that the workpiece material is self quenched, leading to structural changes and residual stresses into workpiece subsurface. This superficial layer of thermo-mechanically modified work material has been observed by many researchers and has been referred to as the white layer, due to its non etching property.

As is evident in the micrographs shown in Figure 4.21 the surfaces obtained in conventional machining as well as in LAM were devoid of a white layer or microstructural alterations. However to check if the material subsurface has been thermally influenced, microhardness measurements were performed on a LECO micro-hardness tester (model M-400-H2), using a load of 1kg.

The results presented in Figure 4.22 do not reveal significant difference between the bulk material hardness and the hardness in the vicinity of the generated surfaces obtained in LAM.
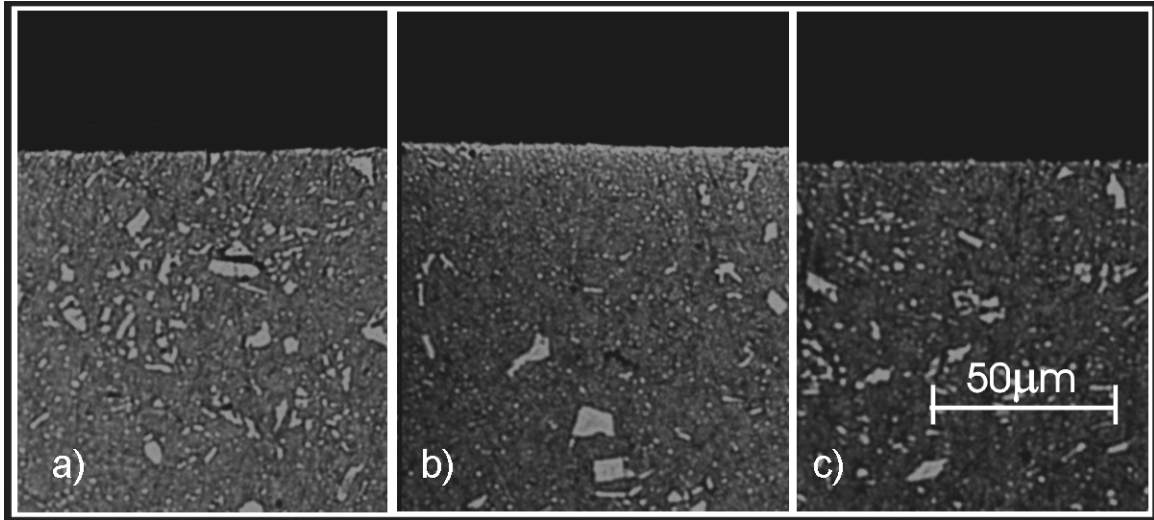
Figure 4.21: Subsurface microstructure obtained in: a) Conventional cutting, b) LAM 20m/min, c) LAM 30m/min.

It is to be noted though that in this case the workpiece was subject to only about 20 heating cycles after which it was cooled down to the room temperature. Had this not been the case it is possible that the temperature in the generated subsurface attains temperatures high enough for steel tempering to occur resulting in a reduction of hardness. Depending on the application, if this is undesirable, it is essential that the work temperature is controlled by resorting to some external means of localized cooling or appropriate continuous control of laser power. It is likely that repetitive heating leading to heat accumulation in the workpiece resulted in the heat affected zone identified in reference [34]. Also, if surface integrity is critical, the final pass could be accomplished conventionally without laser assist to remove any heat affected material.

4.3 Longitudinal Turning

Although the Ashby and Easterling model predicts temperatures as low as 100 °C in the uncut chip thickness for a cutting speed of 100 m/min, experimental tem-
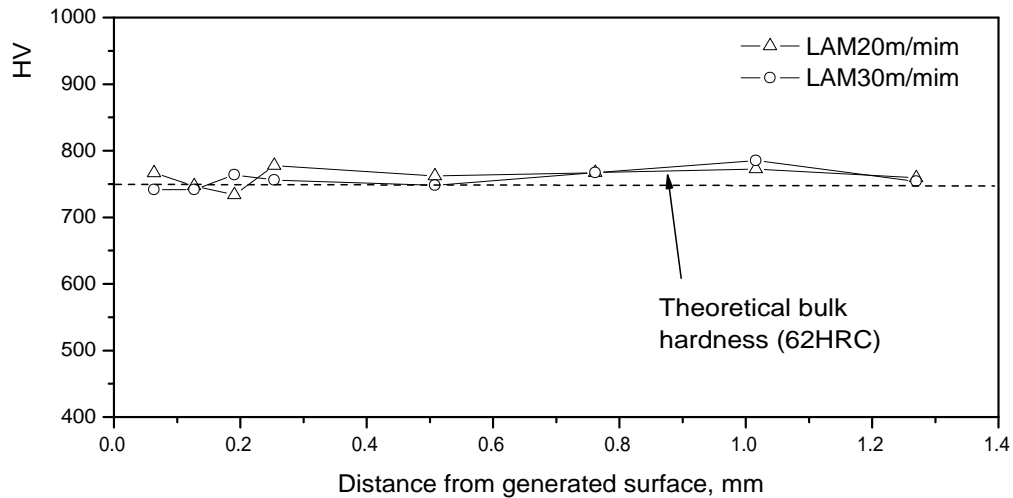
Figure 4.22: Microhardness profile of LAM generated surfaces.

perature measurements during grooving tests indicated that repetitive heating leads to heat accumulation in the workpiece. In a longitudinal laser assisted machining set-up, since the laser spot width is much higher than the feed per revolution, repetitive heating is more pronounced in comparison to grooving. Hence it could be assumed that higher cutting speeds are possible in longitudinal turning in comparison to grooving experiments ($\approx$ 30 m/min). Since the diode laser has a spot size of 0.9 x 4 mm (along the slow and fast axes) the repetitive heating effect will depend on orientation of the laser for a constant feed per revolution and laser power. Tests were performed with two spot orientations with the fast axis oriented parallel (LAM $\parallel$) and perpendicular (LAM $\perp$) to the workpiece axis. Cutting tests were performed at 100 and 150m/min, a feed of 0.05 mm/rev and a depth of cut of 0.2 mm. The tests indicated that the tools failed at speeds higher than 100 m/min pointing to this speed being the maximum possible for the laser power available and the carbide tooling used.

4.3.1   Tool Life - Tool Wear Mechanism

Unlike the grooving experiments where the tools failed at cutting speeds above 20 m/min when machining conventionally, the longitudinal turning experiments resulted in a relatively better performance as indicated in Figure 4.23 (a). For a tool failure criterion of a maximum flank wear of 300 μm, the carbide tooling provided a length cut of approximately 160 m. The corresponding tool wear mechanisms comprised abrasive wear and cutting edge microchipping (Figure 4.23 b). The grooves

a)   b)

Figure 4.23:   a) Comparison of flank wear between conventional cutting and LAM using two laser orientations, and b) The corresponding flank wear micrographs.

evident on the flank wear land are indicative of the abrasive action of hard chromium carbide particles in the workpiece.
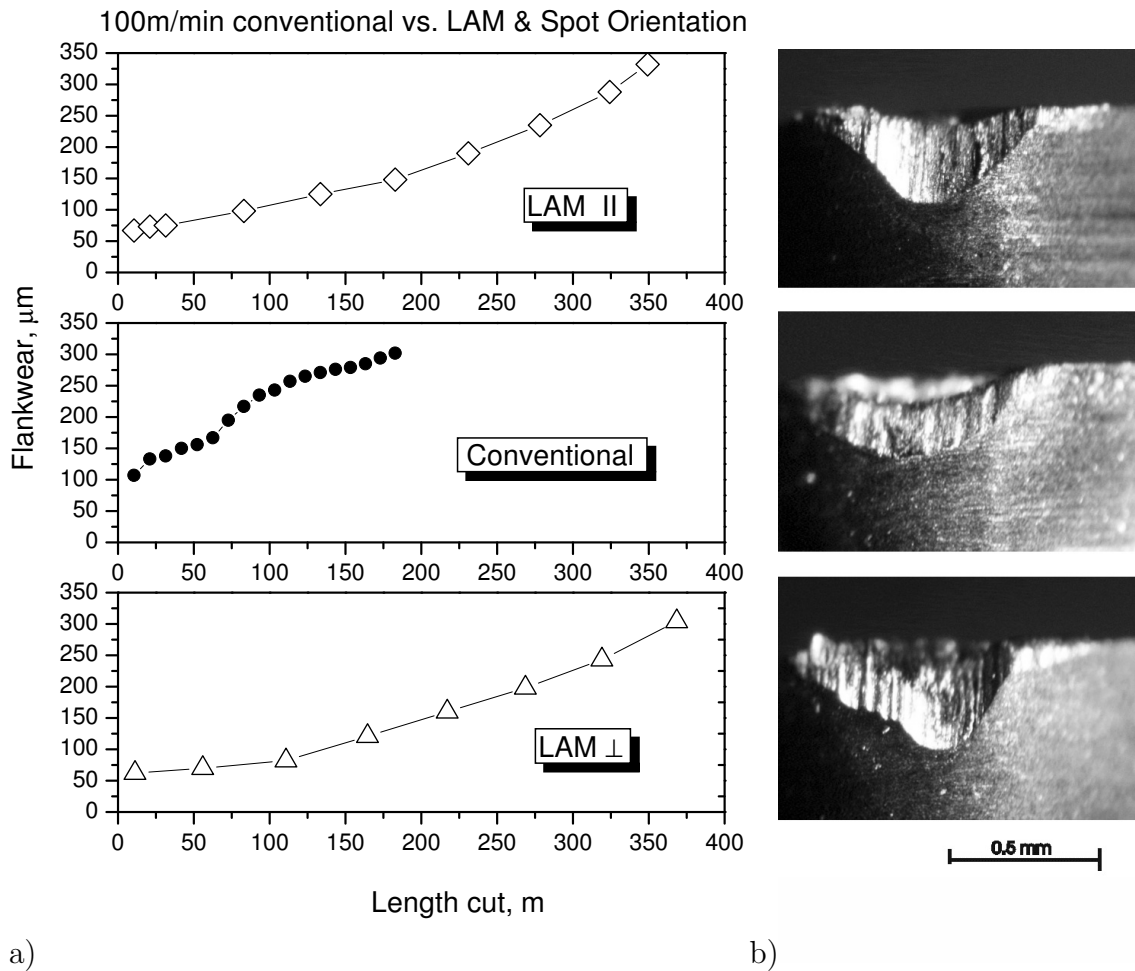
When machining with laser assist, both the laser orientations provided similar tool wear results (despite the number of heating cycles in the parallel orientation being about 4 times higher) in that the length cut was doubled in comparison to conventional cutting for the same tool life criterion. The flank wear corresponding to the LAM configurations indicated abrasive wear. Chipping of the cutting edge was evident, however, it was not of the same scale as in conventional cutting.

4.3.2 Cutting Forces vs. Temperature

With the two laser spot orientations having provided similar tool life results, the effect of laser spot orientation was compared with reference to cutting forces and surface temperature to evaluate their effectiveness in relation to conventional cutting.

Cutting forces obtained during conventional machining (Figure 4.24 a), reveal the hard machining character of the cutting process, with the ratio of the cutting force to the thrust force (F_c/F_p) being around 0.5. The increase in the thrust force during the duration of the cut is indicative of tool wear, with the sudden discontinuity marked in the Figure corresponding to a chipping event taking place at the cutting edge. All three components of the cutting force seem to indicate the presence the vibration of the cutting tool.

Surface temperature measured in front of the cutting tool at a distance of about 10 mm indicated in Figure 4.24 (b) and (c) show the difference between the two LAM configurations and explains the evolution of cutting forces. The maximum temperature reached in the LAM $\parallel$ was about 450°C whereas the corresponding temperature for the LAM $\perp$ was in excess of 600°C, see Figure 4.24 (c).
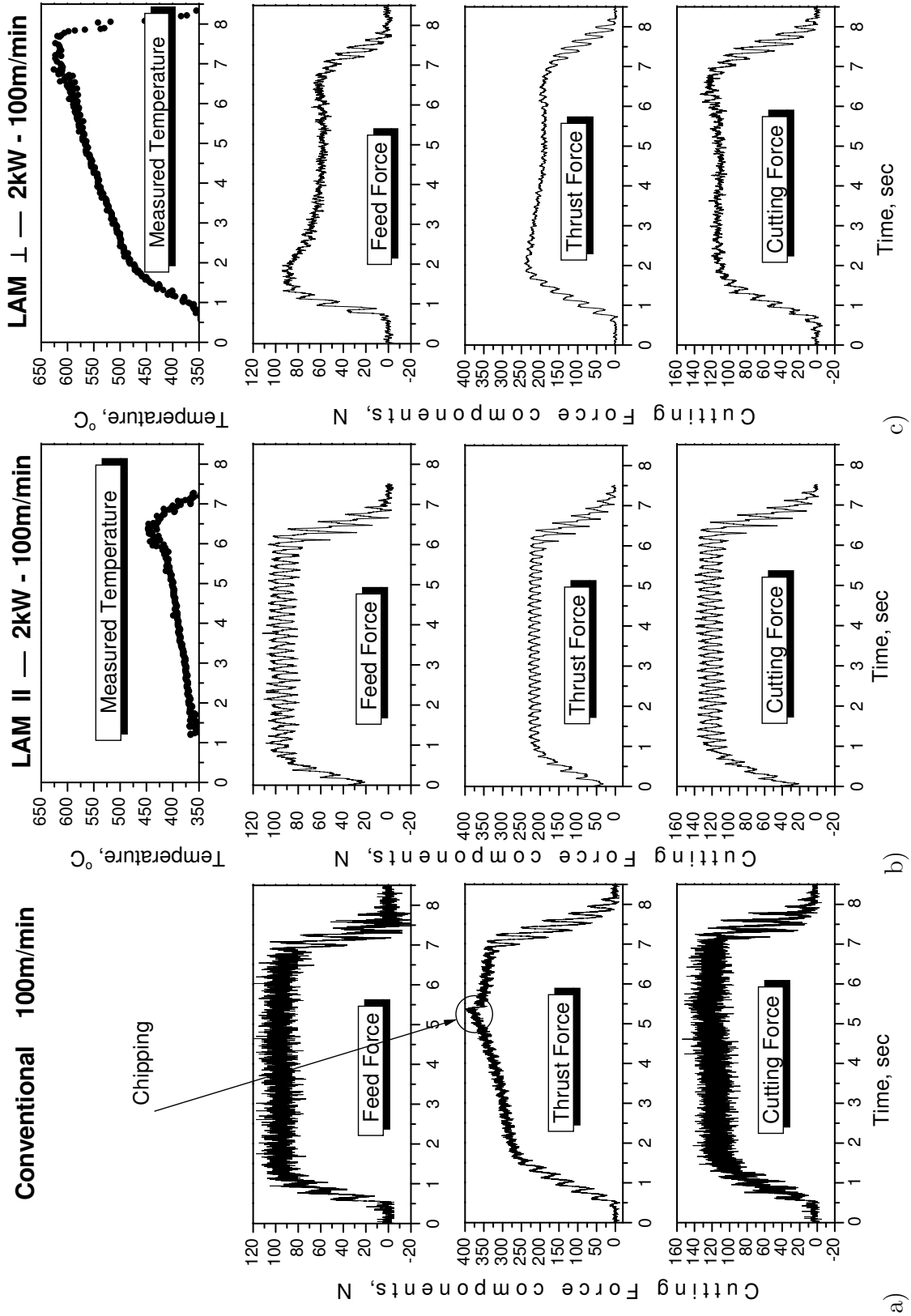
Figure 4.24: Cutting forces and surface temperature: a) Conventional cutting, b) LAM with parallel spot orientation, c) LAM with perpendicular spot orientation.

Cutting force components during LAM ∥, (Figure 4.24 b), show a small improvement in comparison with conventional cutting. The tool vibration is reduced, and while the cutting and feed force components are essentially the same, the thrust force is not only reduced in LAM ∥ but also is maintained constant during the cut. This indicates thermal softening of the workpiece material and reduced wear of the cutting edge.

Due to continuously increasing temperatures achieved during LAM ⊥, cutting force components present a decreasing trend over the duration of the cut unlike in LAM ∥ (Figure 4.24 c). The cutting force to thrust force ratio (F_c/F_p) approaches 1 when machining with laser assist for both the configurations.

The results above indicate that the best laser spot orientation is LAM ⊥. The higher temperatures achieved during LAM ⊥ could be explained by the fact that the uncut chip thickness is irradiated by the laser beam a longer duration during LAM ⊥ than it is during LAM∥ (Figure 4.25). The top hat intensity distribution of the beam along the slow axis (width of the spot) is also more suitable for effective heating as opposed to the gaussian distribution along the fast axis.

a)   b)
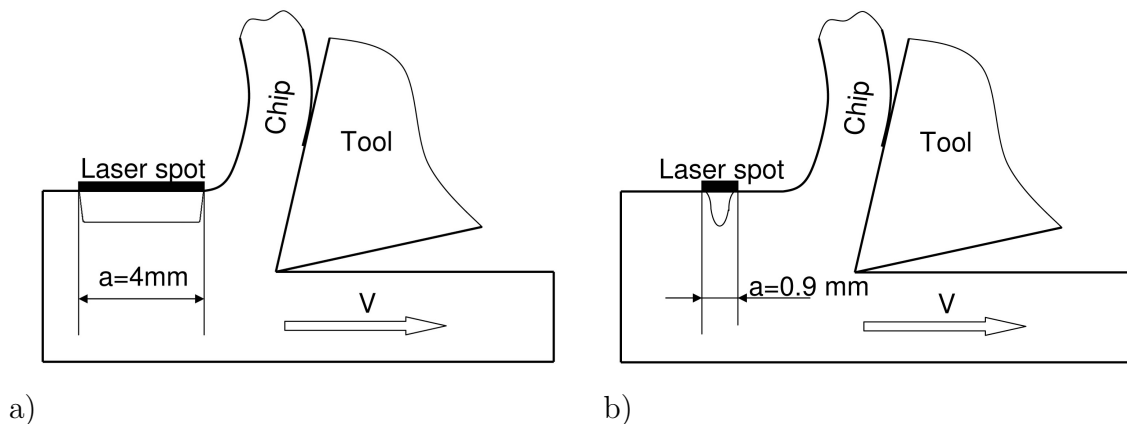
Figure 4.25: Laser spot orientation with regard to the cutting speed: a)LAM ⊥, b) LAM ∥.

4.3.3 Mechanism of Chip Formation

Typical chips produced during longitudinal turning at a cutting speed of 100 m/min in conventional machining and in LAM corresponding to parallel and perpendicular orientations are shown in Figure 4.26. It is evident that the chips produced in conventional as well as in LAM ∥ are segmented whereas the chip produced in LAM ⊥ is largely continuous. This observation is in good agreement with the surface temperature measurements (Figure 4.24) wherein the temperatures obtained in LAM ⊥ was higher the corresponding values in the LAM ∥.
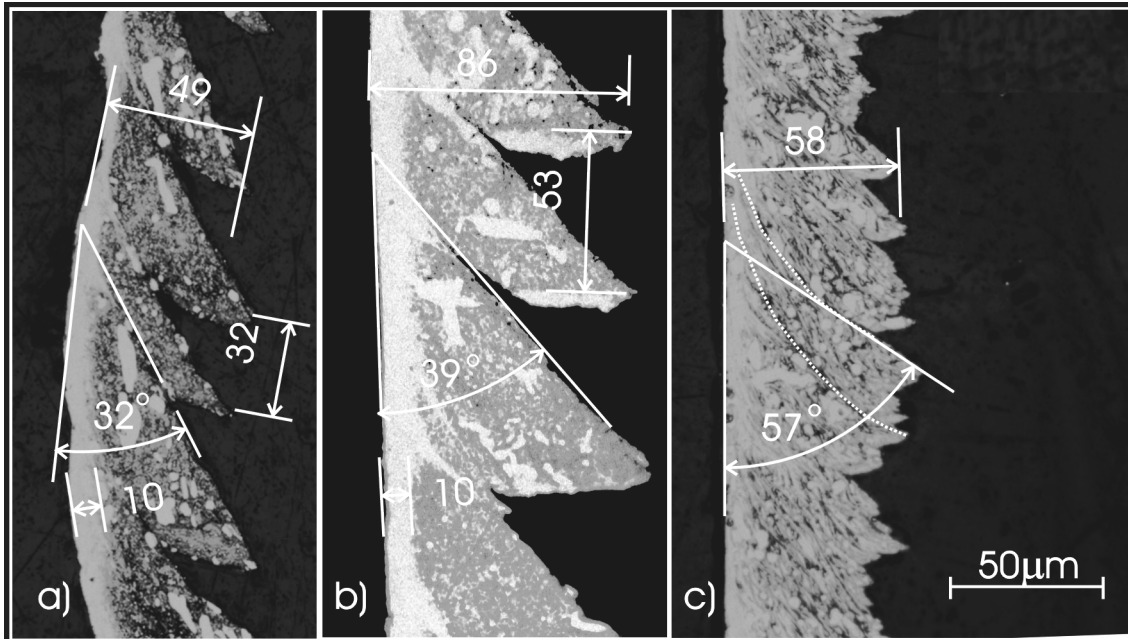
Figure 4.26: Chip cross section: a) Conventional cutting, b) LAM ∥, c) LAM ⊥.

The present work characterizes the chip formation in conventional machining and LAM of D2, as per Lesourd et al. [8], see Figure 4.27, where [h]

- δ = the segmentation distance;

- e = the width primary shear band;
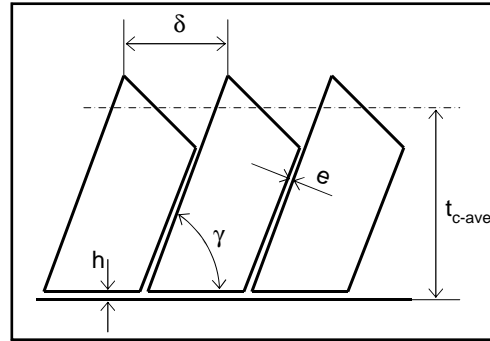
Figure 4.27: Segmented chip characteristics [8].

- h = the width secondary shear zone;

- γ = the slipping angle;

- t_{c-ave} = the average chip thickness.

Although it was observed in reference [8] that a 10-30 % reduction of δ occurs when laser is used to assist the cutting process, for the case studied in present work, respectively LAM $\parallel$ at 100 m/min, δ increased from 32 μm in conventional cutting to 53 μm in LAM $\parallel$.

Slipping angle γ increases with the increase of workpiece temperature from about 32° in conventional cutting to 39° in LAM $\parallel$ ($T \approx 400°C$), respectively to 57° in LAM $\perp$ ($T \approx 600°C$). The slipping angle observation allows a simple way to determine the shear angle, [8]:

$$\gamma + \phi - \alpha = 90°$$

where ϕ is the shear angle, and α is the rake angle. Analyzing the above formula, if γ is increasing, the shear angle is decreasing. This observation is in agreement with the previous results from the grooving/part-off tests, where decreased shear angle was also noticed at elevated workpiece temperatures, and the conclusion in reference [8]

that LAM decreases the shear angle by about 10°.

The chip obtained in LAM ⊥ presents similarities with the chips obtained during LAM in the grooving experiments. Same curved slip lines, marked in Figure 4.26 (c) with dotted line, can be observed. The curvature becomes more significant in the vicinity of the chip-tool interface, and closer to the free surface of the chip the shear lines maintain a constant direction. The curved slip lines are an indication of the work material softening due to laser heating during cutting. Unlike the chips obtained in the grooving experiments, the chips produced in the longitudinal experiment under conditions of conventional cutting and LAM ‖ reveal a white layer of thickness of about 10 μm at the chip tool interface. The white layer represents untempered martensite which forms as a direct result of high temperatures achieved due to localized shearing [45, 51]. The chip obtained during LAM ⊥ (Figure 4.26 c), however, does not show any white layer. It seems to indicate that net rise in temperature at the chip tool interface was not high enough due to the reduction in shear strength of the material brought about by laser heating.

4.3.4 Surface Quality

The micrographs shown in Figure 4.28 a, b and c reveal no trace of white layer at the generated surface. When cutting conventionally or when using laser assist at a cutting speed of 100 m/min the absence of the white layer noticed by other researchers [1] after high speed machining hardened steel, can be explained by the relatively low cutting speed used during present cutting tests. Most of the heat produced by shearing being removed with the chips, the workpiece material remains structurally unchanged. The short length cut employed and workpiece periodic cooling of the workpiece performed during LAM limited the temperature build up into the workmaterial, and thus no structural changes into the workpiece subsurface were

introduced .
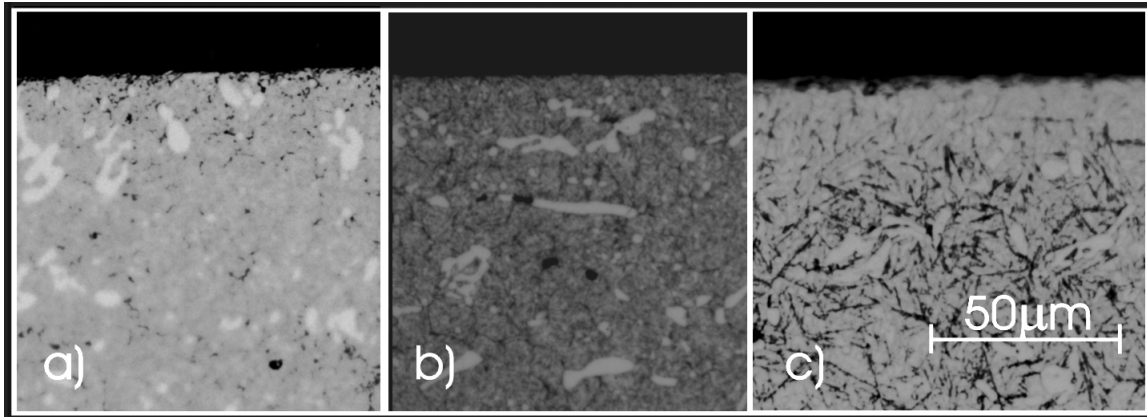
Figure 4.28: Generated Surface Micrographs: a) Conventional cutting, b) LAM ∥, c) LAM ⊥.

To further verify that thermally affected zone is absent in the vicinity of the generated surface, micro-hardness measurements were performed on a LECO micro-hardness tester (model M-400-H2), using a load of 1kg. The results presented in Figure 4.29 do not show much of a difference between the bulk material hardness and the subsurface hardness.
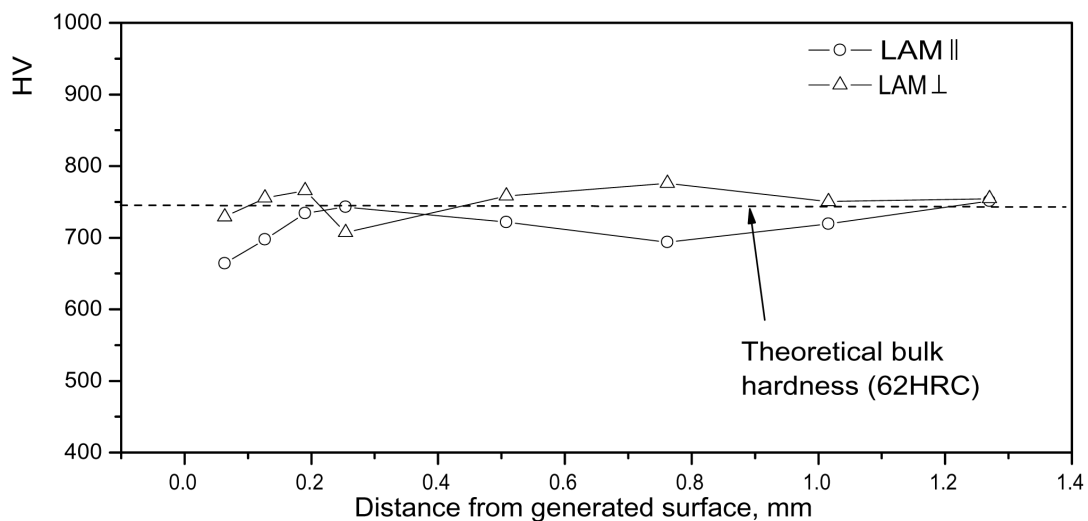
Figure 4.29: Microhardness profile of LAM generated surfaces.

Workpiece surface roughness was also measured for the three cutting methods, at the end of tool life and results are presented in Figure 4.30. The best surface finish, as expected, was obtained in conventional cutting. The results for the two LAM configurations show that the increased material softening due to laser heating in the LAM⊥ generates an increase in surface roughness, which is in good agreement with data presented by Koshy et al. [23] which show roughness as a function of material hardness (Figure 4.31).
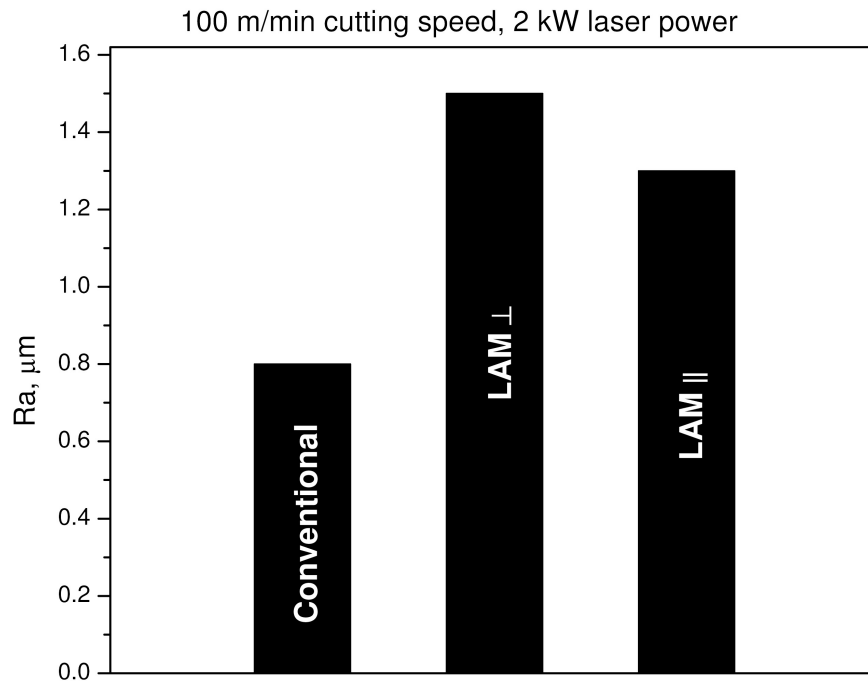
Figure 4.30: Roughness values for Conventional-LAM⊥-LAM∥.
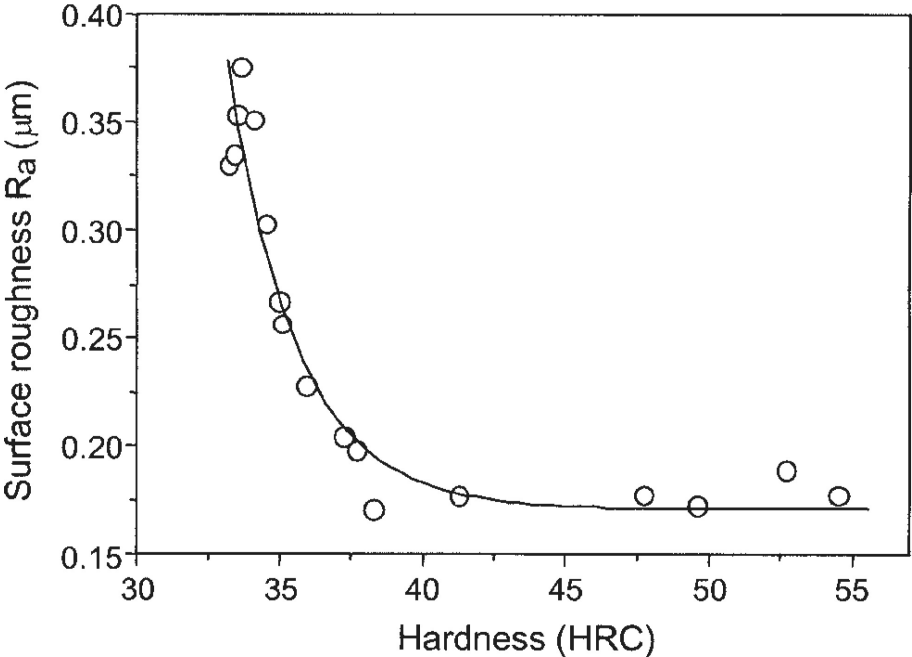
Figure 4.31: Surface roughness as function of work hardness [23].

CHAPTER 5

Conclusions and Future Work

5.1   Conclusions

The present work focused on the application of a high power diode laser for LAM of AISI D2 ($\approx$ 62HRC) tool steel and compare the process performance in reference to conventional machining. Two machining configurations, grooving and longitudinal turning were evaluated using carbide tooling with an emphasis on tool life, cutting forces, mechanism of chip formation, workpiece surface temperature, and surface integrity.

A simple analytical model, used for LAM temperature predictions, was found sufficiently accurate for initial process design, but not appropriate for precise temperature determination in laser assisted turning. For the complete characterization of laser assisted heating in a turning set-up, the model has to be further developed in order to account for repetitive heating and workpiece heat accumulation during the duration of the cut.

On the basis of experimental data obtained during tests and presented in this thesis, the following conclusions can be drawn:

⋄ It was found that AISI D2 steel softens sufficiently at around 300°C. If this temperature is achieved in the superficial layer of the workpiece in front of the cutting tool, continuous chips are obtained with an improvement in tool life of about 100% (in the case of longitudinal turning at 100 m/min) and enabling grooving operations at a cutting speed of 30 m/min. LAM also resulted in reduced thrust forces.

◇ The main mechanisms of tool wear identified during both conventional and LAM were cutting edge chipping, flank face abrasion, and adhesion. With the application of laser assist adhesion becomes the predominant wear mechanism in comparison to chipping and abrasion.

◇ The parameters identified to have the highest influence on LAM are:

  ○ Laser Power: Higher laser power conveys more thermal energy into the work material, permitting increased cutting speeds, and thus higher material removal rates.

  ○ Beam spot size: Beam spot size controls the power density and the localization heating.

  ○ Scanning speed - The cutting speed appropriate for laser assisted turning. Higher cutting speeds require more powerful lasers in order to keep the work zone temperature in a particular range.

◇ The spot orientation more suitable for laser assisted longitudinal turning was found to be the one with the spot fast axis parallel to workpiece axis. In comparison to the slow axis along the workpiece axis this orientation provides a more localized heating in front of the cutting edge.

◇ The larger spot sizes of high power diode lasers in comparison to other industrial lasers presents challenges in terms of generating a heat affected zone beneath the generated surface. This can be addressed by interactively controlling the laser power such that workpiece surface temperature is kept within a certain range, which was not in the scope of the present work. Alternatively the final finishing pass could be accomplished conventionally with no laser assist.

⬦ The mechanism of chip formation for D2 workmaterial transforms from segmental to continuous if the average temperature in the uncut chip thickness just in front of the cutting edge exceeds 300°C. Chip thickening was noticed when using LAM, which suggests a decrease of about 10° in the shear angle.

⬦ Due to the relatively large rectangular spot of the diode laser employed (0.9 x 4 mm), a laser power of 2kW represents a laser power density of only 55.6 kW/cm² which imposes limitations on the cutting speed. So HPDL are more suitable for assisting low speed operations such as grooving/part off that involve large chip cross sectional areas. Longitudinal turning operations that involve feed per revolutions that are small in comparison to the laser spot dimension results in repetitive heating of the workpiece that leads continuous heat accumulation in the workpiece body. Depending on the workmaterial this could result in thermal damage.

The limitations described above suggest that a laser with a higher power density resulting from a smaller spot size would be more appropriate for laser assisted longitudinal turning. However if work material thermal structural changes are not of concern, HPDL could be used successfully for this application as well.

5.2 Future Work

Successful LAM performed at low scanning speed, and the large beam spot size of HPDLs, capable of covering a large workpiece surface area, suggests that Laser Assisted Milling would be the next step of research in the LAM research field. For a milling set-up the scanning speed becomes similar to the feed speed. This implies that the cutting speed will not be directly limited anymore by the laser power. The laser track on the workpiece surface could be linear, hence the Ashby and Easterling

model could be used for accurate temperature prediction.

The model described in the present work can be further developed in order to incorporate the diode laser characteristic of the rectangular laser spot shape, with its different intensity distributions on the two axes. Experimental repetitive heating noticed during turning cutting tests can also be modelled and added to the Ashby and Easterling model in order to predict workpiece subsurface temperatures in the uncut chip thickness.

Other difficult to machine materials such as high silicon aluminum alloys or titanium alloys, which currently present problems with regard to their machinability could be the focus of future LAM research. Titanium alloys are currently widely used in the aerospace industry, successful implementation of LAM in machining these alloys could lead to productivity improvements.

The technology employed for LAM could also be further developed and easily adapted to realize in-process case hardening of components. For laser case hardening the laser beam will follow the cutting tool as opposed to LAM where the laser beam precedes the cutting tool, generating a hardened superficial layer. This process could be applicable for a wide range of industrial steel products and could lead to a reduction in production costs by eliminating the heat treatment operation.

References

[1] H.K. Tönshoff, C. Arendt, and R. Ben Amor. Cutting of hardened steel. *Annals of the CIRP*, vol. 49(2): pp. 547–566, 2000.

[2] Lin Li. The advances and characteristics of high-power diode laser materials processing. *Optics and Lasers in Engineering*, vol. 34: pp. 231–253, 2000.

[3] AISI D2 Cold work tool steel. *www.bucorp.com*, Sep. 2004.

[4] W. Konig and A.K. Zaboklicki. Laser-assisted hot machining of ceramics and composite materials. *National Institute of Science and Technology*, NIST Special Publication 847: pp. 455–463, 1993.

[5] Edward M Mielnik. Hot machining in retrospect and review. *Proceedings of the NAMRC XXII Conference*, MR94-142: pp. 1–12, May 1994.

[6] S.T. Lei, Y.C. Shin, and F.P. Incropera. Deformation mechanisms and constitutive modeling for silicon nitride undergoing laser-assisted machining. *International Journal of Machine Tools & Manufacture*, vol. 40 (15): pp. 2213–2233, Dec. 2000.

[7] Y. Wang, L.J. Yang, and N.J. Wang. An investigation of laser-assisted machining of Al_2O_3 particle reinforced aluminum matrix composite. *Journal of Materials Processing Technology*, vol. 129 (1-3): pp. 268–272, Oct. 2002.

[8] B. Lesourd, F. LeMaître, and T. Thomas. The chip formation in conventional and laser assisted machining - application to the milling process. *Laser Assisted Net shape Engineering - Proceedings of the LANE*, vol. 1: pp. 465–476, 1994.

[9] W. Ben Salem, A. Melahaoui, P. Cohen, F. Ahdad, and J.P. Longuemard. L'usinage assisté par laser. *Mécanique Industrielle et Matériaux*, vol. 48/1: pp. 29–30, Mar.1995.

[10] J.F. Gratias, L.J. Fan, J. Marot, P. Cohen, and Moisan A. Proposition of a method to optimize the machining of XC42 steel with laser assistance. *Annals of the CIRP*, vol. 42/1: pp. 115–118, 1993.

[11] B. Lesourd and T. Thomas. L'usinage assisté par laser. *Mécanique Industrielle et Matériaux*, vol. 48/1: pp. 22–24, 1995.

[12] P.A. Rebro, Y.C. Shin, and F.P. Incropera. Laser-assisted machining of reaction sintered mullite ceramics. *Journal of Manufacturing Science And Engineering-Transactions of the ASME*, vol. 124 (4): pp. 875–885, Nov. 2002.

[13] L. Ma, Y. Wang, D. Xie, L. Yang, and X. Liu. Laser assisted hot machining of cold-hard cast iron. *Journal of Harbin Institute of Technology*, vol. 34/2: pp. 228–231, 2002.

[14] S.T. Lei, Y.C. Shin, and F.P. Incropera. Experimental investigation of thermo-mechanical characteristics in laser-assisted machining of silicon nitride ceramics. *Journal of Manufacturing Science And Engineering-Transactions of the ASME*, vol. 123 (4): pp. 639–646, Nov. 2001.

[15] J.C. Rozzi, F.E. Pfefferkorn, F.P. Incropera, and C. Yung Shin. Transient, three-dimensional heat transfer model for the laser assisted machining of silicon nitride: I. Comparison of predictions with measured surface temperature histories. *International Journal of Heat and Mass Transfer*, vol. 43: pp. 1409–1424, 2000.

[16] M. A. Ashby and K. E. Easterling. The transformation hardening of steel surfaces by laser beams - I. Hypo-eutectoid steels. *Acta Metallica*, vol. 32 (11): pp. 1935–1948, 1984.

[17] S.P.F.C. Jaspers and J.H. Dautzenberg. Material behaviour in conditions similar to metal cutting: flow stress in the primary shear zone. *Journal of Materials Processing Technology*, vol. 122: pp. 322–330, 2002.

[18] M. Haag and T. Rudlaff. High-power diode-lasers and their direct industrial applications. *SPIE proceedings*, vol. 2382: pp. 78–88, 1995.

[19] G. Poulachon, B.P. Bandyopadhyay, I.S. Jawahir, S. Pheulpin, and E. Seguin. Wear behavior of CBN tools while turning various hardened steels. *Wear*, vol. 256/3-4: pp. 302–310, 2003.

[20] T.I. El-Wardany, H.A. Kishawy, and M.A. Elbestawi. Surface integrity of die material in high speed machining, Part I: Micrographical analysis. *Journal of Manufacturing Science and Engineering*, vol. 122: pp. 620–631, 2000.

[21] J.C. Ion, H.R. Shercliff, and M.F. Ashby. Diagrams for laser materials processing. *Acta Metallica et Materialia*, vol. 40: pp. 1539–1551, Jul. 1992.

[22] Kenneth Budinski. *ENGINEERING MATERIALS - Properties and Selection*. Reston Publishing Company Inc., 2nd edition, 1983.

[23] P. Koshy and P. Dumitrescu. A simple technique to characterize the role of work hardness in hard part machining. *Jounal of Engineering Manufacture*, vol. 217: pp. 1485–1489, 2003.

[24] W. König, R.Komanduri, H.K. Tönshoff, and G Ackershott. Machining of hard materials. *Annals of the CIRP*, vol. 33(2): pp. 417–427, 1984.

[25] G. Chryssolouris, N. Anifantis, and S. Karagiannis. Laser assisted machining: An overview. *Journal of Manufacturing Science And Engineering-Transactions of the ASME*, vol. 119 (4B): pp. 766–769, Nov. 1997.

[26] Milton C. Shaw. Metal cutting principles. *Oxford Science Publications*, 4th edition, 1997.

[27] W. Ben Salem, G. Marot, A. Moisan, and J.P. Longuemard. Lasser assisted turning during finishing operation applied to hardened steels and inconel 718. *Laser Assisted Net shape Engineering - Proceedings of the LANE*, vol. 1: pp. 456–464, 1994.

[28] J.C. Rozzi, F.E. Pfefferkorn, F.P. Incropera, and Y.C. Shin. Transient thermal response of a rotating cylindrical silicon nitride workpiece subjected to a translating laser heat source, Part I: Comparison of surface temperature measurements with theoretical results. *Journal of Heat Transfer*, vol. 120: pp. 899–905, Nov. 1998.

[29] J.C. Rozzi, F.P. Incropera, and Y.C. Shin. Transient thermal response of a rotating cylindrical silicon nitride workpiece subjected to a translating laser heat source, Part II: Parametric effects and assessment of a simplified model. *Journal of Heat Transfer*, vol. 120: pp. 907–915, Nov. 1998.

[30] J.C. Rozzi, F.P. Incropera, and C. Yung Shin. Transient, three-dimensional heat transfer model for the laser assisted machining of silicon nitride: II. Assessment of parametric effects. *International Journal of Heat and Mass Transfer*, vol. 43: pp. 1425–1437, 2000.

[31] J.C. Rozzi, F.E. Pfefferkorn, Y.C. Shin, and F.P. Incropera. Experimental evaluation of the laser assisted machining of silicon nitride ceramics. *Journal of*

Manufacturing Science And Engineering-Transactions of the ASME, vol. 122 (4): pp. 666–670, Nov. 2002.

[32] P.A. Rebro, Y.C. Shin, and F.P. Incropera. Design of operating conditions for crackfree laser-assisted machining of mullite. *International Journal of Machine Tools & Manufacture*, vol. 44(7-8): pp. 669–676, 2004.

[33] F.E. Pfefferkorn, Y.C. Shin, Y. Tian, and F.P. Incropera. Laser-assisted machining of magnezia-partially-stabilized zirconia. *Journal of Manufacturing Science And Engineering-Transactions of the ASME*, vol. 126: pp. 42–51, 2004.

[34] A.R. Khan. Laser assisted machining. Master's thesis, McMaster University, 2003.

[35] B.S. Yilbas. Laser heating process and experimental validation. *International Journal of Heat and Mass Transfer*, vol. 40/5: pp. 1131–1143, Mar.1997.

[36] J.C. Rozzi. *Experimental and theoretical evaluation of the Laser Assisted Machining of Silicon Nitride Ceramics*. PhD thesis, Purdue University, 1997.

[37] J.J. Ewing and C.A. Brau. Laser actions on the bands of KrF and XeCl. *Journal of Applied Physics*, vol. 27:350, Jul. 1975.

[38] F. Bachmann. Industrial applications of high power diode lasers in materials processing. *Applied Surface Science*, vol. 208-209: pp. 125–136, 2003.

[39] F. Klocke, A. Demmer, and A. Zaboklicki. Investigation into the use of high power diode lasers for hardening and thermal conduction welding of metals. *SPIE proceedings*, vol. 3097: pp. 592–598, 1997.

[40] M. Haag and T. Rudlaff. Assessment of different high power diode lasers for material processing. *SPIE proceedings*, vol. 3097: pp. 583–591, 1997.

[41] W. Schulz and R. Poprawe. Manufacturing with novel high power diode lasers. *IEEE Journal of selected topics in quantum electronics*, vol. 6/4: pp. 696–705, 2000.

[42] Bill Bryson. *Heat Treatment, Selection, and Application of Tool Steels*. Hanser Gardner Publications - Cincinati, 1997.

[43] T. Hodgson and P.H.H. Trendler. Turning hardened tool steel with cubic boron nitride inserts. *Annals of the CIRP*, vol. 30/1: pp. 63–66, 1981.

[44] H.A. Kishawy. An experimental evaluation of cutting temperatures during high speed machining of hardened D2 tool steel. *Machining Science and Technology*, vol. 6(1): pp. 67–79, 2002.

[45] G. Poulachon, B.P. Bandyopadhyay, I.S. Jawahir, S. Pheulpin, and E. Seguin. The influence of the microstructure of hardened tool steel workpiece on the wear of PCBN cutting tools. *International Journal of Machine Tools & Manufacture*, vol. 43: pp. 139–144, 2003.

[46] P. Koshy, R.C. Dewes, and D.K. Aspinwall. High speed end milling of hardened AISI D2 tool steel (∼58 HRC). *Journal of Materials Processing Technology*, vol. 127: pp. 266–273, 2002.

[47] T.I. El-Wardany, H.A. Kishawi, and M.A. Elbestawi. Surface integrity of die material in high speed machining, Part II: Microhardness variations and residual stresses. *Journal of Manufacturing Science and Engineering*, vol. 122: pp. 632–641, 2000.

[48] C.E. Becze, M.J. Worswick, and M.A. Elbestawi. High strain rate shear

evaluation and characterization of AISI D2 tool steel in its hardened state. *Machining Science and Technology*, vol. 5(1): pp. 131–149, 2001.

[49] H. Bande, G. L'Espérance, M.U. Islam, and A.K. Koul. Laser hardening of AISI O1 tool steel and its microstructure. *Materials Science and Technology*, vol. 7: pp. 452–457, May 1991.

[50] A. Vyas and M.C. Shaw. Mechanics of saw-tooth chip formation in metal cutting. *Journal of Manufacturing Science And Engineering-Transactions of the ASME*, vol. 121: pp. 163–172, 1999.

[51] A. Vyas and M.C. Shaw. The significance of the white layer in a hard turned steel chip. *Machining Science and Technology*, vol. 41(1): pp. 169–175, 2000.

[52] M.A. Davies, Y. Chou, and C.J. Evans. On chip morphology, tool wear and cutting mechanics in finish hard turning. *Annals of the CIRP*, vol. 45(1): pp. 77–82, 1996.

[53] W. Pentland, J.L. Wennberg, and Clarence L. Mehl. Researches in elevated temperature machining of high strength materials. *American Society of Tool and Manufacturing engineers*, MR60-165.

[54] T. Kitigawa and K. Maekawa. Plasma hot machining for new engineering materials. *Wear*, vol. 139: pp. 251–267, 1990.

[55] Carl E. Leshock, Jin-Nam Kim, and C. Shin Yung. Plasma enhanced machining of inconel 718: modeling workpiece temperature with plasna heating and experimental results. *International Journal of Machine Tools & Manufacture*, vol. 41: pp. 877–897, 2001.

[56] G. Marot, L.J. Fan, A. Tarrats, P. Cohen, and J.P. Longuemard. Workpiece material-laser interaction and the laser-assisted machining. *Annals of the CIRP*, vol. 40/1: pp. 91–94, 1991.

[57] O. Manca and V. Naso. Solution to steady-state three-dimensional conduction for a rectangular surface heat source on a semi-infinite body. *International Communications in Heat and Mass Transfer*, vol. 21/6: pp. 799–808, 1994.

[58] I.R. Pashby, S. Barnes, and B.G. Bryden. Surface hardening of steels using a high power diode laser. *Journal of Materials Processing Technology*, 139/1-3: pp. 585–588, Aug. 2003.

[59] Michael Bass. *Physical Processes in Laser-Materials Interactions*. Plenum Press, New York, 1983.